A UNITED STATES DEPARTMENT OF COMMERCE PUBLICATION

ESSA Technical Memorandum WBTM TDL 30

U.S. DEPARTMENT OF COMMERCE
ENVIRONMENTAL SCIENCE SERVICES ADMINISTRATION
Weather Bureau

Summary of Selected Reference Material on the Oceanographic Phenomena of Tides, Storm Surges, Waves, and Breakers

N. ARTHUR PORE

Systems Development Office
SILVER SPRING
MARYLAND
May 1970

ESSA TECHNICAL MEMORANDA

Weather Bureau, Techniques Development Laboratory Series

The primary purpose of the Techniques Development Laboratory of the Office of Systems Development is to translate increases in basic knowledge in meteorology and allied disciplines into improved operating techniques and procedures. To achieve this goal, TDL conducts and sponsors applied research and development aimed at improvement of diagnostic and prognostic methods for producing weather information. The laboratory carries out studies both for the general improvement of prediction methodology used in the National Meteorological Service System and for more effective utilization of weather forecasts by the ultimate user.

ESSA Technical Memoranda in the Weather Bureau Techniques Development Laboratory series facilitate rapid distribution of material which may be preliminary in nature and which may be published formally elsewhere at a later date. The first five papers in the TDL series are part of the former Weather Bureau Technical Notes series.

Papers listed below are available from the Clearinghouse for Federal Scientific and Technical Information, U.S. Department of Commerce, Sills Bldg., 5285 Port Royal Road, Springfield, Va. 22151. Price: $3.00 hard copy; $0.65 microfiche. Order by accession number shown in parentheses at end of each entry.

TN 10 TDL 1 Objective Prediction of Daily Surface Temperature. William H. Klein, Curtis W. Crockett, and Carlos R. Dunn, October 1965. (PB-168 590)

TN 11 TDL 2 Hurricane Cindy Galveston Bay Tides. N. A. Pore, A. T. Angelo, and J. G. Taylor, September 1965. (PB-168 608)

TN 29 TDL 3 Atmospheric Effects on Re-Entry Vehicle Dispersions. Karl R. Johannessen, December 1965. (PB-169 381)

TN 45 TDL 4 A Synoptic Climatology of Winter Precipitation from 700-mb. Lows for the Intermountain Areas of the West. D. L. Jorgensen, W. H. Klein, and A. F. Korte, May 1966. (PB-170 635)

TN 47 TDL 5 Hemispheric Specification of Sea Level Pressure from Numerical 700-mb. Height Forecasts. William H. Klein and Billy M. Lewis, June 1966. (PB-173 091)

WBTM TDL 6 A Fortran Program for the Calculation of Hourly Values of Astronomical Tide and Time and Height of High and Low Water. N. A. Pore and R. A. Cummings, January 1967. (PB-174 660)

WBTM TDL 7 Numerical Experiments Leading to the Design of Optimum Global Meteorological Networks. M. A. Alaka and F. Lewis, February 1967. (PB-174 497)

WBTM TDL 8 An Experiment in the Use of the Balance Equation in the Tropics. M. A. Alaka, D. T. Rubsam, and G. E. Fisher, March 1967. (PB-174 501)

WBTM TDL 9 A Survey of Studies of Aerological Network Requirements. M. A. Alaka, May 1967. (PB-174 984)

WBTM TDL 10 Objective Determination of Sea Level Pressure from Upper Level Heights. William Klein, Frank Lewis, and John Stackpole, May 1967. (PB-179 949)

WBTM TDL 11 Short Range, Subsynoptic Surface Weather Prediction. H. R. Glahn and D. A. Lowry, July 1967. (PB-175 772)

WBTM TDL 12 Charts Giving Station Precipitation in the Plateau States from 700-Mb. Lows During Winter. D. L. Jorgensen, A. F. Korte, and J. A. Bunce, Jr., October 1967. (PB-176 742)

WBTM TDL 13 Interim Report on Sea and Swell Forecasting. N. A. Pore and W. S. Richardson, December 1967. (PB-177 038)

WBTM TDL 14 Meteorological Analysis of 1964-65 ICAO Turbulence Data. DeVer Colson, September 1968. (PB-180 268)

WBTM TDL 15 Prediction of Temperature and Dew Point by Three-Dimensional Trajectories. Ronald M. Reap, September 1968. (PB-180 727)

(Continued on inside back cover)

U.S. DEPARTMENT OF COMMERCE
Environmental Science Services Administration
Weather Bureau

ESSA Technical Memorandum WBTM TDL 30

SUMMARY OF SELECTED REFERENCE MATERIAL ON THE OCEANOGRAPHIC PHENOMENA OF TIDES, STORM SURGES, WAVES, AND BREAKERS

N. Arthur Pore

Systems Development Office
Techniques Development Laboratory

SILVER SPRING, MD.
May 1970
Reprinted May 1971

UDC 551.466.2:551.466.33:551.466.45:551.466.713:
551.466.7:525.6:551.465.75

551.46		Physical oceanography
.465		Sea waves and tides
.466.2		Principles of interpretation and methods of analysis of sea waves
	.33	Forecasting of sea waves
	.45	Breaker waves
	.713	Methods of tidal analysis and prediction
	.7:525.6	Astronomic aspects
551.465		Structure, dynamics and circulation of seas
	.75	Storm surges

CONTENTS

FOREWORD

The Weather Bureau of the Environmental Science Services Administration is responsible for providing on a routine basis timely warnings and forecasts of meteorological and oceanographic conditions both for the high seas and for coastal and inland waterways. This service includes forecasting of storm surges and abnormal tides which are of great concern to coastal communities.

The purpose of this memorandum is to collect together information on the calculation and forecasting of various oceanographic phenomena. Specifically, the phenomena discussed are; astronomical tide, storm surges (extratropical and hurricane), ocean surface waves, and breakers. Selected methods of calculating and forecasting these variables are described. Extensive use is made of illustrations and graphs taken mainly from the references. There are other methods that could be described in the various sections but in order to keep the document relatively short only the methods which are considered of most interest to forecasters of the Marine Weather Service are included.

Each section is written independently of the other four sections. This is the reason for the slight duplication in the description of the important generating processes for hurricane storm surges and extratropical storm surges.

SUMMARY OF SELECTED REFERENCE MATERIAL ON THE OCEANOGRAPHIC PHENOMENA OF TIDES, STORM SURGES, WAVES, AND BREAKERS

N. Arthur Pore

I. ASTRONOMICAL TIDES

Introduction

The longest period waves in the oceans are the tides which are periodic rises and falls of the water level. Tide information is of importance to the shipping industry for navigation and for the operation of ports, to amphibious military operations, to sportsmen in coastal areas, and to Weather Bureau personnel with responsibility for issuing storm surge forecasts.

The tides are caused by the difference in the gravitational attraction of the sun and moon on the solid earth and the water of the oceans. The tide producing force of an astronomical body is directly proportional to the mass of that body and inversely proportional to the cube of the distance from that body to the earth. The relative tide producing force of the moon to that of the sun is determined by considering the mass of the sun to be 27 million times that of the moon and the sun's distance from earth to be 389 times the moon's distance from earth. Consequently, the moon's tide generating force is 2.17 times as great as that of the sun.

The following sections include descriptions of datum planes used in recording tide heights, a discussion of tide tables and a description of the various types of tide. Also included is a discussion of the calculation of astronomical tide by the harmonic method.

Tidal Datum Planes

Tide heights are normally reported with respect to a tidal datum plane. For that reason the following definitions of commonly used tidal datum planes from Schureman (1963) are presented:

Mean sea level (MSL). - The average height of the surface of the sea for all stages of the tide over a 19-year period, usually determined from hourly height readings.

Mean high water (MHW). - The average height of the high waters over a 19-year period. For shorter periods of observations, corrections are applied to eliminate known variations and reduce the result to the equivalent of a mean 19-year value.

All high water heights are included in the average where the type of tide is either semidiurnal or mixed. Only the higher high water heights are included in the average where the type of tide is diurnal. So determined, mean high water in the latter case is the same as mean higher high water.

Mean higher high water (MHHW). - The average height of the higher high waters over a 19-year period. For shorter periods of observations, corrections are applied to eliminate known variations and reduce the result to the equivalent of a mean 19-year value.

Mean low water (MLW). - The average height of the low waters over a 19-year period. For shorter periods of observations, corrections are applied to eliminate known variations and reduce the result to the equivalent of a mean 19-year value.

All low water heights are included in the average where the type of tide is either semidiurnal or mixed. Only the lower low water heights are included in the average where the type of tide is diurnal. So determined, mean low water in the latter case is the same as mean lower low water.

Mean lower low water (MLLW). - Frequently abbreviated lower low water. The average height of the lower low waters over a 19-year period. For shorter periods of observations, corrections are applied to eliminate known variations and reduce the result to the equivalent of a mean 19-year value.

Half-tide level. - Also called mean tide level. A plane midway between mean high water and mean low water.

An excellent reference on tidal datum planes and the measurement, recording and tabulation of tide heights is that of Marmer (1951).

Range of Tide

There is a noticeable tidal cycle during the synodic month, which is the 29½ day interval between conjunctions of the moon and sun. Spring tides, which have greater than normal range, occur at times of conjunction (new moon and full moon). Neap tides, which have less than the normal range, occur at times of quadrature (first quarter and last quarter moon phases). These conditions are illustrated in figure 1.1.

Another effect on the range of the tide is the position of the moon in its orbit around the earth. Thus, at perigee, when the moon is at its closest point to earth, the tide range is increased. The range is decreased at the time of the moon's apogee.

Tide Tables

Tide Tables of the U.S. Coast and Geodetic Survey give the times and heights of high and low water for a large number of reference stations. A sample page from the 1970 Tide Tables for East Coast, North and South America is shown in figure 1.2. Here the datum plane is mean low water. The times of high and low water are indicated in hours and minutes, local standard time; note that the times are in increments of six minutes. This is because the calculations of high and low water times are made to the nearest tenth of an hour.

The Tide Tables include a list of tidal differences which enable one to determine times and heights of tides at many locations. This is done by applying these average differences, a sample of which is shown in figure 1.3, to the times and heights calculated for a reference station.

Types of Tide

A sample of typical tide curves for United States East and Gulf Coasts ports (Coast and Geodetic Survey, 1970a) is shown in figure 1.4. Similar curves are shown for several West Coast ports (Coast and Geodetic Survey, 1970b) in figure 1.5. As evident in these figures, the tide range and the characteristics of the tides are quite variable at different locations.

Tides are classified into three types; semidiurnal, diurnal, and mixed. Locations which experience a semidiurnal tide have two high waters and two low waters each day. This type of tide, which is the most common, is illustrated in the curves of the East Coast stations in figure 1.4. Tides of the diurnal type consist of one high and one low water each day. The curve for Pensacola in figure 1.4 shows a diurnal tide. Tides are classified as mixed when they are of the diurnal type on some days and of the semidiurnal type on other days. In such cases, tides are semidiurnal around the times the moon is on the equator but become diurnal near times of the moon's maximum north or south declination. The Galveston curve in figure 1.4 shows mixed tide characteristics.

Figures 1.6 and 1.7 from Schureman (1958) illustrate the reason for the occurrence of two tide cycles per day at most locations according to the equilibrium theory of tides. This theory does not accurately describe the natural tide, but it is a good way to visualize some of the features of the semidiurnal tide. The differences in gravitational attraction of the moon on the solid earth, the water on the side of the earth toward the moon, and the water on the side of the earth opposite the moon results in two bulges of water on the earth. As the earth rotates daily, each point on the earth will pass through the two bulges resulting in two high tides and two low tides daily. With the moon directly over the equator the two daily high tides at any location will be equal as shown in figure 1.6. When the moon is north or south of the equator as illustrated in figure 1.7, the two daily high tides will be of different heights except for points on the equator. Such diurnal inequality is evident in most of the curves of figure 1.4.

Tidal Constituents and Prediction

An excellent description of constituent tides has been given by Zetler (1959). The complicated motions of the moon and sun are simulated by a number of hypothetical tide-producing bodies. Each of these has a fixed period and produces a tide constituent with an amplitude which can be calculated.

The tidal constituents used for making the tide calculations for the United States Coasts consist of lunar and solar long period terms, lunar and solar diurnal terms, lunar and solar semidiurnal terms, lunar terdiurnal terms, and shallow water constituents ranging from semidiurnal to eighth diurnal. To make tide predictions the harmonic method of tide prediction combines these elementary tidal constituents into a composite tide. The height of the tide at any time as given by Schureman (1958) is:

$$h = H_o + \sum fH \cos[at + (V_o + u) - k]$$

where

h = height of tide at time t,

H_o = mean height of water level above datum used for prediction,

H = mean amplitude of any constituent A,

f = factor for reducing mean amplitude H to year of prediction,

a = speed of constituent A,

t = time reckoned from some initial epoch such as beginning of year of predictions,

$(V_o + u)$ = value of equilibrium argument of constituent A when $t = 0$, and

k = epoch of constituent A.

The periods of constituent tides are known from the theory of tidal forces. The amplitudes and phases cannot be derived theoretically because of the complex coastlines of the continents and the complicated bottom topography of the oceans. The amplitudes and phases are determined by harmonic analysis of a series of tidal observations as described by Schureman (1958).

The best type of observational data for harmonic analysis is that from automated tide gages, from which the tide height may be tabulated at any desired time interval. The Coast and Geodetic Survey uses hourly heights for harmonic analysis.

The length of series which is subjected to harmonic analysis is important and should conform approximately to multiples of periods of the important tidal constituents. The 369-day series is used as the standard length of record in the Coast and Geodetic Survey. Shorter series are used when the available record is shorter than 369 days.

The United States Coast Survey began publishing tide tables in 1867. The first 100 years of tide predictions by this agency are described by Hicks (1967). In this paper, Hicks describes the work of the early tide experts such as Ferrel, Harris, Shidy, Marmer, and Schureman. The harmonic method has been used in tide prediction since 1884. The mechanical analog tide prediction machine was put into operation in the United States in 1855. This machine of Ferrel's would sum 19 constituent tides. Harris and Fischer designed a 37 constituent machine which was put into operation in 1912. This machine was used for over half a century.

The shift to digital predictions by electronic computer was gradual. The first program was prepared in 1956 to predict hourly tide heights only, for use in storm surge research (Harris, Pore, Cummings, 1965). The greatest advantage to digital prediction at that time was the elimination of the hour or more required to set up a new problem on the analog tide predicting machine, when highly accurate predictions were needed for many short periods. Later, as more efficient computers became available, this program was expanded to include the computation of high and low tides.

The program, to a large degree, reproduced the same calculations formerly made on the analog tide predicting machine, and with comparable accuracy. The greater versatility of this system invites experimentation, not feasible with the analog computer. The 1966 Tide Tables of the Coast and Geodetic Survey were the first published tide tables produced by electronic computer.

The tide prediction program has recently been modified (Pore, Cummings, 1967) so it will be adaptable to any large scale computer equipped with a FORTRAN system. This is the program used to meet Weather Bureau needs for the operation of the telemetered tide gage network (Pore, 1964c) used in storm surge forecasting.

A sample of each type of printed output for Hampton Roads is shown in figure 1.8. The top half of the figure is a set of hourly tide heights and the lower portion is a set of times and heights of high and low water. The datum plane is 1.25 feet and 15 tidal constituents were included in the calculations. Each day of hourly tide heights requires two lines of printing. The first number of each line is the date of the month and the other twelve numbers are the hourly tide heights expressed in feet. The first line of each day contains heights from 0000 to 1100 Local Standard Time. The second line covers the period 1200 through 2300 Local Standard Time. The section of the output containing the highs and lows shows the time of high or low tide in hours and minutes with no separation or punctuation between hours and minutes. For example figure 1.8 shows the first low tide on March 1 to be at 0430 LST. Heights are printed in feet.

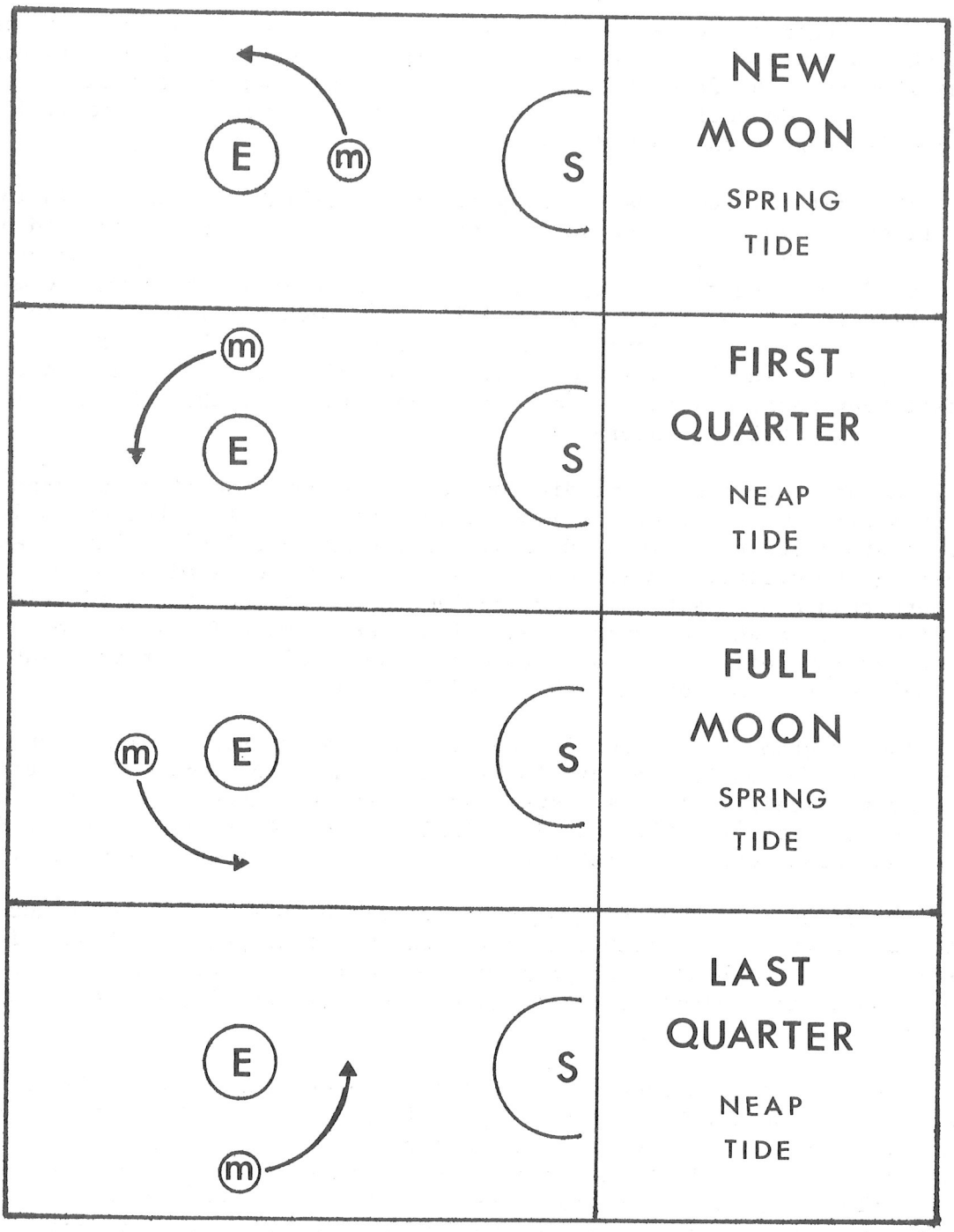

Figure 1.1. Relative positions of the sun, earth and moon at times of different moon phases during the synodic month.

HAMPTON ROADS (SEWELLS PT.), VA., 1970

TIMES AND HEIGHTS OF HIGH AND LOW WATERS

JANUARY						FEBRUARY						MARCH					
DAY	TIME H.M.	HT. FT.	DAY	TIME H.M.	HT. FT.	DAY	TIME H.M.	HT. FT.	DAY	TIME H.M.	HT. FT.	DAY	TIME H.M.	HT. FT.	DAY	TIME H.M.	HT. FT.
1 TH	0248	2.0	16 F	0418	2.3	1 SU	0412	2.3	16 M	0542	2.2	1 SU	0236	2.3	16 M	0406	2.1
	0900	0.2		1042	0.1		1036	0.1		1212	0.2		0900	0.3		1036	0.4
	1454	1.8		1636	1.7		1624	1.7		1806	1.7		1454	1.8		1630	1.7
	2106	-0.1		2236	-0.2		2230	-0.2					2100	0.0		2236	0.3
2 F	0342	2.2	17 SA	0518	2.3	2 M	0518	2.4	17 TU	0006	0.0	2 M	0348	2.4	17 TU	0506	2.2
	1006	0.2		1148	0.1		1148	0.0		0636	2.2		1018	0.2		1136	0.3
	1554	1.7		1730	1.6		1736	1.8		1300	0.1		1606	1.8		1736	1.8
	2206	-0.1		2336	-0.1		2342	-0.3		1854	1.8		2218	-0.1		2336	0.3
3 SA	0442	2.3	18 SU	0612	2.3	3 TU	0618	2.6	18 W	0054	0.0	3 TU	0500	2.5	18 W	0600	2.2
	1106	0.1		1242	0.0		1248	-0.2		0724	2.3		1124	0.1		1224	0.2
	1654	1.8		1830	1.6		1842	2.0		1342	0.0		1718	2.0		1824	2.0
	2300	-0.2								1942	1.9		2330	-0.2			
4 SU	0542	2.5	19 M	0030	-0.1	4 W	0042	-0.5	19 TH	0142	-0.1	4 W	0606	2.6	19 TH	0030	0.2
	1206	-0.1		0700	2.4		0718	2.8		0806	2.4		1224	-0.1		0648	2.3
	1800	1.8		1330	0.0		1342	-0.4		1424	-0.1		1824	2.2		1306	0.1
				1918	1.7		1936	2.2		2024	2.0					1912	2.1
5 M	0000	-0.4	20 TU	0118	-0.2	5 TH	0142	-0.7	20 F	0224	-0.1	5 TH	0036	-0.4	20 F	0118	0.1
	0636	2.7		0748	2.4		0812	2.9		0842	2.4		0700	2.7		0730	2.4
	1306	-0.2		1412	-0.1		1430	-0.5		1454	-0.2		1318	-0.3		1342	0.0
	1854	1.9		2006	1.8		2030	2.4		2100	2.1		1924	2.5		1948	2.3
6 TU	0100	-0.5	21 W	0200	-0.2	6 F	0242	-0.8	21 SA	0300	-0.2	6 F	0136	-0.6	21 SA	0200	0.0
	0736	2.8		0830	2.4		0906	2.9		0918	2.4		0754	2.9		0806	2.4
	1400	-0.4		1454	-0.2		1524	-0.7		1530	-0.2		1412	-0.4		1418	-0.1
	1954	2.1		2048	1.8		2124	2.6		2136	2.2		2018	2.7		2024	2.4
7 W	0154	-0.6	22 TH	0242	-0.2	7 SA	0336	-0.8	22 SU	0336	-0.2	7 SA	0230	-0.7	22 SU	0236	-0.1
	0830	3.0		0906	2.4		0954	2.9		0948	2.4		0848	2.9		0842	2.4
	1454	-0.5		1530	-0.2		1606	-0.7		1600	-0.2		1454	-0.6		1448	-0.1
	2048	2.2		2124	1.9		2218	2.7		2206	2.3		2106	2.9		2100	2.5
8 TH	0248	-0.7	23 F	0324	-0.2	8 SU	0430	-0.8	23 M	0412	-0.2	8 SU	0318	-0.7	23 M	0312	-0.2
	0918	3.0		0942	2.4		1042	2.8		1024	2.3		0936	2.9		0918	2.4
	1542	-0.6		1600	-0.2		1654	-0.7		1630	-0.2		1542	-0.6		1524	-0.1
	2142	2.3		2200	2.0		2306	2.7		2242	2.3		2154	3.0		2136	2.6
9 F	0348	-0.8	24 SA	0400	-0.2	9 M	0518	-0.7	24 TU	0448	-0.1	9 M	0412	-0.7	24 TU	0348	-0.2
	1012	3.0		1018	2.3		1130	2.6		1054	2.2		1018	2.7		0954	2.4
	1630	-0.7		1636	-0.2		1742	-0.6		1700	-0.2		1624	-0.6		1554	-0.1
	2236	2.4		2236	2.0		2354	2.7		2318	2.4		2242	3.0		2212	2.7
10 SA	0442*	-0.7	25 SU	0436	-0.1	10 TU	0612	-0.5	25 W	0530	-0.1	10 TU	0500	-0.5	25 W	0430	-0.1
	1100	2.9		1048	2.3		1218	2.4		1130	2.1		1106	2.6		1030	2.3
	1718	-0.6		1706	-0.2		1824	-0.5		1736	-0.1		1712	-0.5		1630	-0.1
	2330	2.5		2312	2.0					2354	2.4		2330	2.9		2248	2.7
11 SU	0536	-0.6	26 M	0512	-0.1	11 W	0048	2.6	26 TH	0612	0.0	11 W	0548	-0.3	26 TH	0506	-0.1
	1154	2.7		1124	2.2		0706	-0.3		1206	2.0		1148	2.4		1106	2.2
	1812	-0.6		1736	-0.2		1306	2.1		1812	-0.1		1754	-0.3		1706	-0.1
				2348	2.0		1918	-0.3								2330	2.6
12 M	0018	2.5	27 TU	0554	0.0	12 TH	0142	2.5	27 F	0036	2.4	12 TH	0018	2.7	27 F	0554	0.0
	0630	-0.5		1200	2.1		0806	0.0		0700	0.1		0636	-0.1		1148	2.1
	1242	2.4		1812	-0.2		1400	1.9		1248	1.9		1236	2.1		1748	0.0
	1900	-0.5					2006	-0.2		1900	-0.1		1842	-0.2			
13 TU	0118	2.4	28 W	0030	2.1	13 F	0242	2.3	28 SA	0130	2.3	13 F	0106	2.5	28 SA	0018	2.6
	0730	-0.3		0636	0.0		0906	0.1		0754	0.2		0730	0.1		0842	0.2
	1336	2.2		1236	1.9		1454	1.7		1348	1.8		1324	1.9		1236	2.0
	1948	-0.4		1848	-0.1		2100	-0.1		1954	0.0		1930	0.0		1836	0.1
14 W	0218	2.4	29 TH	0112	2.1	14 SA	0342	2.2				14 SA	0206	2.4	29 SU	0112	2.5
	0836	-0.1		0724	0.1		1012	0.2					0830	0.3		0736	0.3
	1436	2.0		1324	1.8		1600	1.6					1424	1.8		1330	1.9
	2048	-0.3		1930	-0.1		2206	0.0					2024	0.2		1942	0.1
15 TH	0318	2.3	30 F	0200	2.1	15 SU	0448	2.2				15 SU	0306	2.2	30 M	0218	2.4
	0936	0.0		0824	0.2		1118	0.3					0930	0.4		0848	0.3
	1530	1.8		1412	1.7		1706	1.6					1524	1.7		1442	1.9
	2142	-0.2		2024	-0.1		2306	0.1					2130	0.3		2054	0.1
			31 SA	0300	2.2										31 TU	0330	2.4
				0930	0.2											0954	0.3
				1518	1.7											1600	2.0
				2124	-0.1											2212	0.1

TIME MERIDIAN 75° W. 0000 IS MIDNIGHT. 1200 IS NOON.
HEIGHTS ARE RECKONED FROM THE DATUM OF SOUNDINGS ON CHARTS OF THE LOCALITY WHICH IS MEAN LOW WATER.

Figure 1.2. Sample page from Tide Tables, East Coast North and South America, Coast and Geodetic Survey, 1970.

TABLE 2.—TIDAL DIFFERENCES AND OTHER CONSTANTS

No.	PLACE	POSITION		DIFFERENCES				RANGES		Mean Tide Level
		Lat.	Long.	Time		Height		Mean	Spring	
				High water	Low water	High water	Low water			
		° ′	° ′	h. m.	h. m.	feet	feet	feet	feet	feet
	MARYLAND, Outer Coast	N.	W.	on SANDY HOOK, p.70						
				Time meridian, 75°W.						
1907	Fenwick Island Light	38 27	75 03	-0 13	-0 19	-0.9	0.0	3.7	4.5	1.8
1909	Ocean City	38 20	75 05	-0 28	-0 30	-1.2	0.0	3.4	4.1	1.7
1911	North Beach Coast Guard Station	38 12	75 09	-0 28	-0 29	-1.2	0.0	3.4	4.1	1.7
	MARYLAND and VIRGINIA									
	Chincoteague Bay									
1913	Assateague Beach, Toms Cove	37 52	75 22	+0 06	+0 16	-1.0	0.0	3.6	4.4	1.8
1915	Chincoteague Point	37 54	75 25	+0 05	+0 11	*0.57	*0.57	2.6	3.1	1.3
1917	Bogues Bay, Chincoteague Inlet	37 53	75 30	+0 38	+0 57	-1.6	0.0	3.0	3.6	1.5
1918	Wishart Point, Bogues Bay	37 53	75 30	+0 20	+0 42	-2.0	0.0	2.6	3.1	1.3
1919	Chincoteague, Chincoteague Channel	37 56	75 23	+0 40	+0 47	*0.37	*0.37	1.7	2.1	0.9
1921	Piney Island, Assateague Channel	37 56	75 21	+1 05	+1 13	*0.46	*0.46	2.1	2.5	1.0
1923	Greenbackville	38 00	75 23	+2 19	+2 48	*0.13	*0.13	0.6	0.7	0.3
1925	George Island Landing	38 02	75 22	+2 53	+3 02	*0.13	*0.13	0.6	0.7	0.3
1927	Assacorkin Island	38 04	75 19	+3 33	+3 42	*0.09	*0.09	0.4	0.5	0.2
1928	Public Landing	38 09	75 17	+4 58	+5 27	*0.09	*0.09	0.4	0.5	0.2
	VIRGINIA, Outer Coast									
1929	Gargathy Neck	37 47	75 34	+1 05	+0 56	-1.6	0.0	3.0	3.6	1.5
1931	Metomkin Inlet	37 40	75 36	+0 35	+0 12	-1.0	0.0	3.6	4.4	1.8
1932	Folly Creek, Metomkin Inlet	37 42	75 38	+0 58	+0 41	-1.3	0.0	3.3	4.0	1.7
1933	Wachapreague Inlet (inside)	37 35	75 37	+0 09	+0 03	-0.7	0.0	3.9	4.7	1.9
1935	Quinby Inlet entrance	37 28	75 40	+0 04	-0 12	-0.6	0.0	4.0	4.8	2.0
1937	The Swash, south end	37 30	75 40	+0 19	+0 14	-0.7	0.0	3.9	4.7	1.9
1939	Great Machipongo Inlet (inside)	37 24	75 43	+0 36	+0 23	-0.7	0.0	3.9	4.7	1.9
1941	Upshur Neck, south end	37 28	75 48	+0 50	+0 52	-0.2	0.0	4.4	5.3	2.2
1943	Sand Shoal Inlet (C. G. Station)	37 18	75 47	+0 08	-0 11	-0.5	0.0	4.1	4.9	2.0
1945	Ship Shoal Inlet	37 13	75 48	+0 26	+0 09	-0.6	0.0	4.0	4.8	2.0
1947	Smith Island (C. G. Station)	37 07	75 55	+0 23	+0 59	-1.1	0.0	3.5	4.2	1.7
	Chesapeake Bay, Eastern Shore			on HAMPTON ROADS, p.94						
1949	Fisherman Island	37 06	75 59	-0 47	-1 00	+0.5	0.0	3.0	3.6	1.5
1951	Kiptopeke Beach (Ferry)	37 10	75 59	-0 40	-0 35	+0.2	0.0	2.7	3.2	1.4
1953	Old Plantation Flats	37 14	76 03	-0 27	-0 15	-0.1	0.0	2.4	2.9	1.2
1955	Cape Charles Harbor	37 16	76 01	-0 18	-0 03	-0.1	0.0	2.4	2.8	1.2
1957	Nassawadox Creek	37 28	75 58	+0 56	+0 48	-0.7	0.0	1.8	2.2	0.9
1959	Occohannock Creek	37 33	75 55	+2 02	+2 32	-0.8	0.0	1.7	2.0	0.9
1961	Pungoteague Creek	37 40	75 50	+2 22	+2 37	-0.8	0.0	1.7	2.0	0.8
1963	Onancock, Onancock Creek	37 43	75 45	+2 52	+3 09	-0.7	0.0	1.8	2.2	0.9
1965	Watts Island	37 48	75 54	+2 59	+3 02	-0.9	0.0	1.6	1.9	0.8
1967	Tangier Sound Light	37 47	75 58	+2 51	+2 48	*0.64	*0.64	1.6	1.9	0.8
1969	Muddy Creek Entrance	37 51	75 40	+3 14	+3 43	-0.3	0.0	2.2	2.6	1.1
	MARYLAND									
	Chesapeake Bay, Eastern Shore									
1971	Ape Hole Creek, Pocomoke Sound	37 58	75 49	+3 24	+3 48	-0.2	0.0	2.3	2.8	1.1
	Pocomoke River									
1973	Shelltown	37 59	75 38	+3 29	+4 06	-0.1	0.0	2.4	2.9	1.2
1975	Pocomoke City	38 05	75 34	+5 46	+6 05	-0.9	0.0	1.6	2.0	0.8
1977	James Island Light	37 58	75 55	+3 51	+3 50	-0.7	0.0	1.8	2.2	0.9
1979	Crisfield, Little Annemessex River	37 59	75 52	+3 47	+3 55	-0.5	0.0	2.0	2.4	1.0
1981	Long Point, Big Annemessex River	38 03	75 48	+4 16	+4 36	-0.4	0.0	2.1	2.5	1.0
1983	Teague Creek, Manokin River	38 06	75 50	+4 35	+4 55	-0.4	0.0	2.1	2.5	1.0
1985	Ewell, Smith Island	38 00	76 02	+3 56	+4 21	*0.64	*0.64	1.6	1.9	0.8
1987	Solomons Lump Light	38 03	76 01	+4 13	+4 15	-0.8	0.0	1.7	2.0	0.8
1989	Holland Island Bar Light	38 04	76 06	+4 13	+4 20	*0.56	*0.56	1.4	1.7	0.7
1991	Sharkfin Shoal Light	38 12	75 59	+4 43	+4 56	-0.3	0.0	2.2	2.6	1.1
1993	Great Shoals Light, Monie Bay	38 13	75 53	+4 57	+5 12	-0.2	0.0	2.3	2.8	1.2

*Ratio.

Figure 1.3. Sample page from Table 2 of Tide Tables, East Coast North and South America, Coast and Geodetic Survey, 1970)

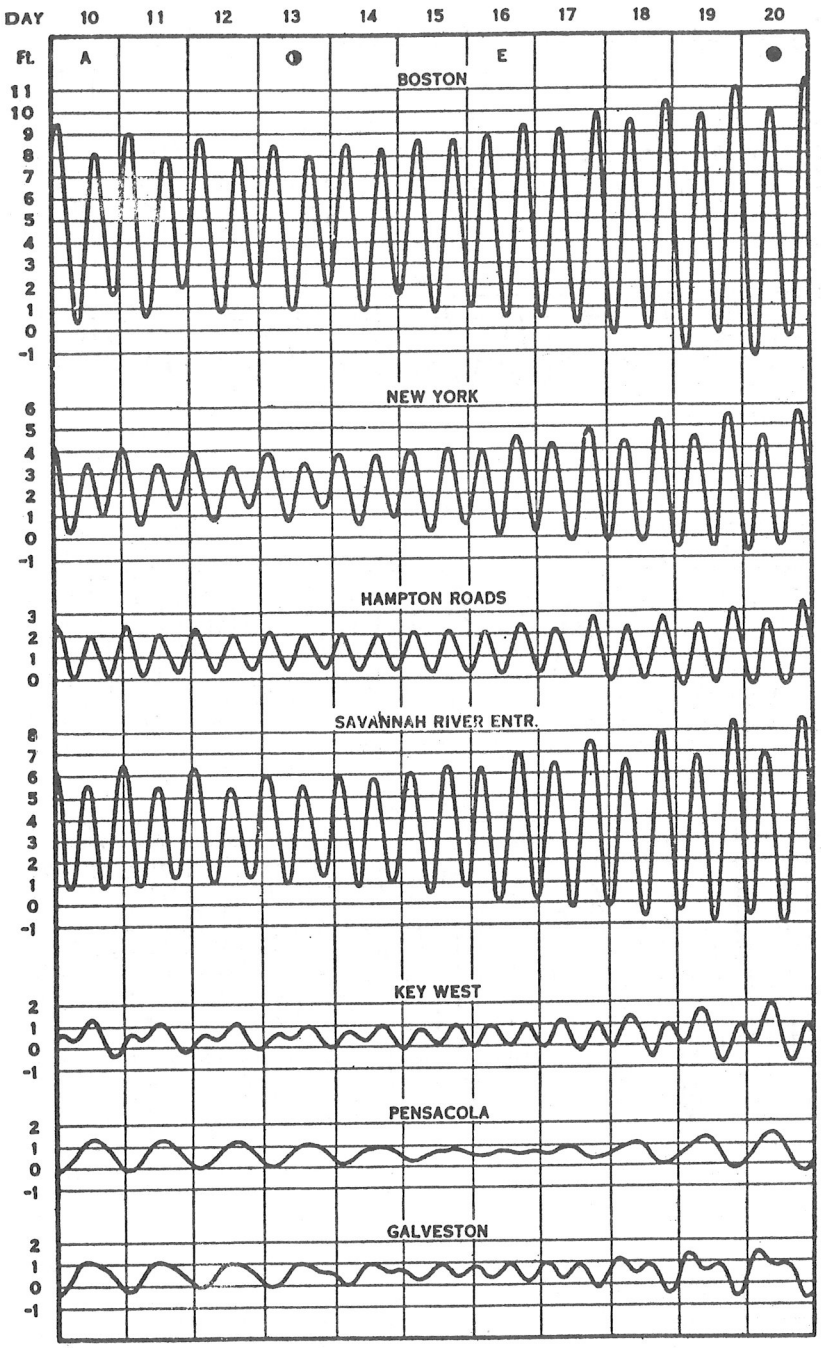

Figure 1.4. Typical tide curves for several United States East and Gulf Coasts ports. (Tide Tables, East Coast North and South America, Coast and Geodetic Survey, 1970)

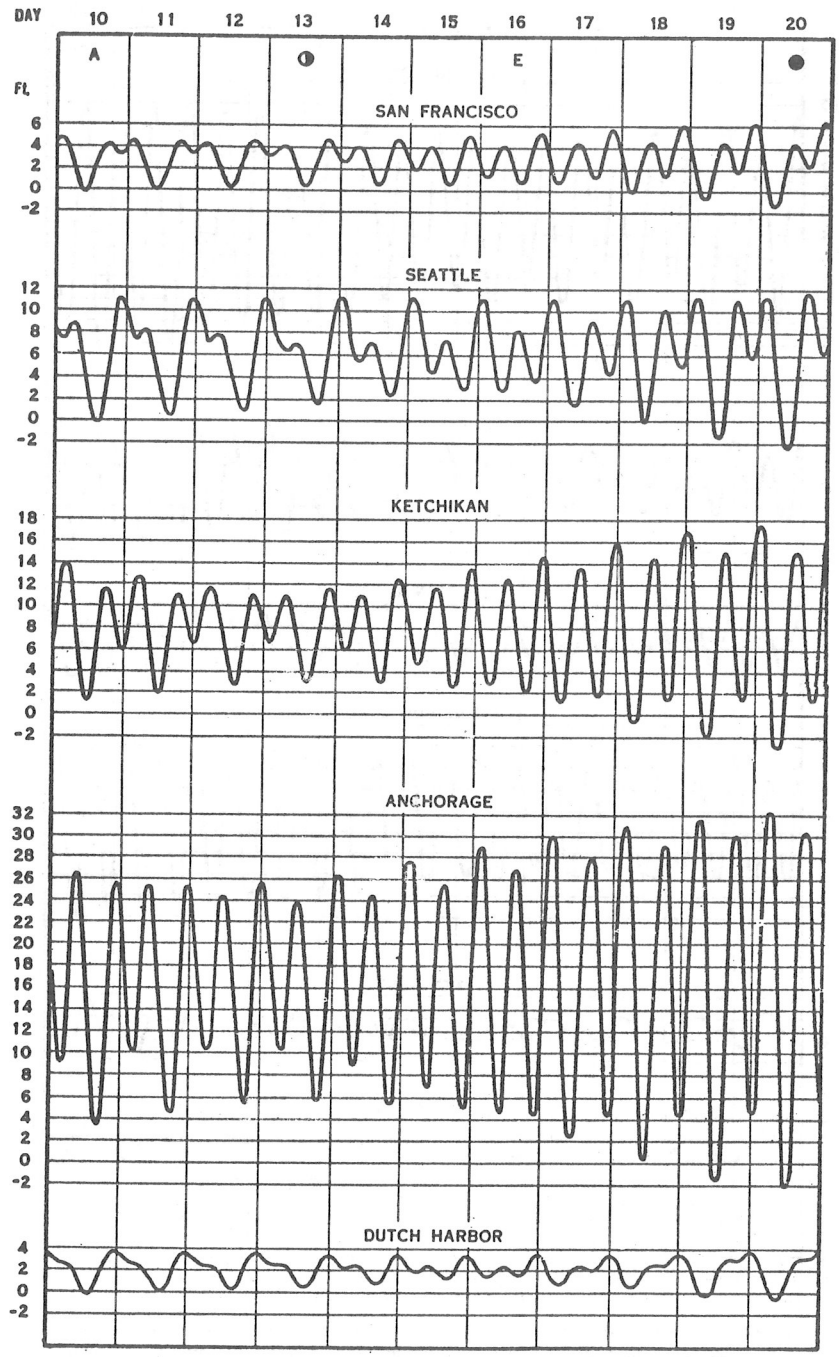

Lunar data: max. S. declination, 9th; apogee, 10th; last quarter, 13th; on equator, 16th; new moon, 20th; perigee, 22d; max. N. declination, 23d.

Figure 1.5. Typical tide curves for several United States West Coast ports. (Tide Tables, West Coast North and South America, Coast and Geodetic Survey, 1970)

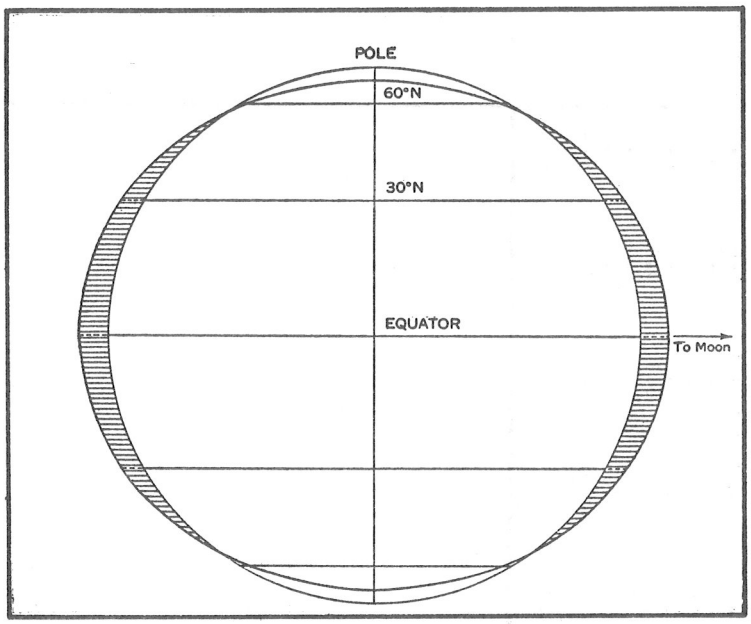

Figure 1.6. Equilibrium tide conditions with moon over the equator with the two high and low tides being of equal range with each rotation of the earth. (Schureman, 1958)

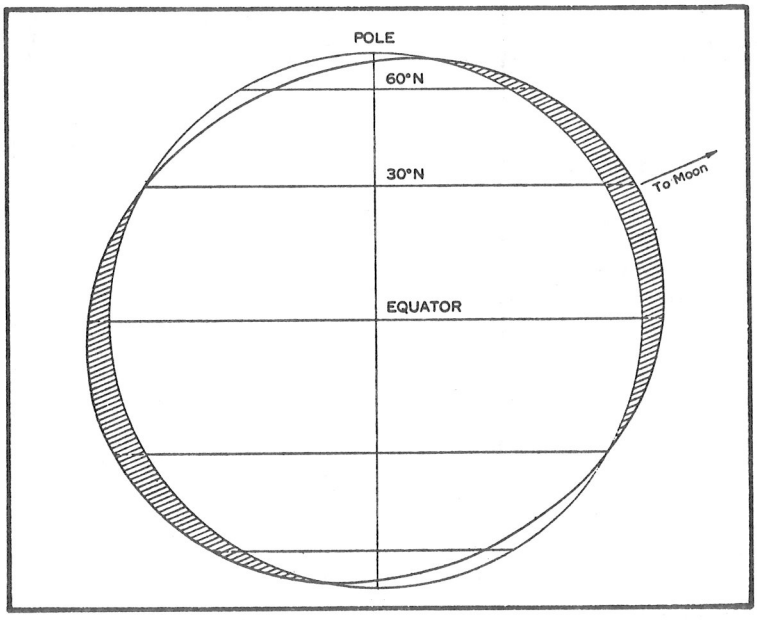

Figure 1.7. Equilibrium tide conditions with moon north of equator with the two high and low waters with each earth rotation being of different range except at the equator. (Schureman, 1958)

HAMPTON ROADS, VA. TIDE PREDICTIONS, 1968
YEAR 1968 MONTH 3 DATUM 1.25 NO. OF CONSTITUENTS 15 CHECKSUM -0.0000000

1	2.0	1.4	0.7	0.1	-0.2	-0.2	0.1	0.7	1.4	2.0	2.3	2.4
1	2.1	1.5	0.8	0.2	-0.2	-0.3	0.0	0.5	1.2	1.9	2.3	2.5
2	2.3	1.8	1.2	0.5	0.1	-0.1	-0.0	0.4	1.0	1.6	2.1	2.3
2	2.2	1.8	1.2	0.6	0.1	-0.2	-0.1	0.3	0.8	1.5	2.0	2.4
3	2.4	2.1	1.6	1.0	0.4	0.1	-0.0	0.2	0.6	1.2	1.7	2.0
3	2.1	1.9	1.5	0.9	0.4	0.0	-0.1	0.1	0.5	1.1	1.7	2.1
4	2.3	2.2	1.9	1.4	0.8	0.4	0.2	0.2	0.4	0.9	1.4	1.8
4	2.0	1.9	1.6	1.2	0.7	0.3	0.0	0.0	0.3	0.8	1.3	1.8
5	2.1	2.2	2.1	1.7	1.2	0.8	0.4	0.3	0.3	0.6	1.0	1.4
5	1.7	1.8	1.7	1.4	1.0	0.6	0.3	0.1	0.2	0.5	1.0	1.5
6	1.9	2.1	2.2	2.0	1.6	1.2	0.7	0.5	0.4	0.5	0.7	1.1
6	1.4	1.7	1.7	1.6	1.3	0.9	0.6	0.3	0.2	0.3	0.6	1.1
7	1.5	1.9	2.1	2.1	1.9	1.5	1.1	0.8	0.5	0.4	0.5	0.8
7	1.1	1.4	1.6	1.6	1.5	1.2	0.9	0.6	0.3	0.3	0.4	0.7
8	1.1	1.5	1.9	2.1	2.1	1.9	1.6	1.2	0.8	0.5	0.4	0.5
8	0.7	1.1	1.4	1.6	1.6	1.5	1.3	0.9	0.6	0.3	0.3	0.4
9	0.7	1.1	1.6	1.9	2.1	2.2	2.0	1.6	1.2	0.7	0.5	0.3
9	0.4	0.7	1.0	1.4	1.6	1.7	1.6	1.3	1.0	0.6	0.3	0.2
10	0.3	0.6	1.1	1.6	2.0	2.3	2.3	2.0	1.6	1.1	0.7	0.3
10	0.2	0.3	0.7	1.1	1.5	1.8	1.9	1.8	1.4	1.0	0.5	0.2

HAMPTON ROADS, VA. TIDE PREDICTIONS, 1968
YEAR 1968 MONTH 3 DATUM 1.25 NO. OF CONSTITUENTS 15 CHECKSUM -0.0000000

TIMES AND HEIGHTS OF HIGH AND LOW WATERS

DAY	TIME	HT.	TIME	HT.	TIME	HT.	TIME	HT.	TIME	HT.	TIME	HT.
1	430	-0.3	1036	2.4	1642	-0.3	2300	2.5				
2	506	-0.2	1112	2.3	1718	-0.2	2336	2.4				
3	548	0.0	1142	2.1	1748	-0.1						
4	12	2.3	624	0.1	1218	2.0	1830	0.0				
5	54	2.2	706	0.3	1300	1.8	1906	0.1				
6	136	2.2	800	0.4	1348	1.7	1954	0.2				
7	230	2.1	854	0.4	1448	1.6	2048	0.3				
8	330	2.1	1000	0.4	1548	1.6	2154	0.3				
9	430	2.2	1100	0.3	1654	1.7	2300	0.2				
10	530	2.3	1200	0.2	1754	1.9						

Figure 1.8. Samples of the printed output of the program. These printouts show (above) the calculated hourly tide and (below) the times and heights of high and low waters for Hampton Roads, Va. for March 1 - 10, 1968. (Pore and Cummings, 1967)

II. EXTRATROPICAL STORM SURGE

Introduction

There are sections of the United States Coast where the highest tides of record have been produced by extratropical storms, even though the abnormal tide levels caused by extratropical storms are usually not as great as those caused by hurricanes. Certainly the frequency of occurrence of extratropical storm surges is greater than that of hurricane storm surges.

The definition of storm surge is the algebraic difference between the observed tide and the normal astronomical tide. Figure 2.1 illustrates this definition with a two-day length of record. Here the observed tide is shown by the upper solid curve, the normal astronomical tide or predicted tide by the dashed line and the storm surge by the lower curve.

Generation of Storm Surge

The principal factors involved in the generation and modification of the extratropical storm surge are:

1. The rise of water caused by the action of the wind stress on the water surface which can be thought to consist of two components. One component is the set-up of water by the onshore wind in which the slope of the water surface is directly proportional to the wind stress and inversely proportional to the water depth. The other component is the effect of wind parallel to shore which generates a current parallel to shore. The effect of the earth's rotation is to have water piled up along the shore if the shore is to the right of the current. The effects of these two wind set-up components are illustrated in figures 2.2 and 2.3 from Harris (1963a);

2. The reduction of atmospheric pressure, generally called the inverted barometer effect, which causes an increase in sea level in areas of low pressure;

3. The transport of water by waves and swells in the shallow water area near shore which is illustrated in figure 2.4. Harris (1963a) reports agreement by various investigators, that the slope of the water surface due to the waves is directly proportional to the gradient of variance in water elevation caused by waves (which is proportional to the wave height squared), and inversely proportional to the depth. This is illustrated in figure 2.4.

4. The modifying effects of coastline configuration and the bathymetry (bottom contours).

Importance of Time of Occurrence

The effect of the time of occurrence of the storm surge with respect to the stage of the normal astronomical tide is shown in figure 2.5. Here two identical storm surges are combined with different phases of the normal tide, one occurring at normal high tide and the other at normal low tide, with the one at high tide resulting in a higher actual tide. The time of occurrence of the storm surge with respect to the normal tide can mean the difference between serious and minor flooding.

Variations in Maximum Water Levels

Of special importance in forecasting the water level is the fact that there is considerable variation in the maximum water level height within a very short distance. This was known to be true in hurricane situations and was shown by a dense set of data for the first time for an extratropical storm after the destructive storm of March of 1962. Figure 2.6 shows water levels established by high water marks measured by the U.S. Army Corps of Engineers, Coast and Geodetic Survey, U.S. Geological Survey and others after the storm. Variations of several feet in a distance of several miles are indicated. Most of the recording tide gages are located in harbors where they are protected from the waves reaching the open coast and therefore do not record water levels as high as those indicated by the high water marks.

Figure 2.7 shows water level data for four selected tide gage locations during the period of March 5-8, 1962. Curves are drawn for the observed tide level, the predicted tide and the storm surge. The observed tide was considerably above normal during five succeeding high tides.

Objective Forecasting Techniques

Hustead (1955) developed an empirical method of forecasting the meteorologically produced tide departures from normal astronomical tide for the Norfolk, Virginia tidal basin for northeast winds. This method is applicable to storms moving northward off the Virginia Capes, east of Cape Henry and Cape Charles. Figure 2.8 shows the tide departure as a function of mean wind movement in a two hour period. Instructions for using the method, as given by Hustead (1955) are: "In practice, forecast the wind movement expected on triple register for the two-hour period prior to hurricane or coastal wave center reaching latitude 37°N. Then divide this forecast wind value by two. With this value located along the abscissa, read the ordinate value of tidal departure on curve. This tidal departure value is then added to the normal tidal value predicted for the USC&GS Sewells Point gage for the forecast time of the storm center to reach 37°N. This tidal height and time is the forecast occurrence for Sewells Point and is then modified for any particular point in the tidal basin by using the time and height differences given in "Table 2 - Tidal Differences and Ranges" as published in TIDE TABLES EAST COAST, NORTH AND SOUTH AMERICA (Including Greenland), U.S. Department of Commerce, Coast and Geodetic Survey."

Tancreto (1958) reasoned that since the Sverdrup-Munk-Bretschneider method of forecasting the height of significant wind-waves represents the transfer of energy from the wind to the waves, there should be some relationship between the forecast wave height and the magnitude of the storm surge. Based on 45 storms the following regression equation, with a correlation coefficient of 0.88, relating the maximum height of the extratropical storm surge (S_h) to the forecast significant wave height (H) was derived for Boston:

$$S_h = 0.24 + 0.11\ H$$

where both S_h and H are expressed in feet.

Figure 2.9 is a scatter diagram showing the points on which this relationship was established along with some independent cases. This equation is based on and is applicable to storms with strong winds with an easterly component along and off the southern New England Coast. Stratification of the cases into two classes, those with east wind components and those with northeast wind components did not significantly improve the relationship.

Miller (1957) studied the effect of geostrophic wind over an offshore circular area 300 miles in diameter on the Atlantic City water level during a six-month period. He concluded that the surge is nearly proportional to the wind speed, that in general there is a time lag of about twelve hours between the wind and the surge, and that maximum setup occurs with east-northeast winds.

The effect of extratropical storms on the tide at several Atlantic Coast stations was studied by Donn (1958), who generally agreed with Miller that the relationship between wind speed and surge seems to be linear, that there is a time lag between the wind and the storm surge.

The principal differences and similarities between the dynamic and statistical numerical methods of storm surge computations have been discussed by Harris (1962). In the dynamic method the numerical integration of the hydrodynamic equations is carried out to reveal information about the physical processes involved even though a practical prediction scheme may not be determined. The statistical approach, although not designed to disclose the physical processes to the extent of the dynamic method, is likely to make more efficient use of the available observational data and lead to relatively simple, easy to use prediction schemes such as a set of regression equations. It was shown that a solution for the linearized hydrodynamic equations for storm surges can be obtained as an integral of the product of the atmospheric forcing function and an influence function which approaches zero with increasing time lags. This solution can be approximated for a given time as the weighted sum of the atmospheric forces during a recent time period. The weighting factors can then be determined as regression coefficients in a multiple correlation problem.

This approach has been followed by Pore (1964a, 1964b, 1965) in the development of techniques for several East Coast ports. The regression equations were determined with use of the multiple correlation screening procedure. A detailed description of the screening procedure is given by Miller (1958). The manner in which the predictors were screened is shown here:

1. $SS = A_1 + B_1X_1$

2. $SS = A_2 + B_2X_1 + C_1X_2$

3. $SS = A_3 + B_3X_1 + C_2X_2 + D_1X_3$

.
.
.

n. $SS = A_n + B_nx_1 + C_{n-1}x_2 + \ldots + nx_n$

where SS is storm surge, A_1, A_2, A_3, etc. are constants X_1, X_2, X_3, etc. are predictors, and B_1, B_2, C_1, C_2, etc. are regression coefficients.

The procedure is to first select the best single predictor (X_1) for regression equation 1. The second regression equation contains the first predictor (X_1) and the predictor (X_2) that contributes most to reducing the residual after the first predictor is considered. This process is continued until some limiting value of additional variance that is explained by additional predictors is reached.

This method has been used to develop techniques for Atlantic City, Breakwater Harbor, Norfolk, and Baltimore. A brief description of the results for each of these locations will be given.

In the Atlantic City study (Pore, 1964a), the following variables were considered with the screening process as predictors of the Atlantic City storm surge:

Onshore wind component, defined to be positive from the southeast, at Nantucket, Atlantic City, and Norfolk;

Alongshore wind component, defined to be positive from the northeast, at Nantucket, Atlantic City, and Norfolk;

Atmospheric pressure at Nantucket, Atlantic City, and Norfolk.

The location of these stations and the definitions of the wind components are shown in figure 2.10. These predictors were considered with various time lags to account for the lag of the ocean response to the atmospheric forces. The wind components were considered with time lags from 0 to 22 hours at 2 hour intervals and the pressure was evaluated with lags of 0, 3, 6, 9, 12, and 18 hours.

The components of the wind speed squared were experimented with and were not found to be more useful predictors than the components of wind speed. The reason for this may be that the method is essentially an interpolation procedure in which the continuous weather conditions of a storm surge generating area are represented by hourly observations at three points. In this system, whenever an observation is not wholly representative of the surge generating area the error will be less amplified in the components of wind speed than in the components of wind speed squared.

Several correlation screening runs were made considering various minimum time lags and after subjective evaluation the following regression equation was given:

$$SS_{ACY} = 10.60 + 0.36\ (p_{-6} - 1000)_{ACK} - 0.69\ (P_{-6} - 1000)_{ORF}$$
$$+ 0.24\ (v_{-6} + v_{-18})_{ACK} - 0.14(u_{-10})_{ORF}$$

Where SS is storm surge in tenths of feet,

p is station pressure in millibars,

v is alongshore component of wind in knots,

u is onshore component of wind in knots,

and the time lag in hours and the station identification are indicated by subscripts. The correlation coefficient of this equation is 0.90 and the root mean square error is 0.5 feet on both the dependent data and independent data.

Tests of this equation on the eighteen storms of the dependent data are shown in figure 2.11. Tests on thirteen independent storms are shown in figure 2.12.

Comparison of storm surge curves for Breakwater Harbor, Delaware and Atlantic City showed that the same storms generate significant storm surges at both stations. For that reason an empirical study (Pore, 1964b) was done for the Breakwater storm surge using data from the same storm periods that were used in the Atlantic City study. The variables considered as predictors were also the same and are illustrated in figure 2.10.

The prediction equation which was considered is:

$$SS_{BWH} = 11.57 - 0.98\ (p_{-6} - 1000)_{ORF} + 0.24\ (v_{-12})_{ACK}$$

$$+ 0.56\ (P_{-6} - 1000)_{ACY} + 0.21\ (v_{-6})_{ACY} + 0.17\ (v_{-24})_{ACK}$$

where the units, station notations, and time lags are similar to those used in the Atlantic City equation above.

Figures 2.13 and 2.14 show the application of this equation to the dependent and independent data respectively. In these figures the calculations with the above equation are shown by the light solid line identified as "short equation" in the legend.

A similar study was made for Chesapeake Bay (Pore, 1965) in which predictor equations were derived for storm surge at Hampton Roads and Baltimore. Meteorological data used as predictors are from Baltimore, Patuxent River, and Norfolk. Figure 2.15 shows the locations of the predictor stations, the tide gage locations, and the definitions of the wind components.

The predictor equation for Baltimore has a correlation coefficient of 0.76 and is:

$$SS_{BAL} = 4.82 - 0.40\ (v_{-12})_{NHK} + 0.43\ (SS_{-18})_{HR} - 0.29(v_{-12})_{ORF}$$

$$+ 0.14\ (u_{-12})_{BAL} + 0.27\ (SS_{-24})_{HR} + 0.16(u_{-12})_{ORF}$$

where the units and station identification are similar to the earlier equations. The importance of the storm surge at Hampton Roads prior to the storm surge at Baltimore is shown here by the Hampton Roads storm surge terms.

The similar equation for Hampton Roads storm surge has a correlation coefficient of 0.84 and is:

$$SS_{HR} = 11.02 + 0.27(v_{-6})_{ORF} + 0.07(u_{-12})_{BAL} - 1.22(p_{-6} - 1000)_{ORF}$$

$$+ 1.06(P_{-6} - 1000)_{BAL} + 0.37(SS_{-6})_{BAL} + 0.21(v_{-12})_{NHK}$$

Tests of the equations for both Baltimore and Hampton Roads are shown in figures 2.16 and 2.17 for the developmental data and in figure 2.18 for the independent data.

An extratropical storm surge forecasting technique is being developed which will be more receptive to the meteorological forecasts produced by the numerical models of the National Meteorological Center (NMC). Changes in the new technique are that meteorological data will only be used at six hour intervals instead of one hour intervals and that input data will be only from NMC standard grid points instead of from fixed land stations.

A feasibility study was carried out using Atlantic City data. The same storm periods used in the development of the earlier technique, based on onshore and alongshore wind components and pressure, were used to develop the new technique. Comparison of the test results between the two techniques shows the method using grid point data at six hour intervals to be promising. A description of the development follows:

The wind in the storm surge generating area of importance to Atlantic City is dependent on the sea level pressure at the 35 NMC points shown in figure 2.19. The sea level pressures at these points with time lags of 0 to 24 hours were considered by the statistical screening procedure. The following equation with a correlation coefficient of 0.91 was obtained for testing:

$$SS_{ACY} = 23.08 + 0.09\ (p_{45} - 900)_0 + 0.47\ (p_1 - 900)_{-12}$$

$$-0.35(p_{12} - 900)_{-6} + 0.39\ (p_9 - 900)_{-6} - 0.93(p_{34} - 900)_0$$

$$-0.16(p_{45} - 900)_{-24} + 0.32(p_{21} - 900)_0$$

where SS_{ACY} is the Atlantic City storm surge in tenths of feet, and p is the sea level pressure in millibars. The identification of the grid points is given as the subscript of p and corresponds to the point location of figure 2.20. The time lag in hours for each pressure term is given as the subscript of the term and is equal to 0, 6, 12, or 24 hours.

The application of this equation to the developmental data is shown in figure 2.21 and to the independent data in figure 2.22.

It is planned to develop similar regression equations for several other locations along the East Coast from Cape Hatteras through New England. Once these are developed it is hoped that they can be used operationally at NMC by direct utilization of the NMC Meteorological prognoses by computer, with the storm surge forecasts transmitted on an appropriate teletype circuit. This type of objective storm surge forecast will not be the final forecast for a community or locality but rather the basic value around which local forecasts would be made. This is so because such a system gives an estimate for the tide gage locations for which it was developed and because of variations in tide height within a short distance during storm conditions.

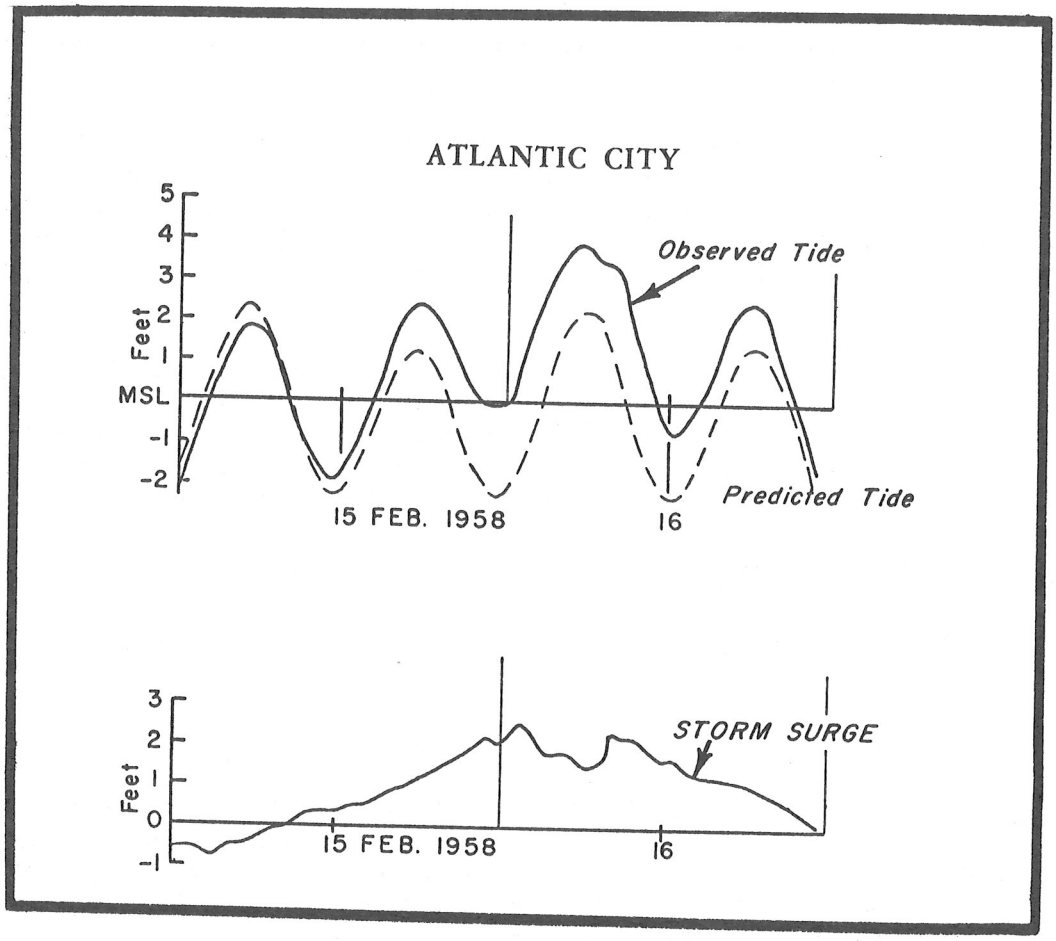

Figure 2.1. Example of Atlantic City tide data showing the observed tide, the predicted astronomical tide and the storm surge. (Pore, 1964a)

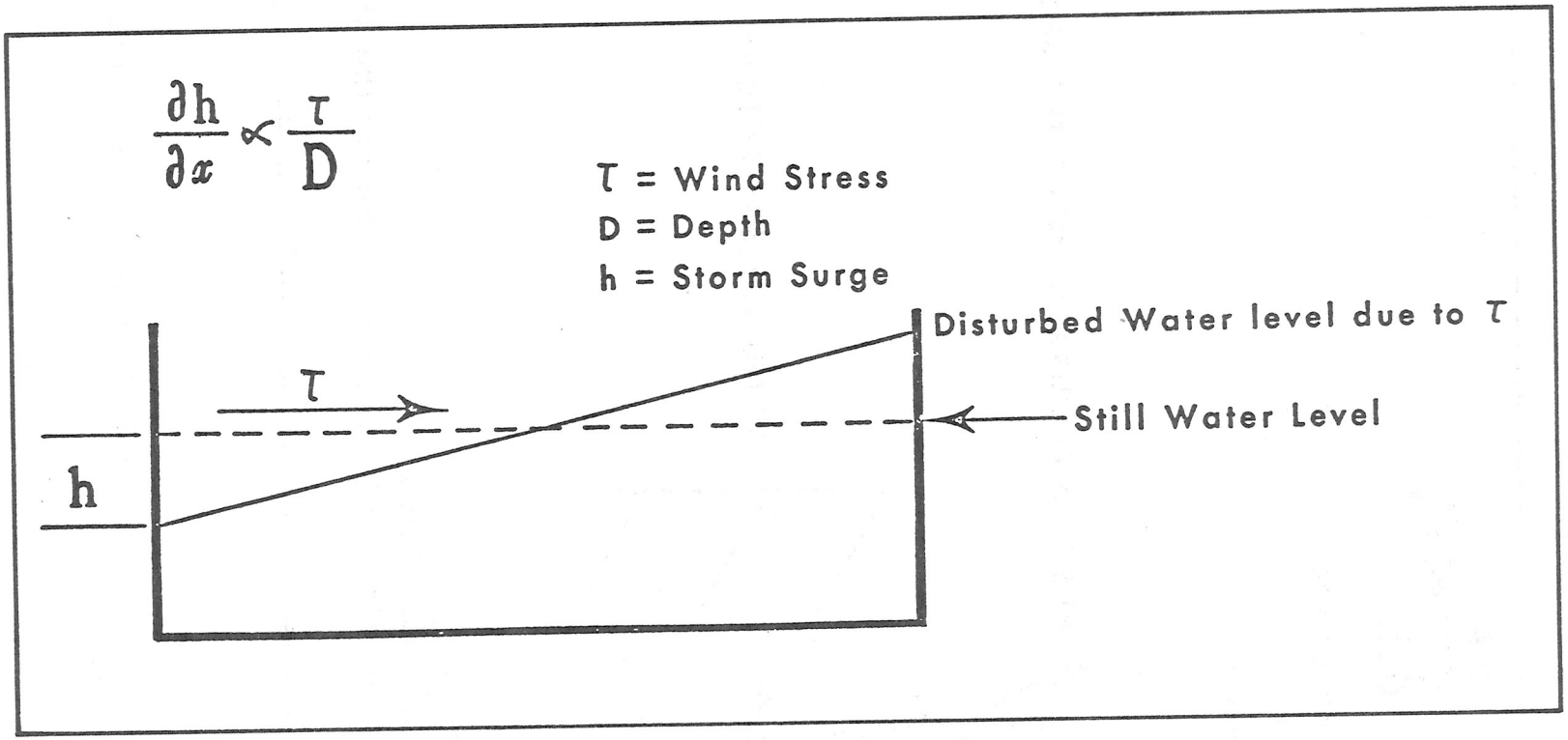

Figure 2.2. Schematic illustration of the effect of an onshore wind on water level. (Harris, 1963a)

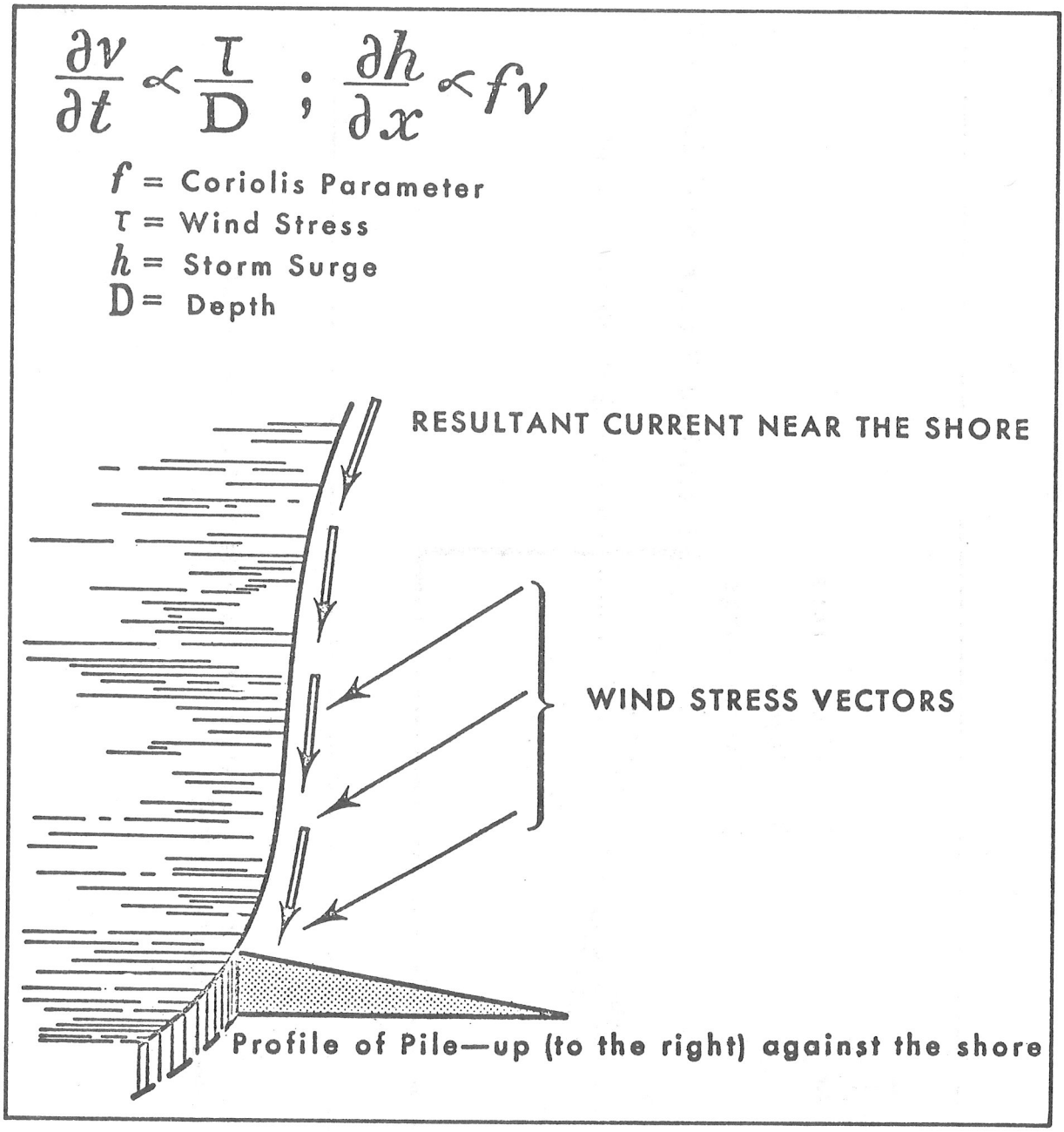

Figure 2.3. Schematic illustration of the effect of an oblique wind on water level. (Harris, 1963a)

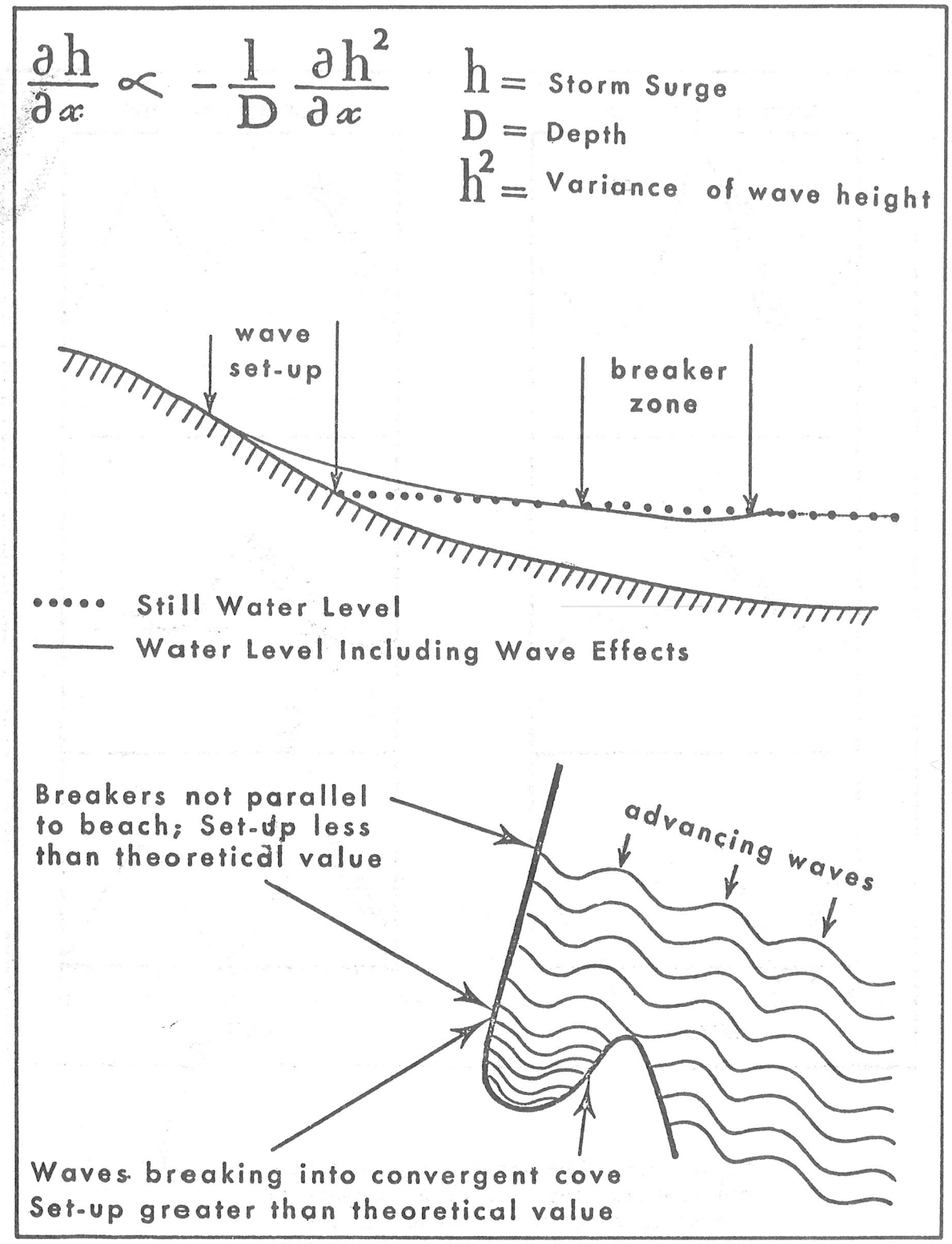

Figure 2.4. Schematic illustration of wave set-up in a vertical plane (above) and in a horizontal plane (below). (Harris, 1963a)

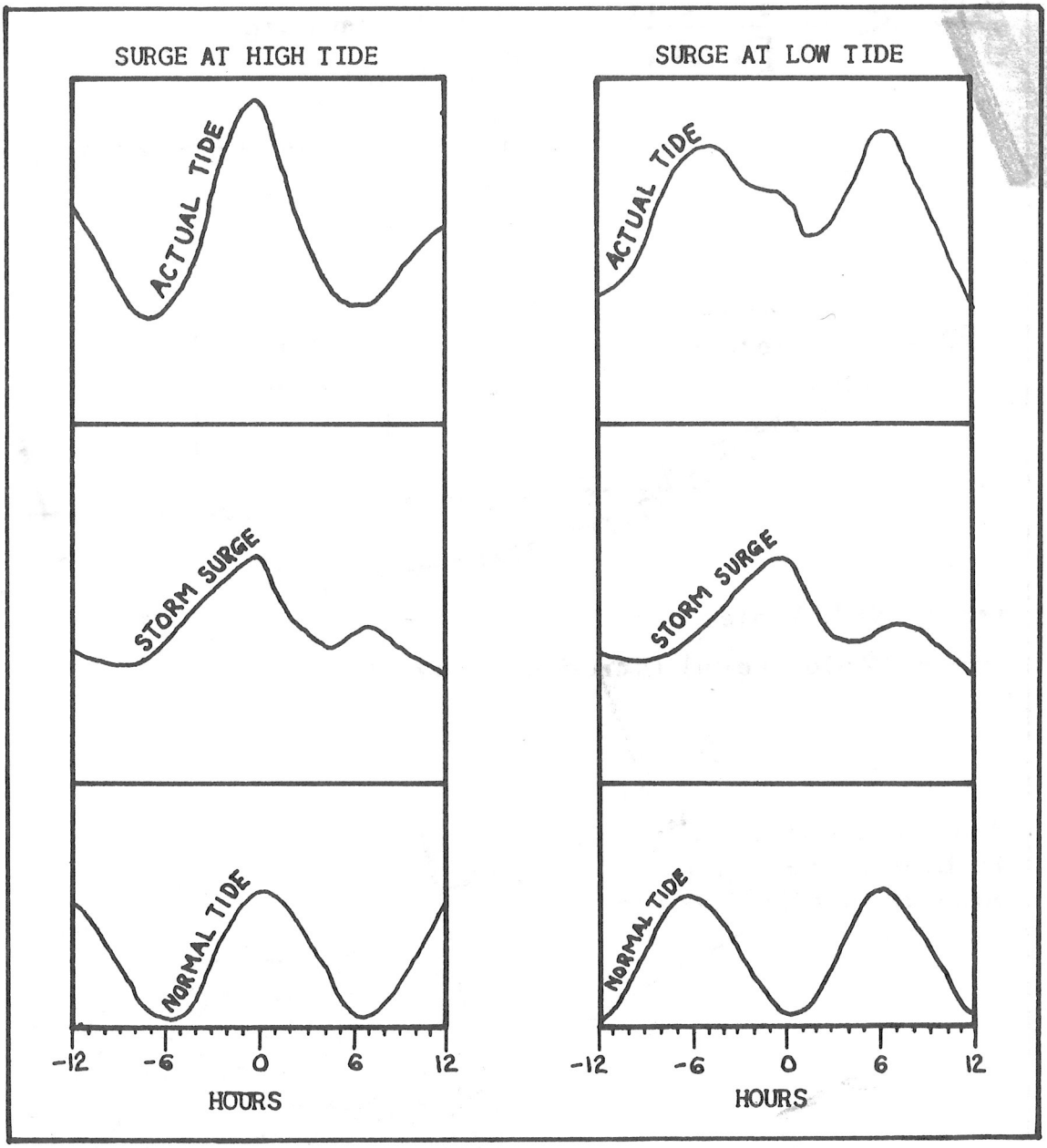

Figure 2.5. The actual tide and its components. The time of occurrence of the storm surge with respect to the normal tide is important in determining the height of the actual tide. (Pore, 1961)

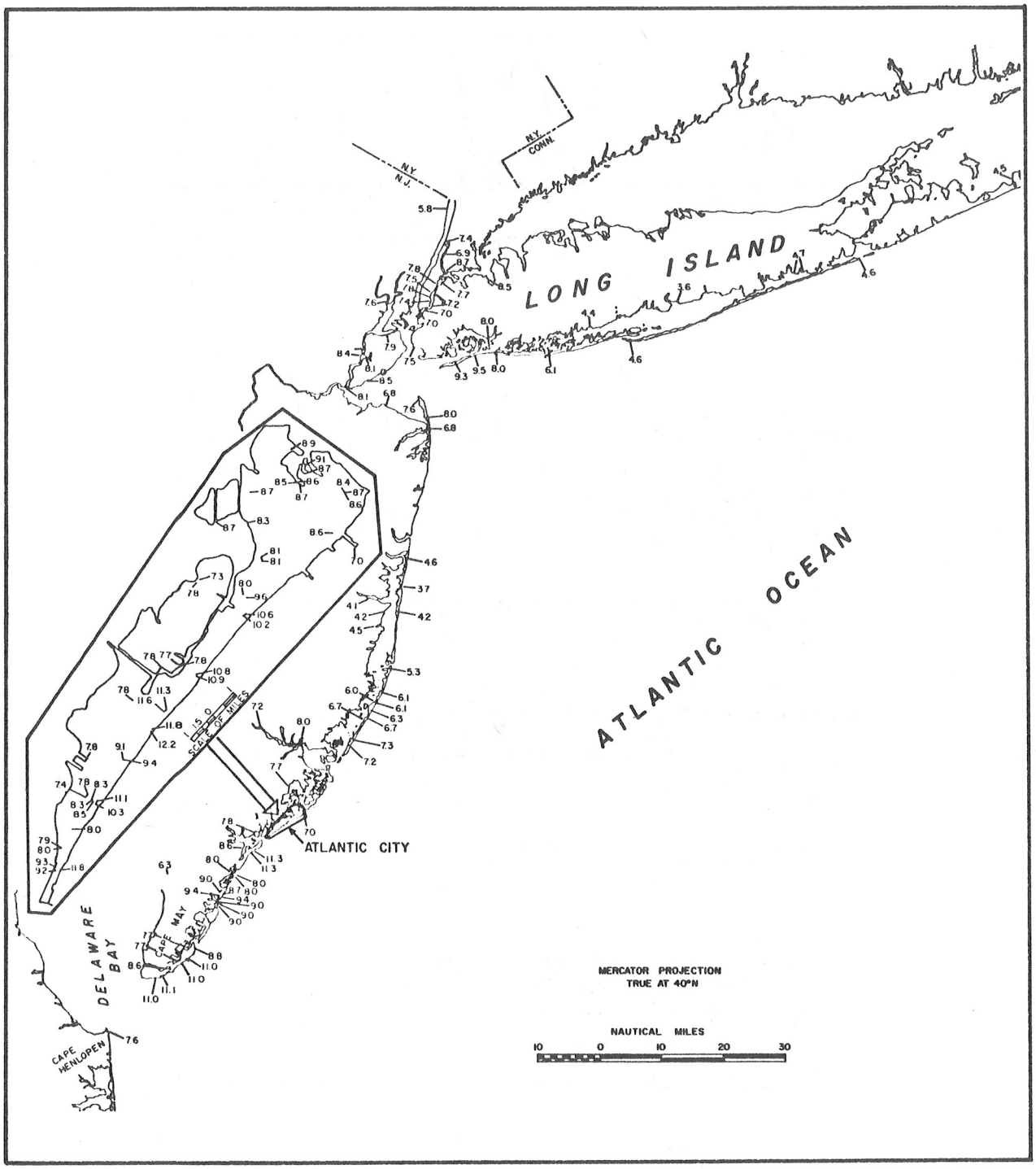

Figure 2.6. High water elevations for the early March storm, 1962. (Harris, 1963a)

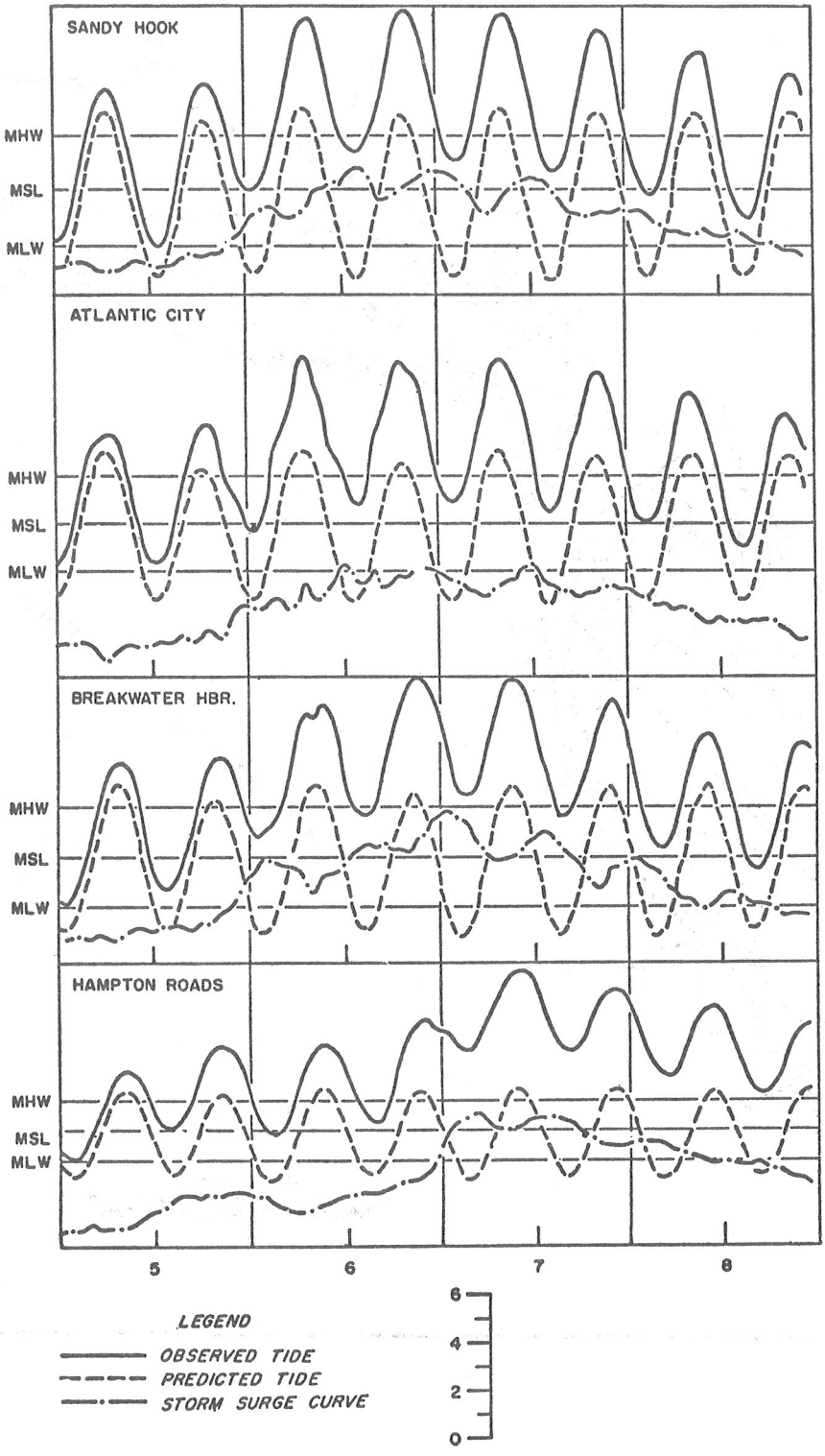

Figure 2.7. Observed tide, predicted tide and storm surge, for selected stations, March 5-8, 1962. (Harris, 1963a)

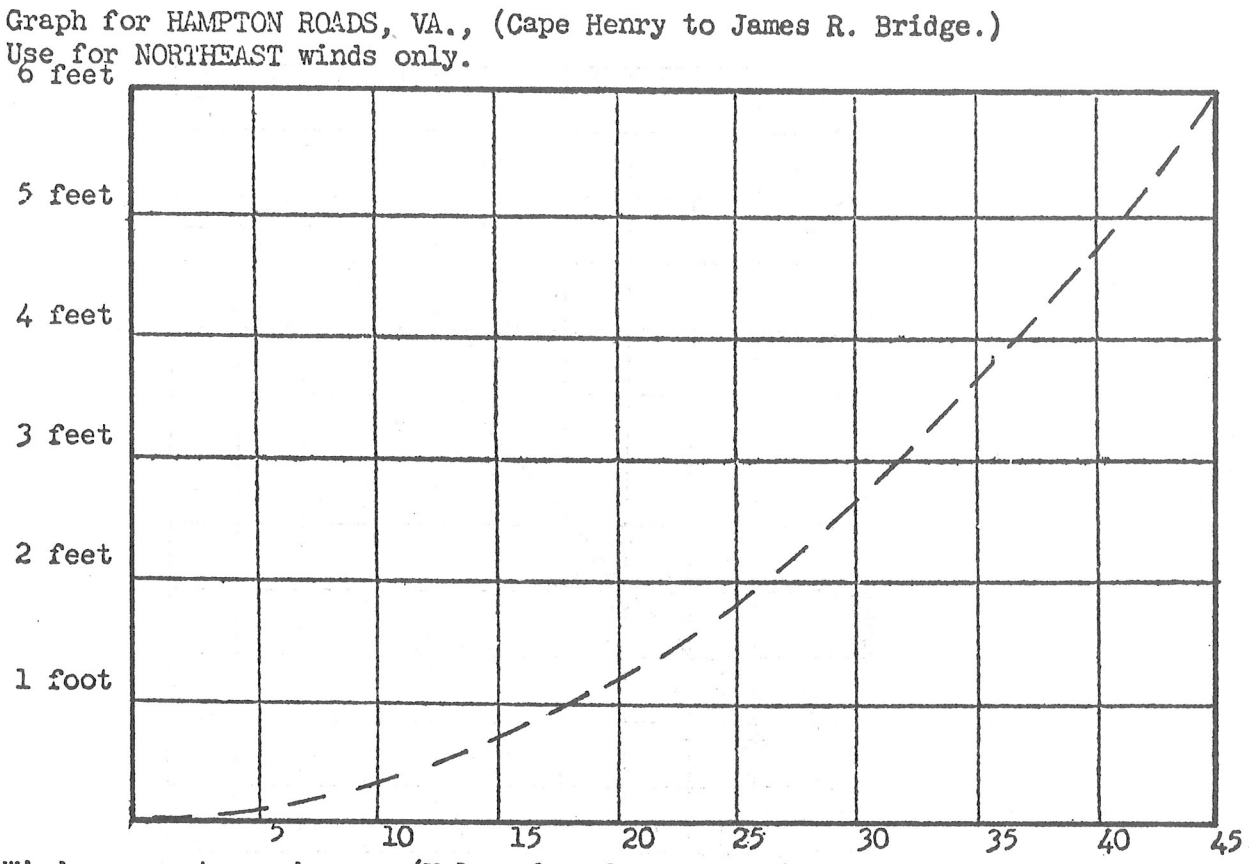

Figure 2.8. Graph showing relationship of storm surge at Hampton Roads, Va. to two-hour wind movement for northeast winds at Norfolk, Va. (Hustead, 1955)

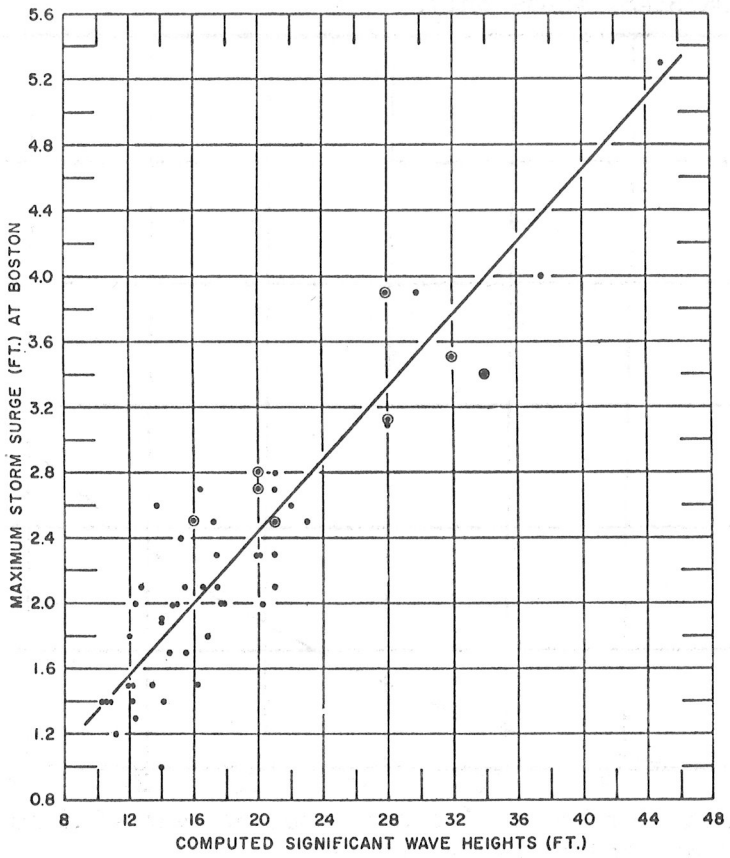

Figure 2.9. The maximum storm surge at Boston as a function of the computed offshore wave heights. The dependent data are plotted as dots and the independent as encircled dots. (Tancreto, 1958)

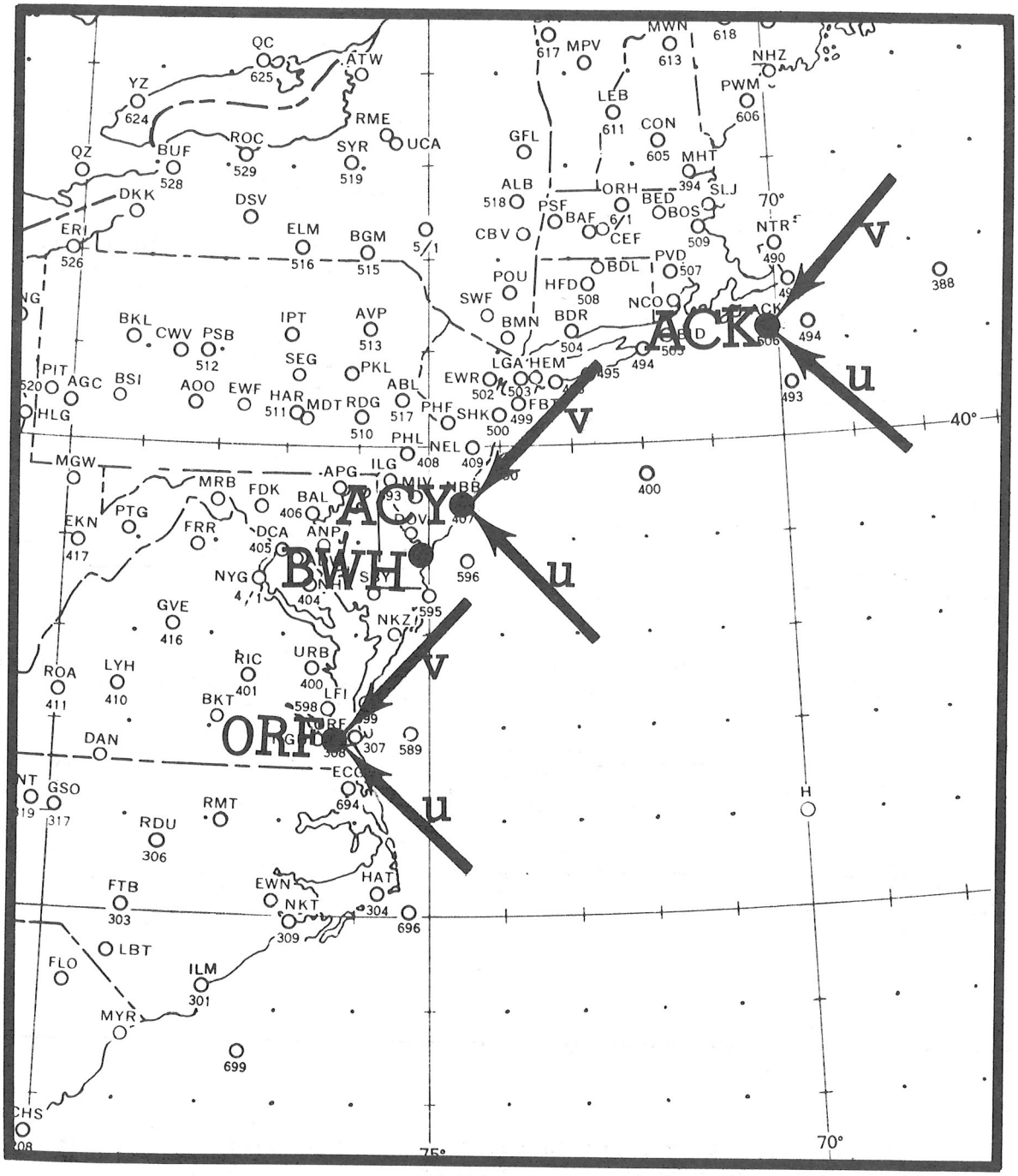

Figure 2.10. Station locations and definitions of the onshore (u) and the alongshore (v) wind components. Station abbreviations are ACK for Nantucket, Mass.; ACY for Atlantic City, N. J.; BWH for Breakwater Harbor, Del.; and ORF for Norfolk, Va. (Pore, 1964b)

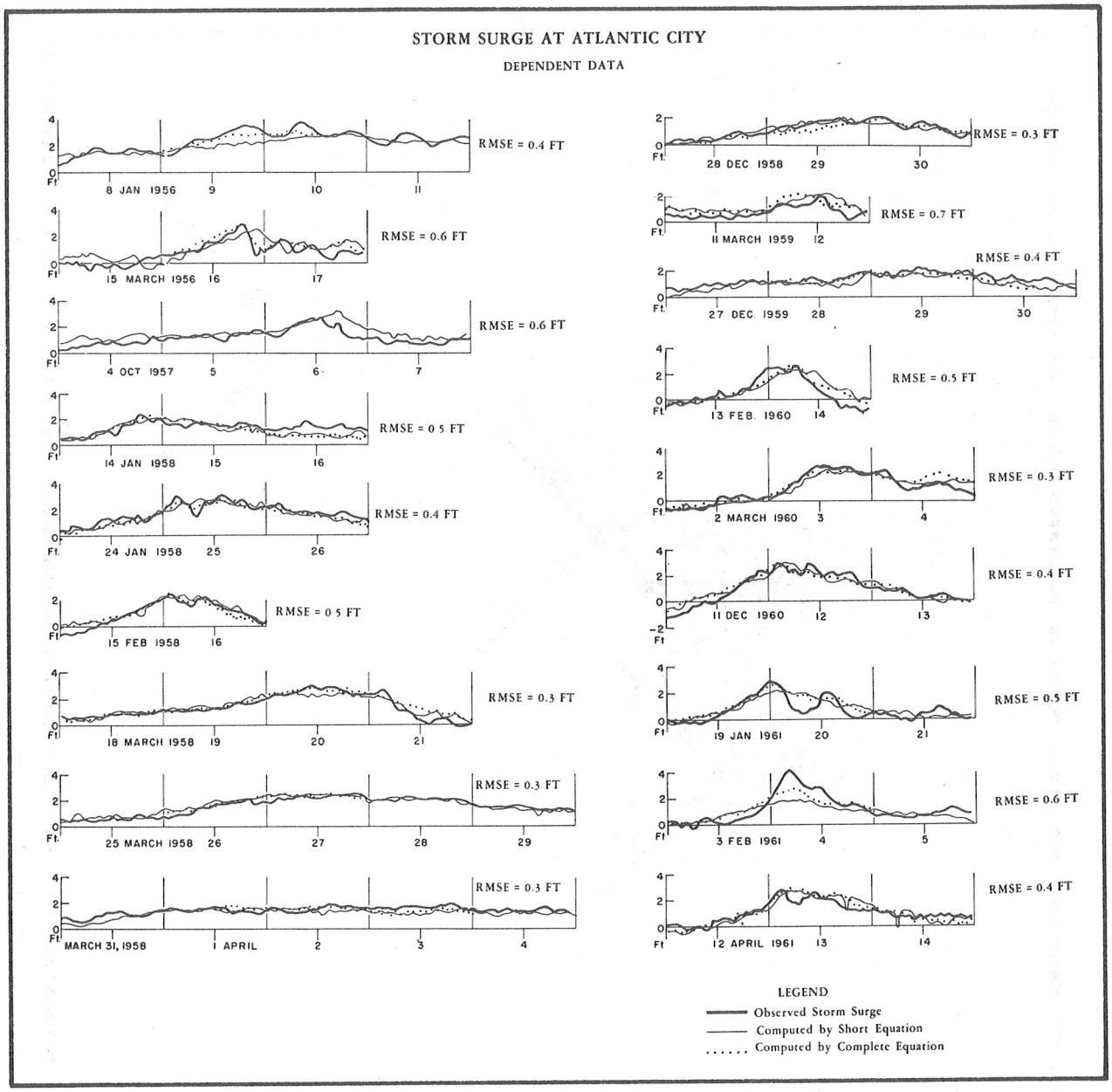

Figure 2.11. Storm surges and calculations of dependent cases. The date for each day is placed at the noon position. The light solid lines show the calculations by the five predictor equation given in the text. The dotted lines show the calculations by a 90 term prediction equation. The root mean square error shown for each storm is for the five predictor equation. The over-all error of the dependent cases is 0.5 feet. (Pore, 1964a)

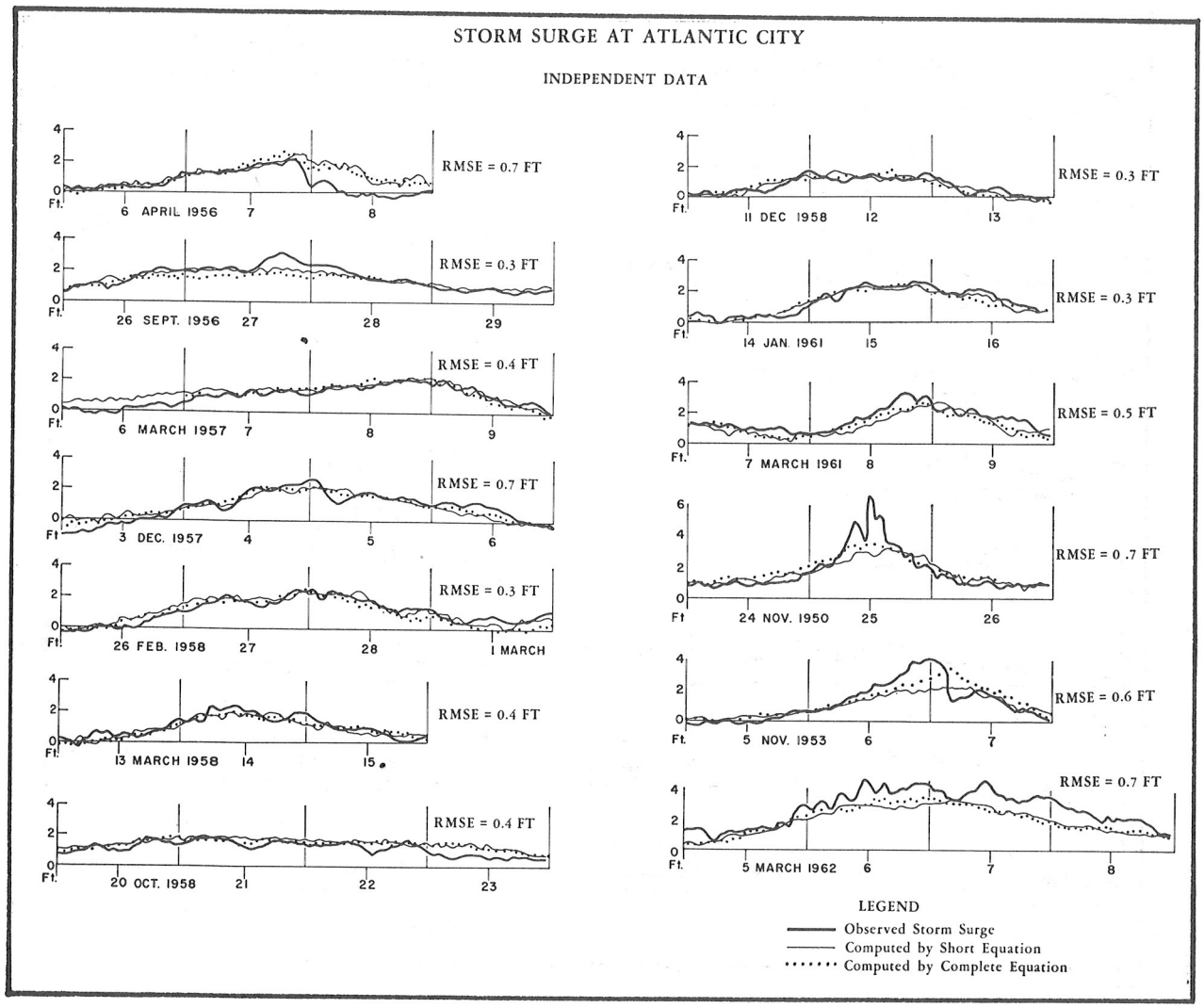

Figure 2.12. Storm surges and calculations of the independent cases. The date for each day is placed at the noon position. The light solid lines show the calculations by the five predictor equation given in the text. The dotted lines show the calculations by a 90 term equation. The root mean square error shown for each storm is for the five predictor equation. The overall rms error of the independent cases is 0.5 ft. (Pore, 1964a)

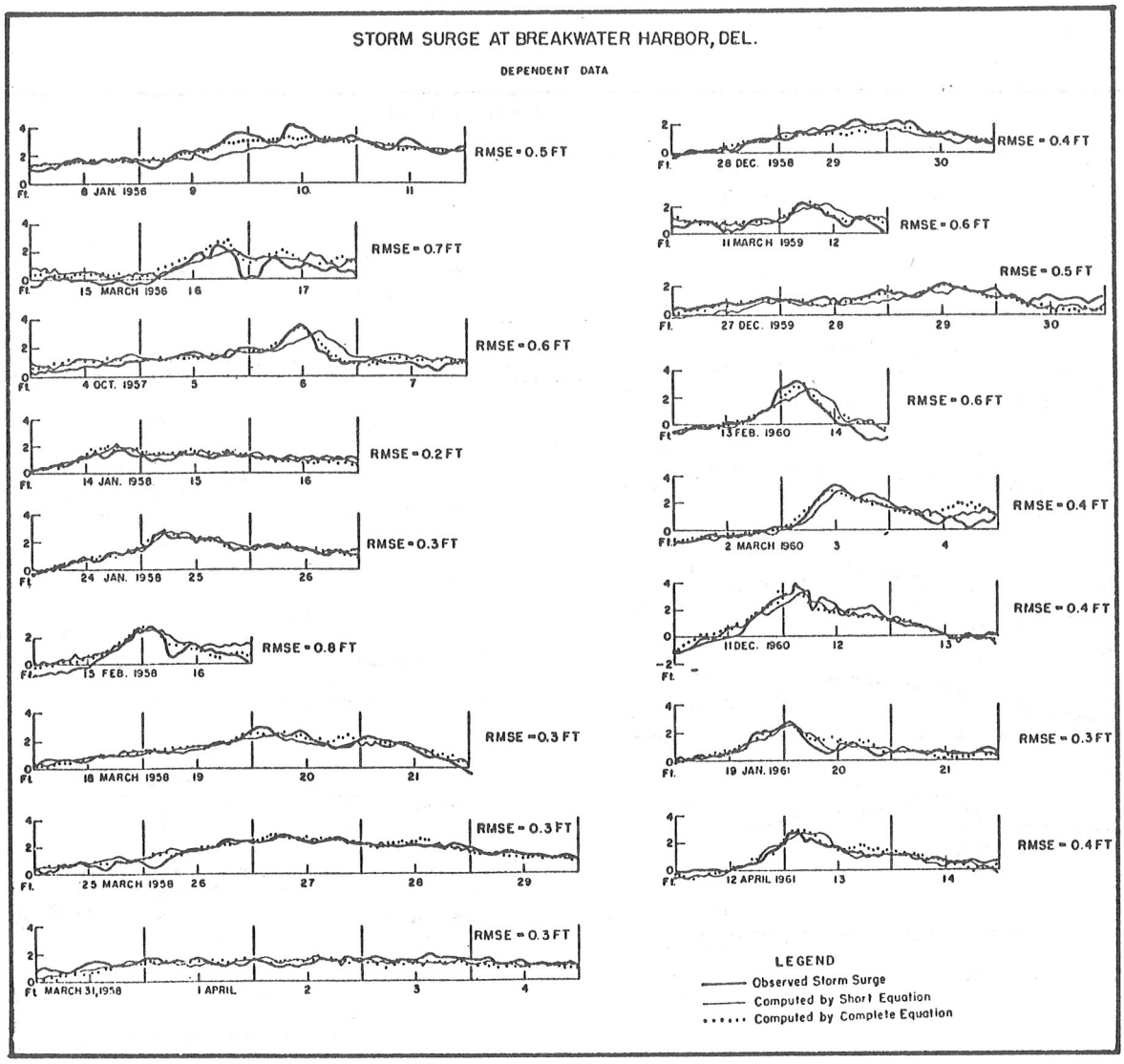

Figure 2.13. Storm surges and calculations of the dependent cases. The date for each day is placed at the noon position. The light solid lines show the calculations by the five term prediction equation given in the text. The dotted lines show the calculations by a 90-term prediction equation. The root mean square error shown for each storm is for the five term equation. The over-all rms error of the dependent cases is 0.4 feet. (Pore, 1964b)

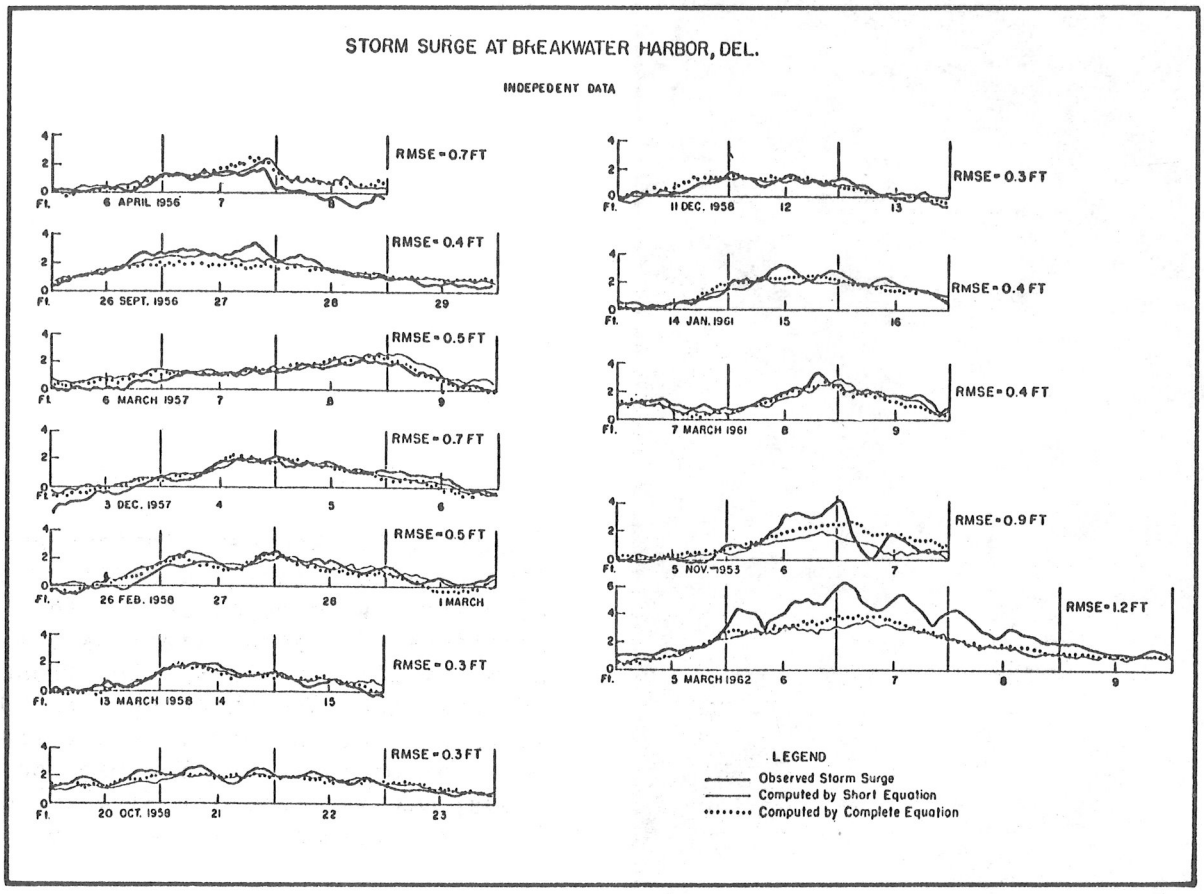

Figure 2.14. Storm surge and calculations of the independent cases. The date is placed at the noon position. The light solid lines show the calculations by the five term prediction equation given in the text. The dotted lines show the calculations by a 90 term prediction equation. The root mean square error shown for each storm is for the five predictor equation. The over-all rms error of the independent cases is 0.6 feet. (Pore, 1964b)

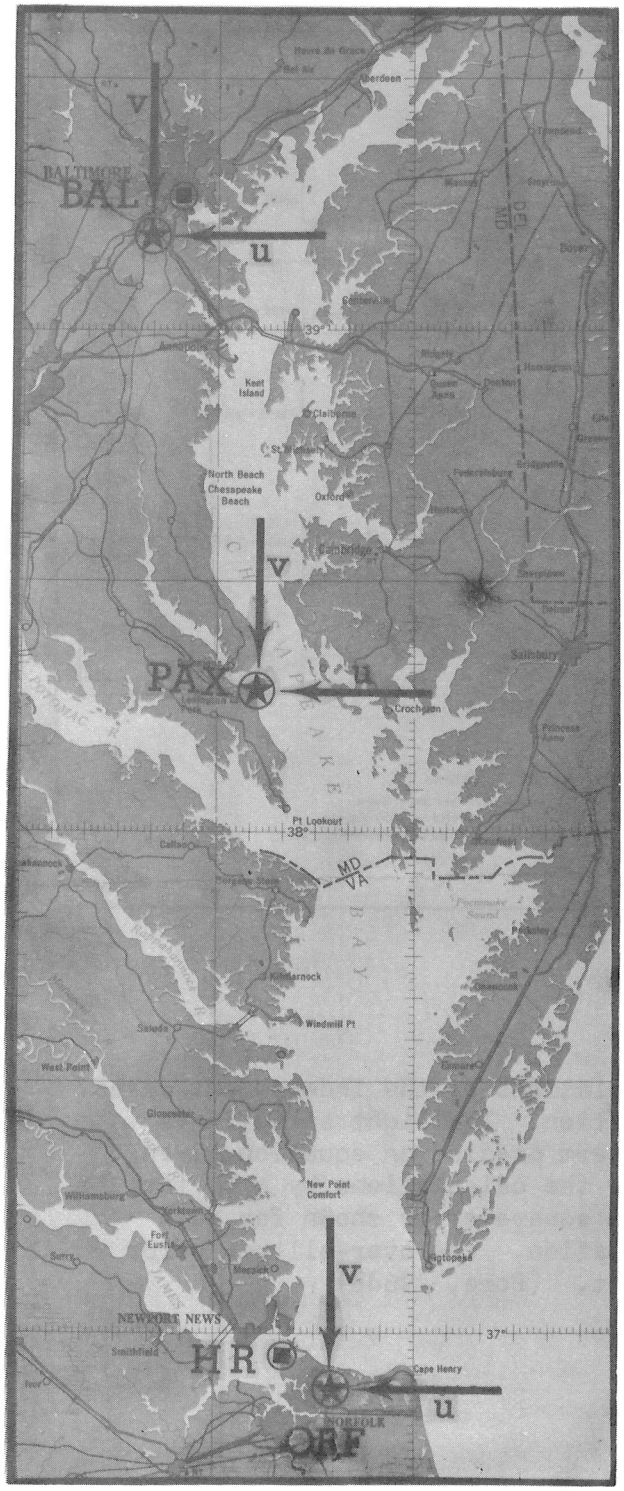

Figure 2.15. Weather stations and tide gage locations and definitions of u and v wind components. The locations of weather stations are shown by circled stars. Locations of tide gages are shown by circled squares. Station abbreviations are ORF for Norfolk; HR for Hampton Roads; PAX for Patuxent River; and BAL for Baltimore. (Pore, 1965)

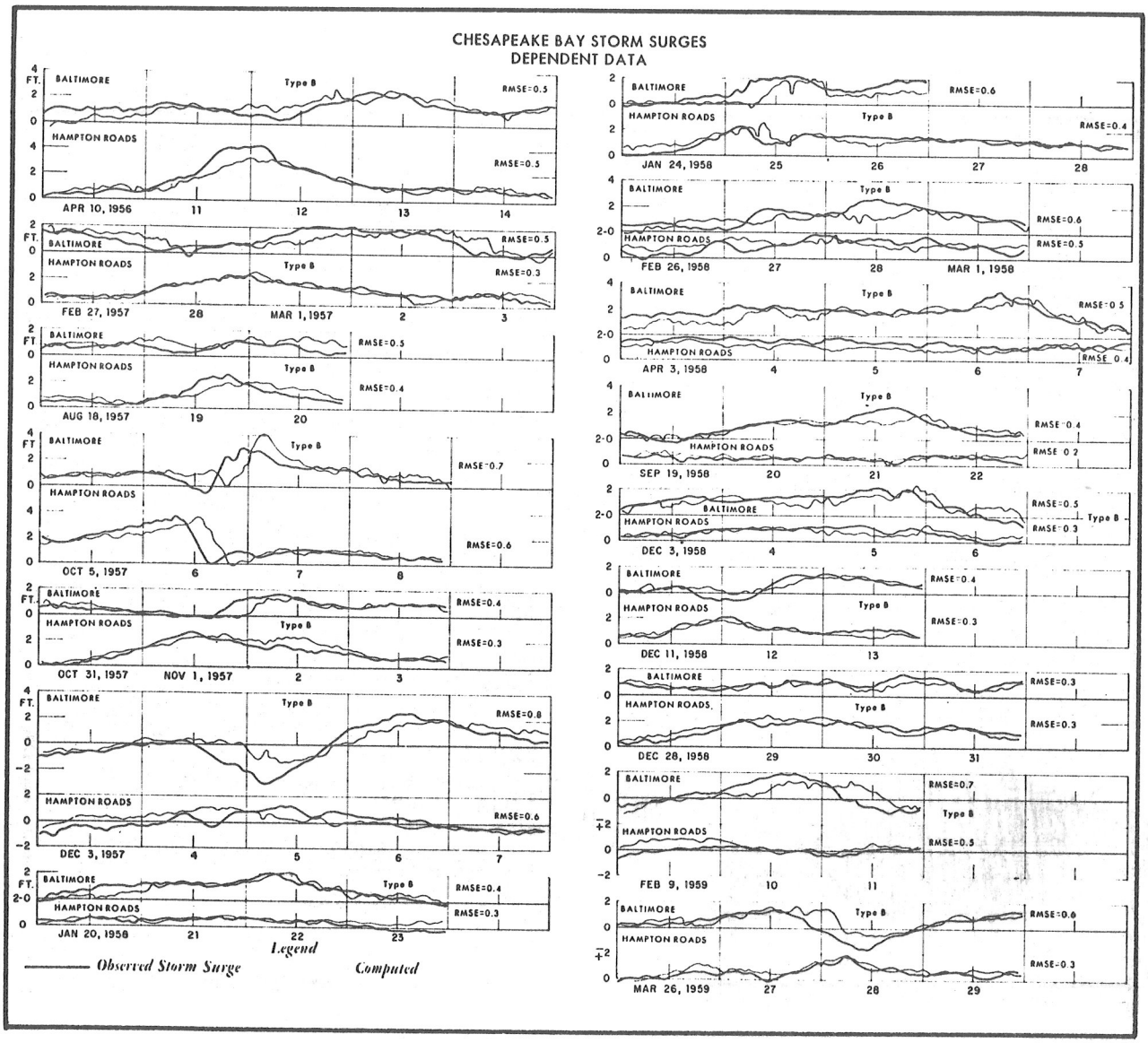

Figure 2.16. Storm surges and calculations of dependent cases. The date for each day is placed at the noon position. The computed curves show the calculated values for Baltimore and Hampton Roads by the prediction equations given in the text. The overall rms errors of the dependent cases are 0.6 ft. for Baltimore and 0.4 ft. for Hampton Roads. Other dependent cases are shown in the next figure. (Pore, 1965)

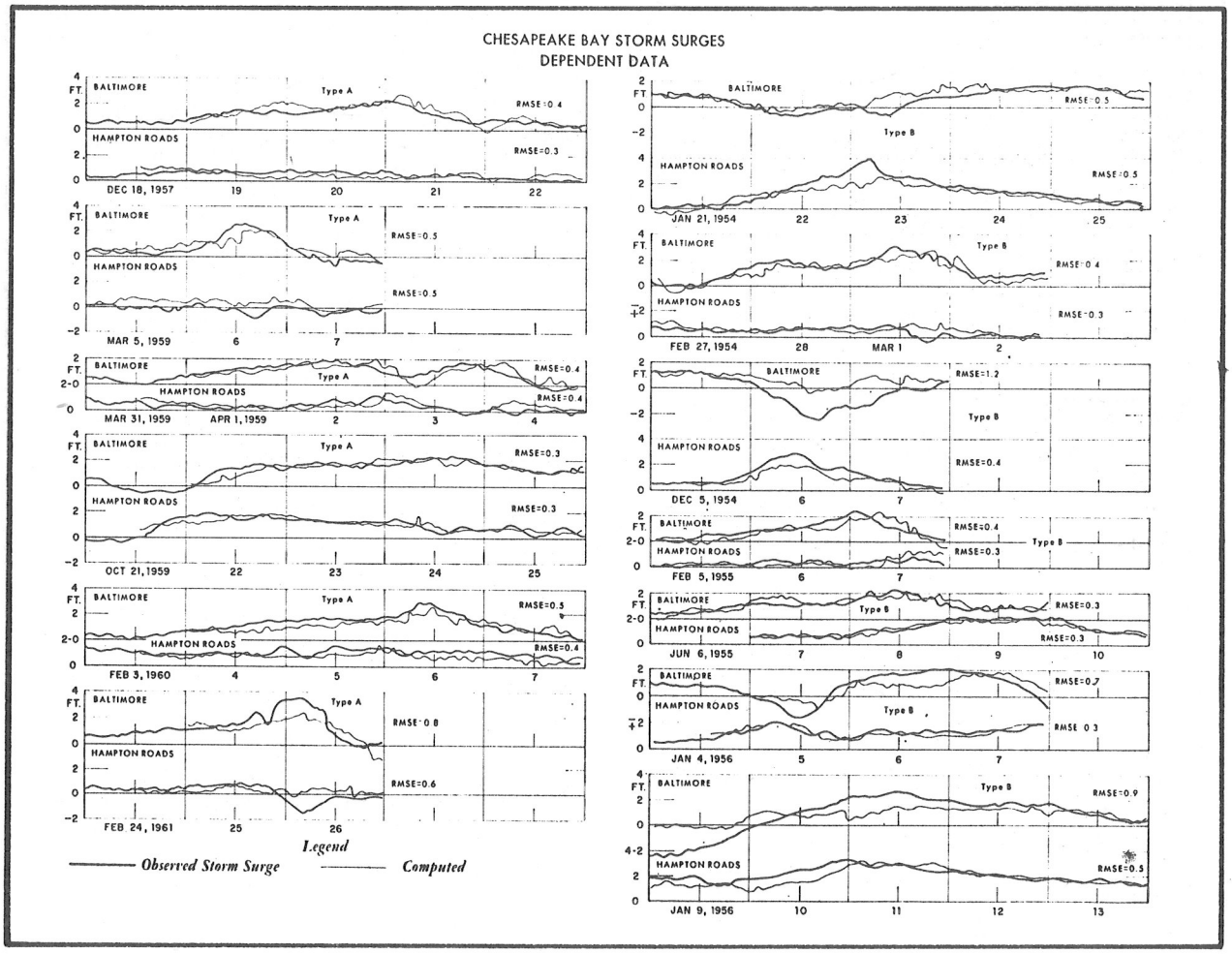

Figure 2.17. Storm surges and calculations of dependent cases. The date for each day is placed at the noon position. The computed curves show the calculated values for Baltimore and Hampton Roads by the prediction equations given in the text. The overall rms errors of the dependent cases are 0.6 ft. for Baltimore and 0.4 ft. for Hampton Roads. Other dependent cases are shown in the previous figure. (Pore, 1965)

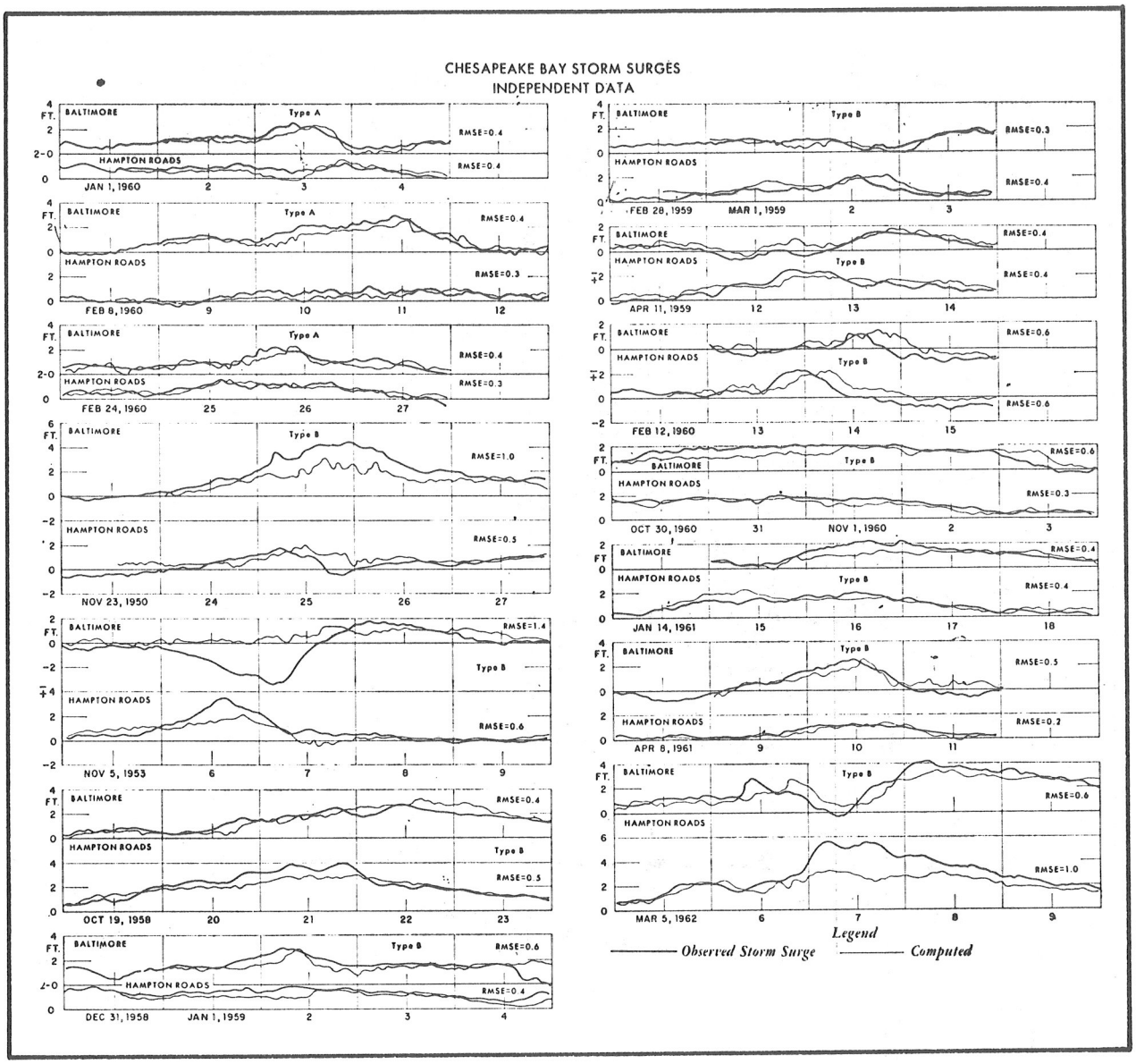

Figure 2.18. Storm surges and calculations of the independent cases. The date for each day is placed at the noon position. The computed curves show the calculated values for Baltimore and Hampton Roads by the prediction equations given in the text. The overall rms errors of the independent cases are 0.7 ft. for Baltimore and 0.5 ft. for Hampton Roads. (Pore, 1965)

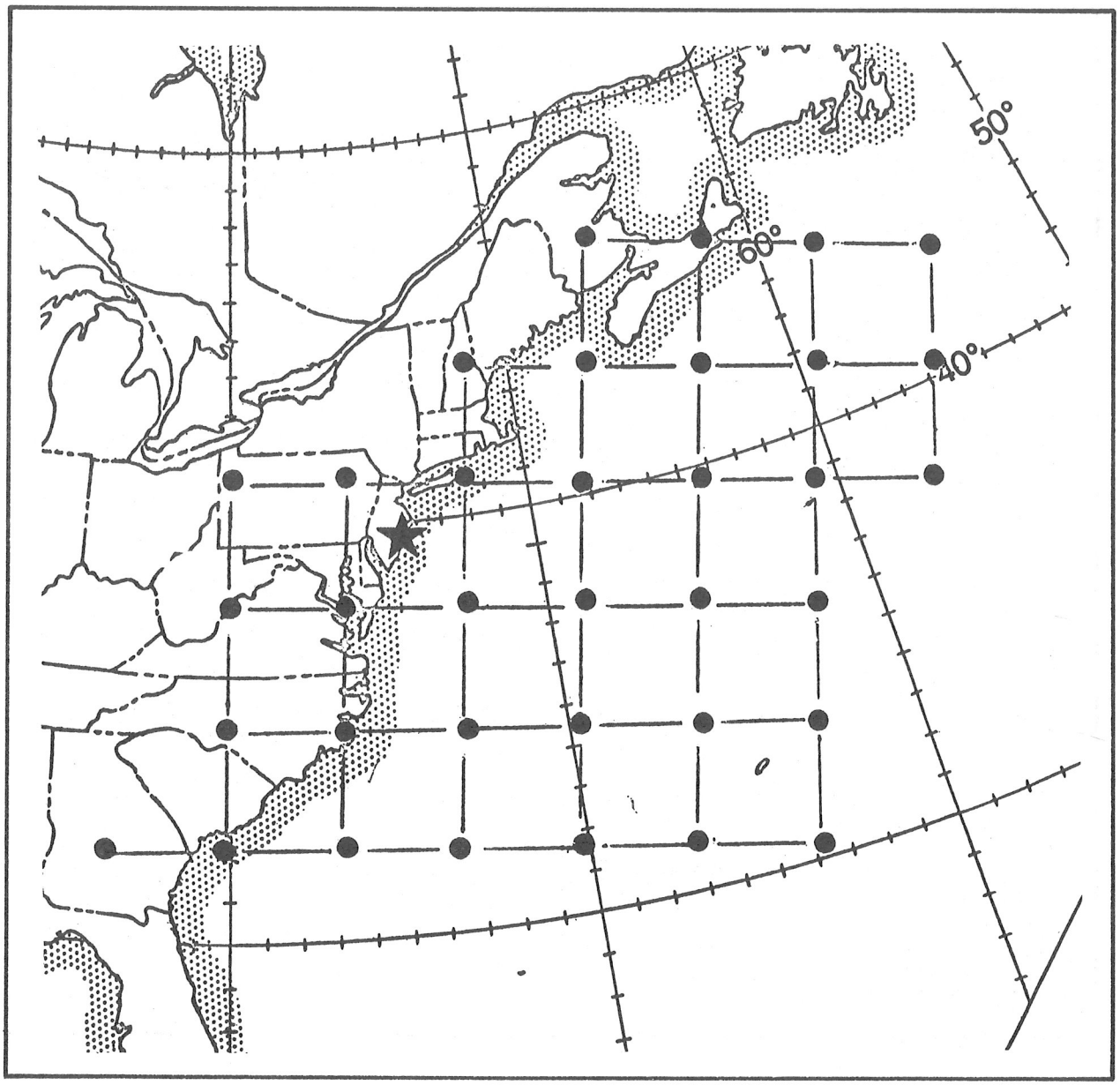

Figure 2.19. Grid points of the National Meteorological Center octagonal grid used in the development of the storm surge forecast technique for Atlantic City.

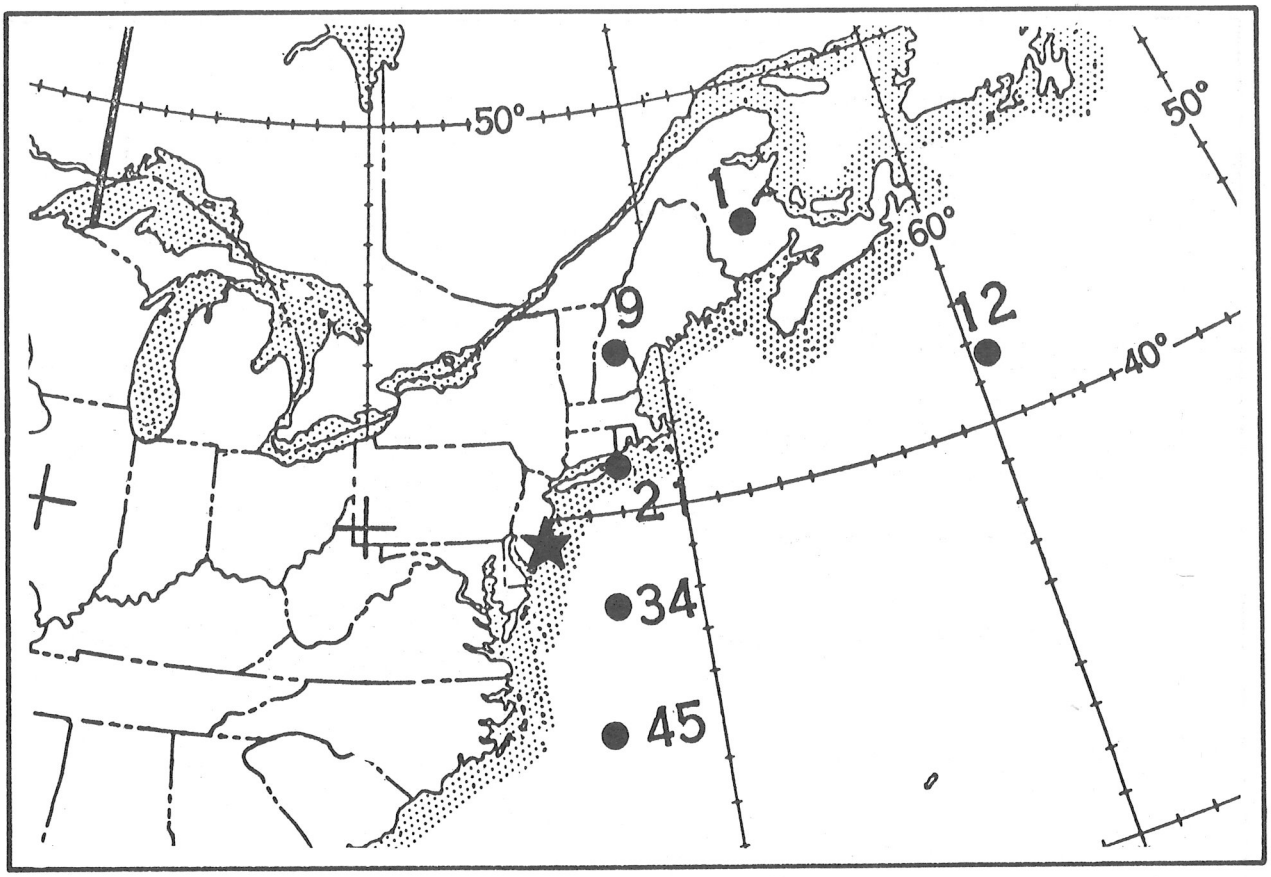

$$SS = A + B(P45)_0 + C(P1)_{-12} + D(P12)_{-6}$$

$$+E(P9)_{-6} + F(P34)_0 + G(P45)_{-24} + H(P21)_0$$

Figure 2.20. Location of grid points and form of the prediction equation for extratropical storm surge at Atlantic City. The subscripts of the terms in the prediction equation refer to the time lags in hours of the sea level pressures at the grid points indicated in parentheses. For example, $(P1)_{-12}$ refers to the pressure at point 1 with a time lag of 12 hours.

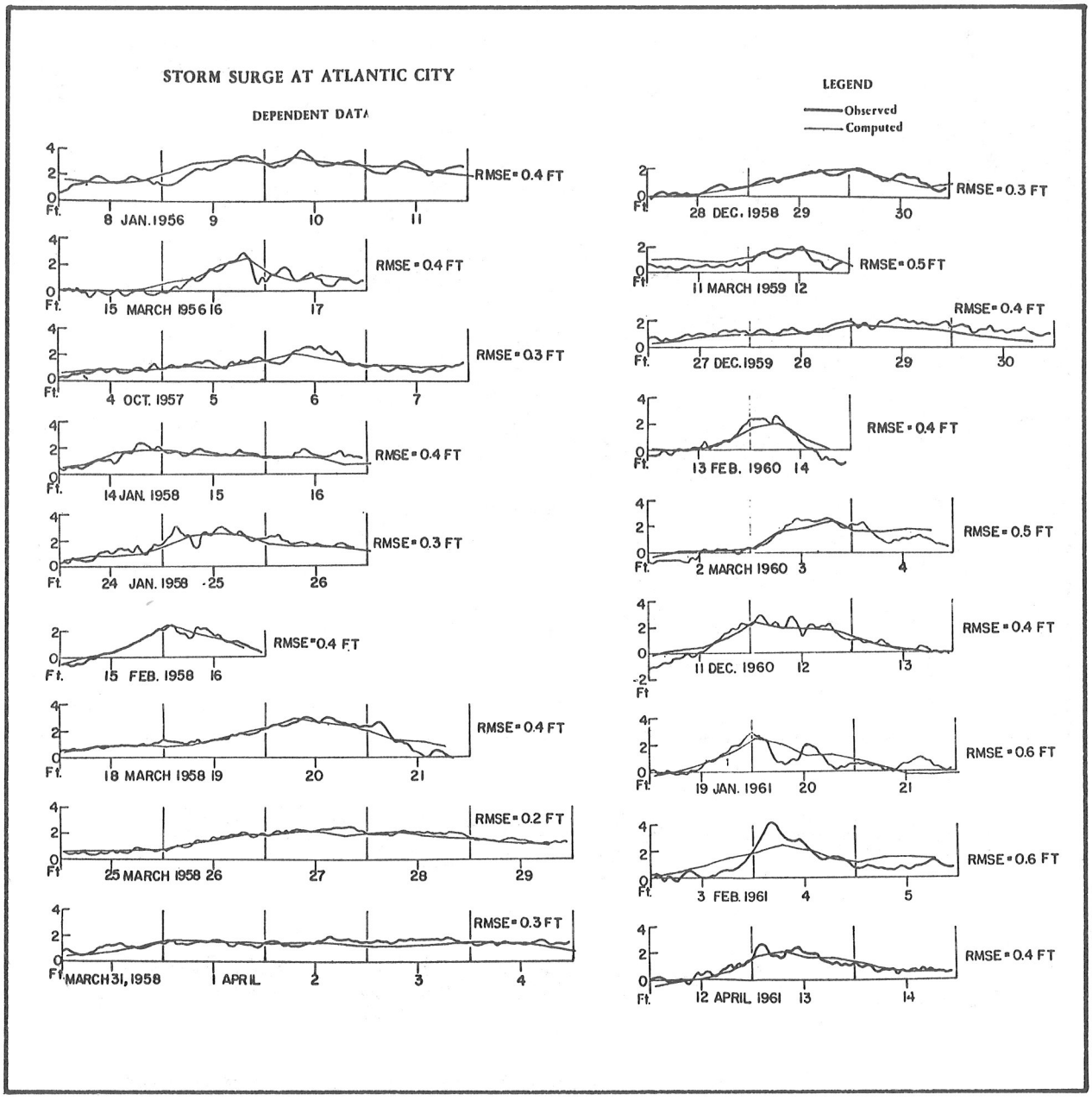

Figure 2.21. Extratropical storm surges and calculations for dependent cases at Atlantic City, using sea level pressure at grid points as predictors. The date for each day is placed at the noon position. Computed curves show values by the prediction equation given in the text.

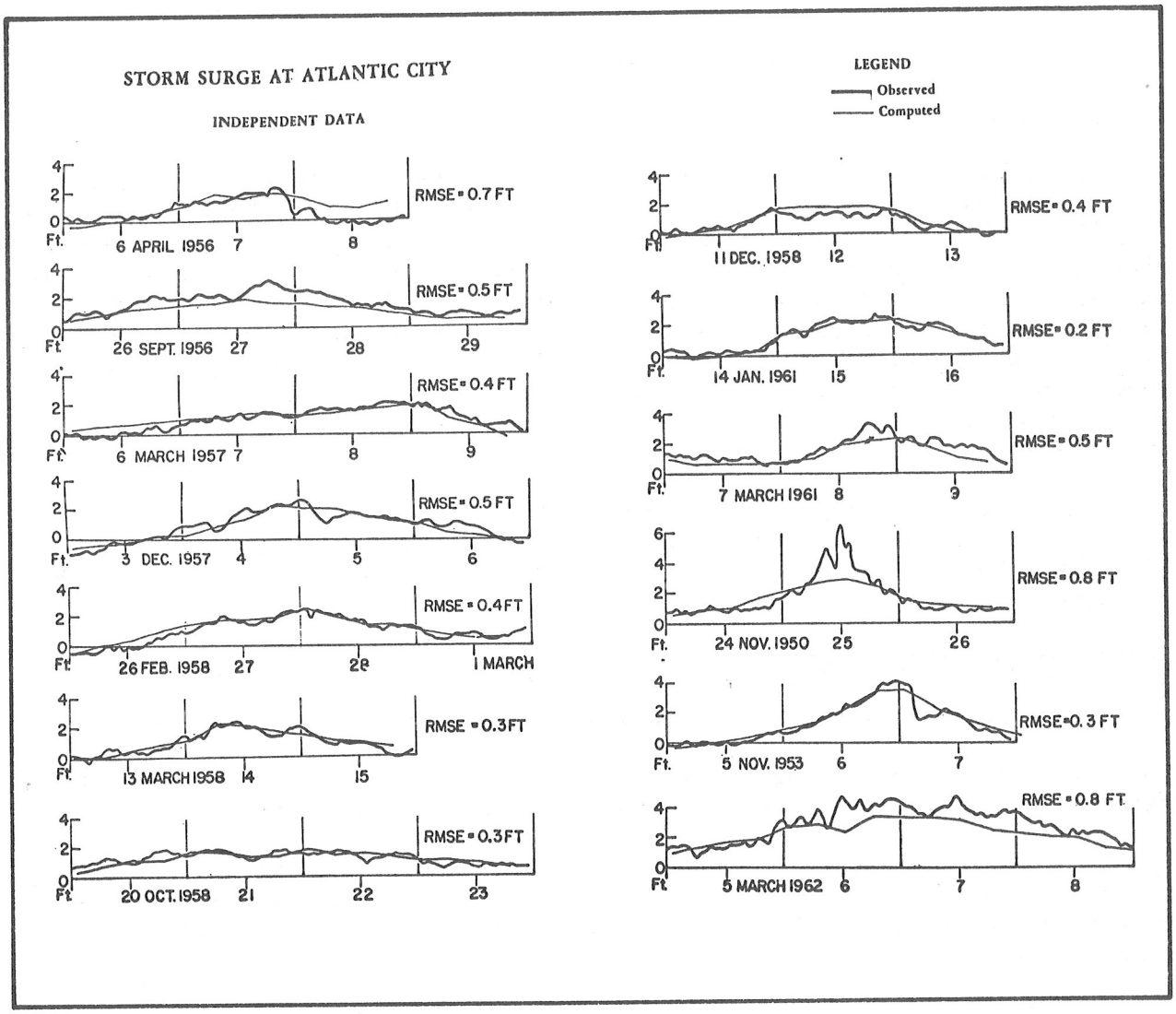

Figure 2.22. Extratropical storm surges and calculations for independent cases at Atlantic City, using sea level pressure at grid points as predictors. The date for each day is placed at the noon position. Computed curves show values by the prediction equation given in the text.

III. HURRICANE STORM SURGE

Introduction

Whenever a hurricane approaches or crosses the coastline the sea level increases from a few feet to more than twenty feet above the normal tide level. Much of the loss of life associated with these storms is caused by the storm-induced rises of sea level. Examples of storms costly in terms of lives are the hurricane of September 1900, in which over 6000 were lost in the Galveston area, hurricane Audrey of June 1957 which claimed several hundred lives in Louisiana, and most recently hurricane Camille of 1969 which was responsible for many lost lives in Mississippi and Louisiana. Tremendous property damage is also caused by the storm surges in harbors and along the open coast.

The storm surge is defined as the rise or fall of the sea level caused by a meteorological disturbance and is closely approximated by the algebraic difference between the observed tide and the normal astronomical tide as shown in figure 2.1.

Generation of Storm Surge

The principal factors in the generation of storm surges are:

1. The stress of wind on the sea surface. The wind blowing over the water piles up the water. This is often called the wind set-up.

2. The reduction of atmospheric pressure in the storm area causes an increase in sea level in the low pressure area. This inverted barometer effect amounts to about 13½ inches of water per inch of mercury drop in atmospheric pressure.

3. The transport of water by waves and swells in the shallow water area near shore, especially that associated with breaking waves.

4. Modifications due to the local conditions in harbors, such as convergence or divergence of the surge depending on the shoreline orientation and the effect of varying depths within the harbor.

Examples of Hurricane Storm Surges

An example of a hurricane-produced storm surge is that in Carol of August 1954, illustrated in figure 3.1. The locations of the tide gages which recorded the storm surge are shown along with the track of the storm, and the location of the storm center at various times. The graphs show the storm surge based on hourly differences of the observed tide and the normal astronomical tide. The maximum values of the surge at each station are indicated on the curves. The highest was 8.8 feet at Woods Hole, Mass. The oscillations in the Atlantic City, Sandy Hook, and Battery curves, which occurred after the main surge, are characteristic of the storm surge in this area when a hurricane passes offshore. At all of the stations except Willets

Point (southern entrance point between East River and Long Island Sound) the maximum surge occurred near the time when the storm was closest to the station. This time is shown by the dashed line through the curves. The time delay at Willets Point is believed to be caused by the time required for the main surge to travel from the ocean through Long Island Sound to Willets Point.

The storm surge data for hurricane Donna of 1960, one of the most destructive hurricanes of record in the United States, is presented in figure 3.2. Because its path was close to shore over a long distance, appreciable surges were produced along most of the East Coast. Willets Point received significant surges through both the East River and Long Island Sound. The maximum surge was the result of the significant surge in New York Harbor, shown by the Battery curve, moving through the East River with the secondary surge coming through the Sound. This is in contrast to conditions during Carol, which passed farther to the east, and resulted in a less significant surge in New York Harbor and a smaller initial peak at Willets Point.

Importance of Time of Occurrence

The effect of the time of occurrence of a storm surge with respect to the stage of the normal astronomical tide is shown in figure 2.5. Here two identical storm surges are combined with different phases of the normal tide, one occurring at normal high tide and the other at normal low tide, with the one at high tide resulting in a higher actual tide. The time of occurrence of the storm surge with respect to the normal tide can mean the difference between serious and minor flooding.

Variations in Maximum Water Levels

The tide heights observed during hurricanes can vary by several feet within a few miles because of local topographic features in the flooded area. Figure 3.3 shows high water marks recorded in Florida during hurricane Donna. In hurricane Audrey (Harris, 1958) these variations amounted to several feet in less than a mile near the coast because of local variations in the exposure to wind and waves. Variations farther inland were observed because of the presence of spoil banks, dikes, and levees.

Accurate observations of storm surge and water level data during hurricanes are difficult to obtain. Until recently there were few systematic collections made that were accurately documented as to the reference datum plane, timing of surge, etc. Harris (1963b) made a search for all the available reliable data on storm surges caused by hurricanes in the United States from 1926 to 1961. This data collection is by far the best available for research on hurricane storm surges or for general reference. Considerable data were earlier presented by Cline (1920, 1926) on the tide and meteorological conditions of hurricanes in the Gulf of Mexico between 1900 and 1919.

Objective Forecasting Techniques

Conner, Kraft, and Harris (1957) developed an empirical method of relating the maximum storm surge to the central pressure of the hurricane. By combining the relationship for the maximum wind speed as given by Myers (1954) and the relationship of wind stress to wind speed they determined an empirical relationship between maximum tide height and the central pressure of the hurricane to be:

$$h_{max} = 0.154\ (1019 - P_o)$$

where h_{max} is the maximum tide height in feet,
and P_o is the central pressure of the hurricane in millibars.
This expression is based on the observations of 30 hurricanes in the Gulf of Mexico and has a correlation coefficient of 0.68. This expression is shown graphically as the straight line of figure 3.4.

Hoover (1957) performed a similar study and derived two regression lines for the maximum storm tide or storm surge as a function of the central pressure. One regression line was for the maximum storm tide on the Gulf of Mexico coast as shown in figure 3.5 and the other was for the maximum storm surge on the Atlantic Coast as shown in figure 3.6. The difference between the study by Hoover and that of Conner, Kraft, and Harris (1957) is that Hoover determined the maximum heights of his developmental data by constructing tide profiles which were used for estimating the maximum tide. Conner, Kraft and Harris used the maximum observed tide in their development. Some examples of Hoover's surge profiles are shown in figure 3.7.

Empirical methods such as those just described are limited because of the small amount of observational data available for development work and the great differences in meteorological conditions observed in hurricanes. For these reasons the numerical approach to the storm surge problem appears more promising.

Jelesnianski (1966, 1967) has developed a useful numerical storm surge model. The model has been used to construct a storm surge prediction system in the form of polar graphs for operational use. These graphs give storm surge characteristics as functions of the strength and movement of the hurricanes.

Jelesnianski (1966) first developed the model for storm surges without the effect of bottom stress in the storm surge equations. These computations were restricted to relatively fast moving storms which crossed the coast at an angle within 60° of perpendicular to the coast. Later, Jelesnianski (1967) added the bottom stress to the equations of motion. This addition made the system applicable to storms of any speed and with any angle of approach to the coastline, including those which travel parallel to the coast.

Jelesnianski's computations were for standard storms traveling over idealized basins. The standard storm used has a "stationary-storm-maximum-wind" of 100 miles per hour with the storm center at latitude 30°. The standard basin has a linear sloping depth profile of 3 feet per mile, a 15 foot depth at the coastal boundary, a shelf length of 60 miles and a depth of 195 feet at the deep water boundary. Computations were made of the standard storm traveling over the idealized basin. By allowing storm parameters such as storm speed, coastal crossing angle, and radius of maximum wind to vary, storm surge profiles have been constructed. These computations have been put into polar graph nomogram form for easy access for use in forecasting storm surges.

The coastal storm surge profile can be portrayed by determining the eight points on the profile shown in figure 3.8. The points labeled A through I indicate such storm surge profile points as maximum surge value, distance from landfall of storm to peak surge and distance from peak surge to zero surge. These points will be more specifically defined in the discussion to follow on the nomograms.

Nine pairs of nomograms are here presented from Jelesnianski (1967). Each pair of nomograms includes one for the standard storm with a radius of maximum wind of 15 statute miles and one for the standard storm with a radius of 30 statute miles. Each nomogram is used by considering the arguments of crossing angles of the storm to the coast and storm speed. The crossing angle of the storm to the coast for use in the nomograms has been defined in the following paragraph from Jelesnianski (1966).

"Let the observer be oriented on a straight-line coast so that water is to his right and land to his left; let the direction he faces be relative north with his back to relative south along the coast. Angular crossings of the storm at the coast will now be defined in the meteorological sense; thus, a storm moving to relative north along the coast has an angular crossing from the south or 180°, one moving from sea to land and crossing the coast at normal incidence has an angular crossing from the east or 90°, one moving to relative south along the coast has an angular crossing from the north or 0°, etc."

The nomograms are presented in figures 3.9 through 3.17 as follows:

Figure 3.9. Distance from landfall position to point of peak surge on the coast. Corresponds to point A in figure 3.8.

Figure 3.10. Peak coastal surge value. Corresponds to point B in figure 3.8.

Figure 3.11. Minimum coastal surge value. Corresponds to point H in figure 3.8.

Figure 3.12. Distance on coast from point of peak surge to point on coast to right of landfall having one-half the peak surge. Corresponds to point D in figure 3.8.

Figure 3.13. Distance on coast from point of peak surge to point on coast to left of landfall having one-half the peak surge. Corresponds to point C in figure 3.8.

Figure 3.14. Distance on coast from point of peak surge to point on coast to right of landfall having one-quarter the peak surge. Corresponds to point F in figure 3.8.

Figure 3.15. Distance from peak surge to zero surge on the coast to left of landfall. Corresponds to point G in figure 3.8.

Figure 3.16. Distance from peak surge to minimum surge. Corresponds to point I in figure 3.8.

Figure 3.17. Arrival time of peak surge after storm landfall.

The nomograms described above apply to storms that make landfall. For storms that do not make landfall, a standard storm traveling parallel to the coast of a standard basin was considered by the model. The series of computations under varying conditions of storm speed and distance of the storm center from the coast resulted in the nomogram shown as figure 3.18 from Jelesnianski (1967). Here the radius of maximum wind was 30 miles. The nomogram covers storm distances from the coast of from 50 miles inland to 100 miles offshore. Curves for three storm speeds, 0, 20 and 40 miles per hour, are included. The maximum and minimum values of the storm surge profile (points B and H of figure 3.8), for storms which do not cross the coast, can be determined from this nomogram. With the assumption that the dispersion of the surge does not depend on the distance of the storm from the coast, the storm surge profile can be completed by determining points A, C, D, F, G, and I from the nomograms of figures 3.9, 3.13, 3.12, 3.14, 3.15, and 3.16.

Variations of latitude changes the computed surge only slightly. This slight correction for latitude was added to the corrections for depth profile for special points on the East and Gulf Coasts of the United States. These correction factors for the peak surge were obtained by making computations with the model considering the depth profiles at these special points. These correction factors are shown for most of the East Coast in figure 3.19 and for Florida and the Gulf Coast in figure 3.20.

The corrected storm surge peak is given by:

$$h_c = h_s (V_r/100)^{2F_D}$$

where h_c is the corrected surge peak, h_s is the standard storm surge peak, V_r is the maximum storm wind, and F_D is the correction factor for depth profile and latitude.

It is pointed out by Jelesnianski (1967) that since the model does not consider curvilinear boundaries such as bays and inlets that the values from the nomograms are to be considered as a preliminary guide which requires some adjustment for the local shoreline. Looking into the future, it is expected that with more natural coastal boundary conditions storm surge forecasts can be made by computer using forecast storm variables and forecast point of landfall.

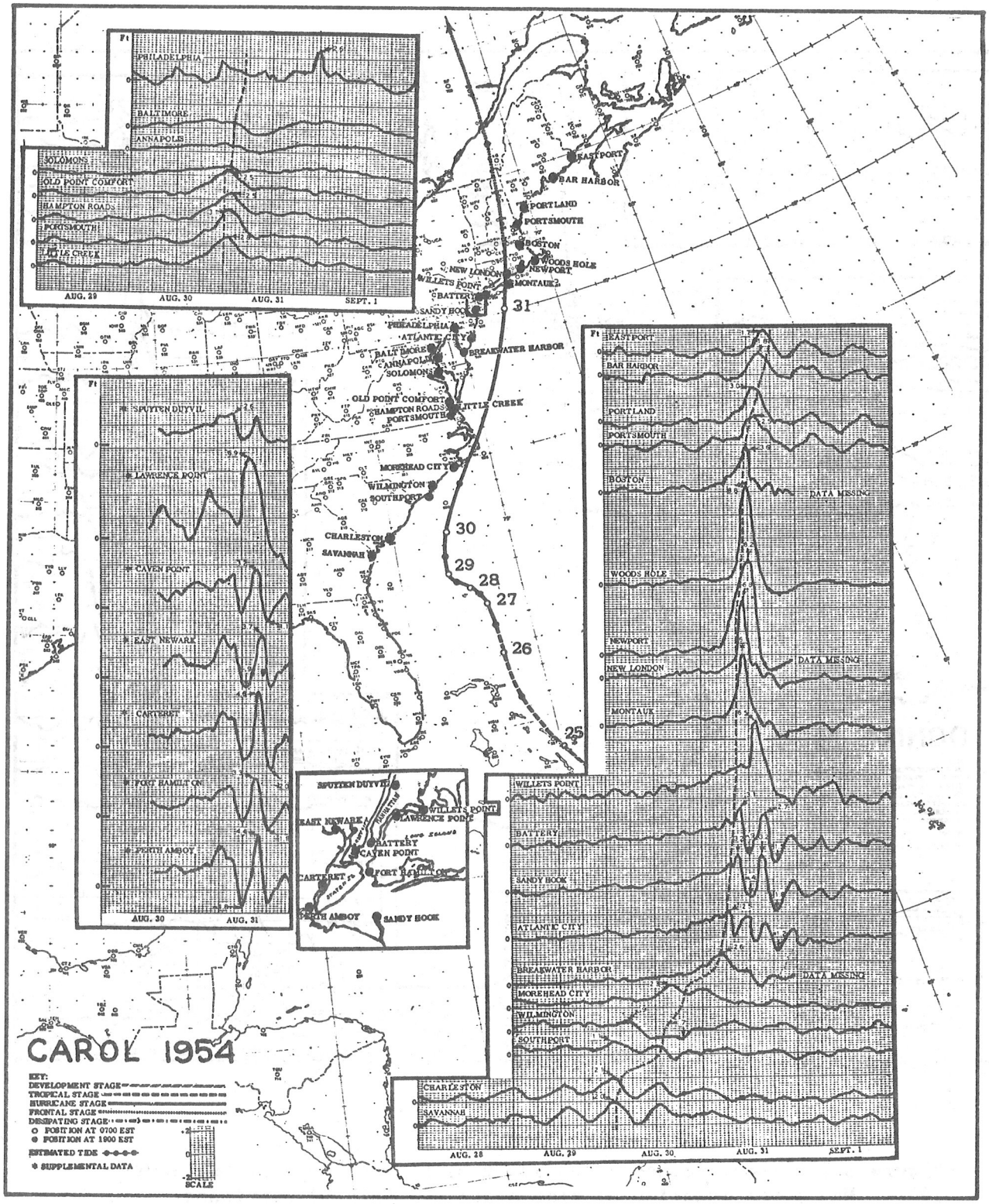

Figure 3.1. Storm surges produced by Hurricane Carol of August 1954. Map gives location of tide gages and path of hurricane. (Harris, 1963b)

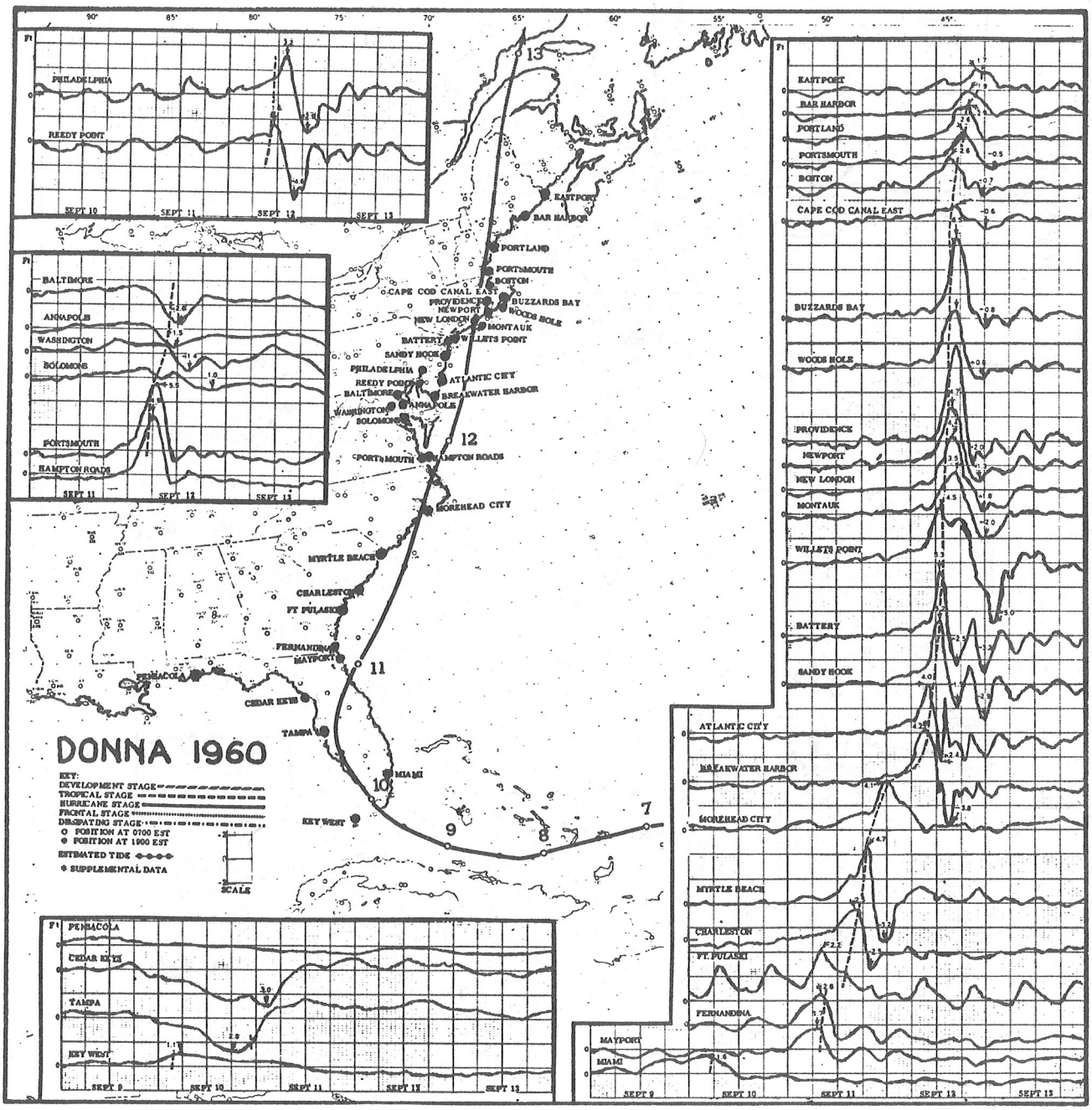

Figure 3.2. Storm surges produced by Hurricane Donna of September 1960. Map gives location of tide gages and path of hurricane. (Harris, 1963b)

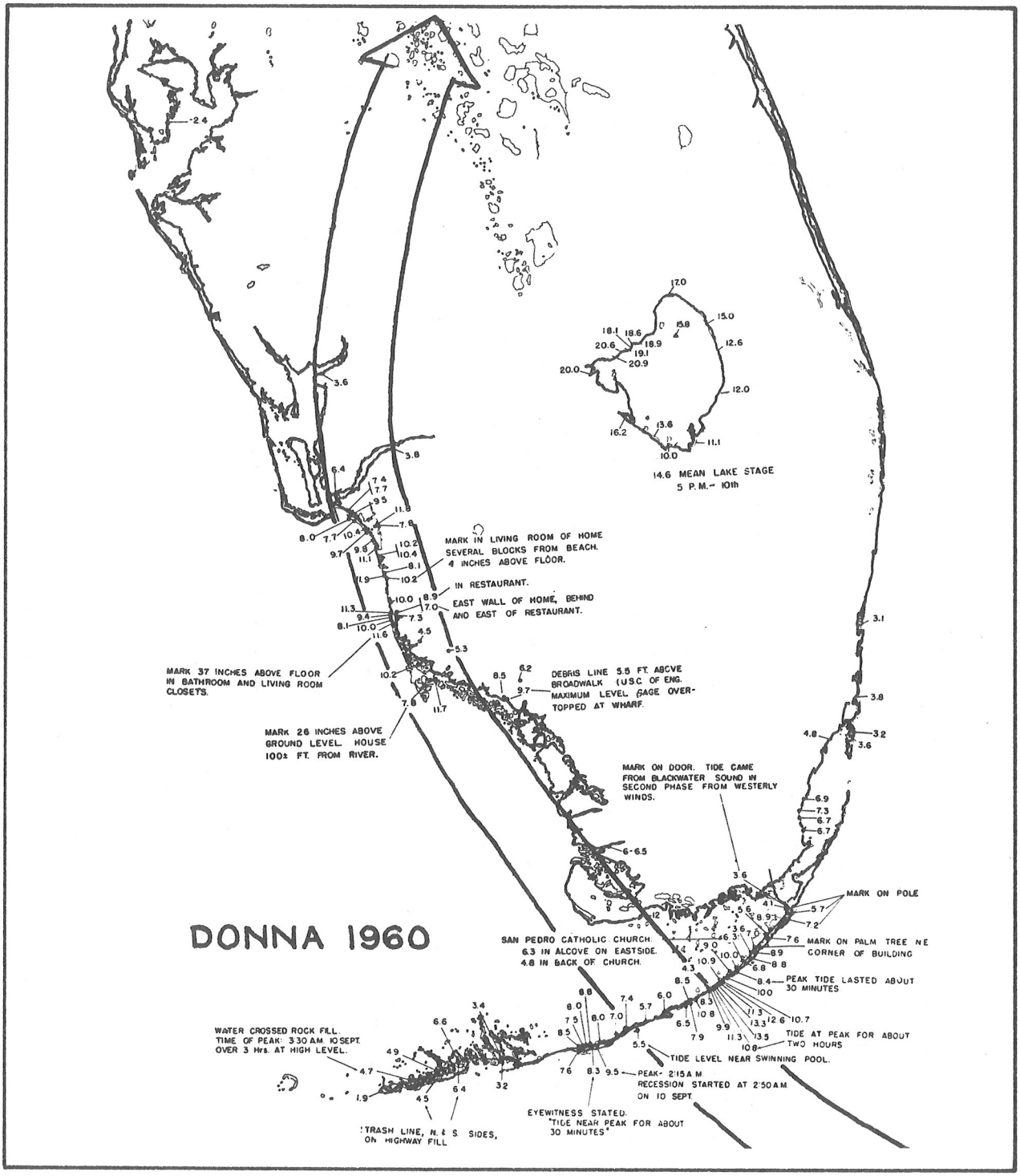

Figure 3.3. High water marks recorded during hurricane Donna of September 1960 in southern Florida. (Harris, 1963b)

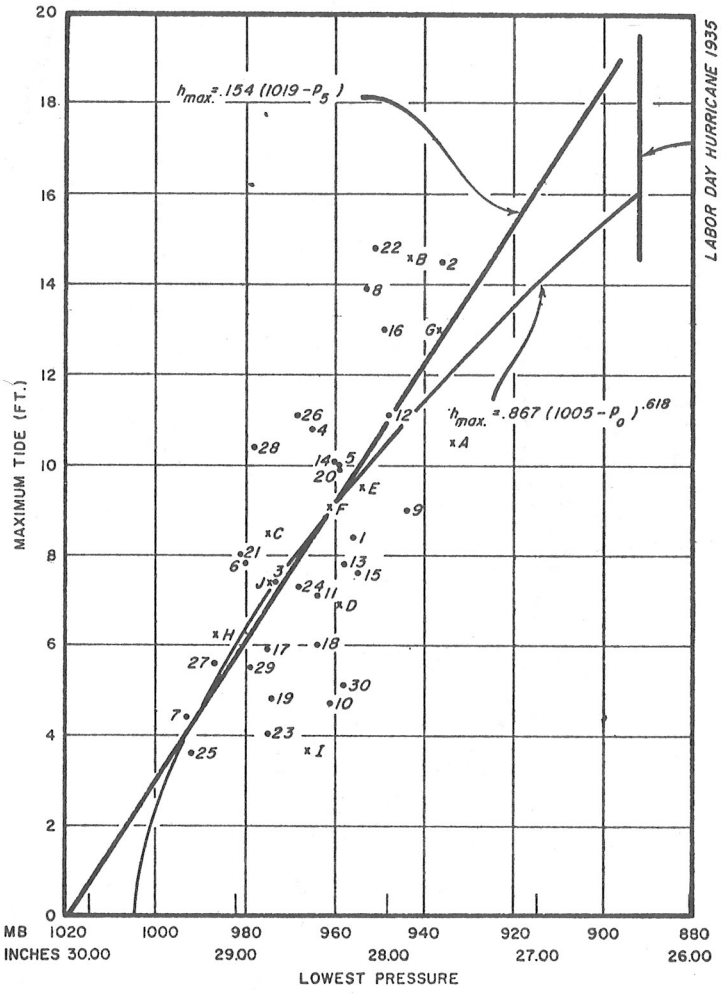

Figure 3.4. Maximum tide or storm surge height on the open coast as a function of the central pressure. Dependent data are plotted as points. Independent data are plotted as crosses. (Conner, Kraft and Harris, 1957)

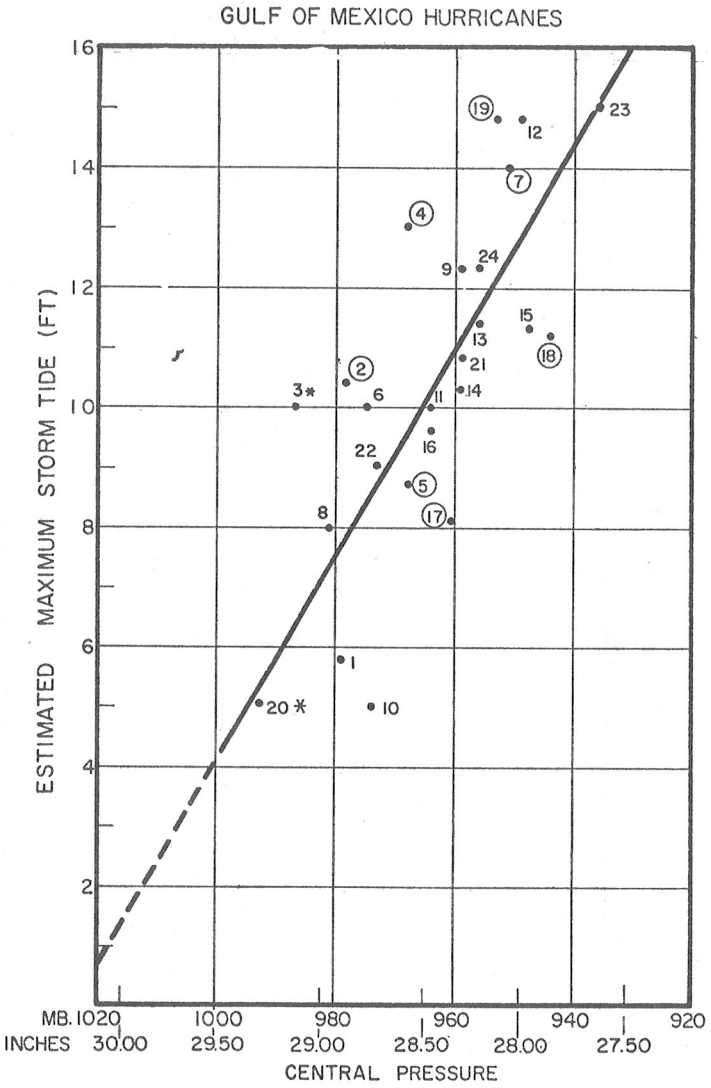

Figure 3.5. Regression of maximum storm tide height on central pressure for hurricanes entering the United States Gulf of Mexico coastline west of Tallahassee, Florida. (Hoover, 1957)

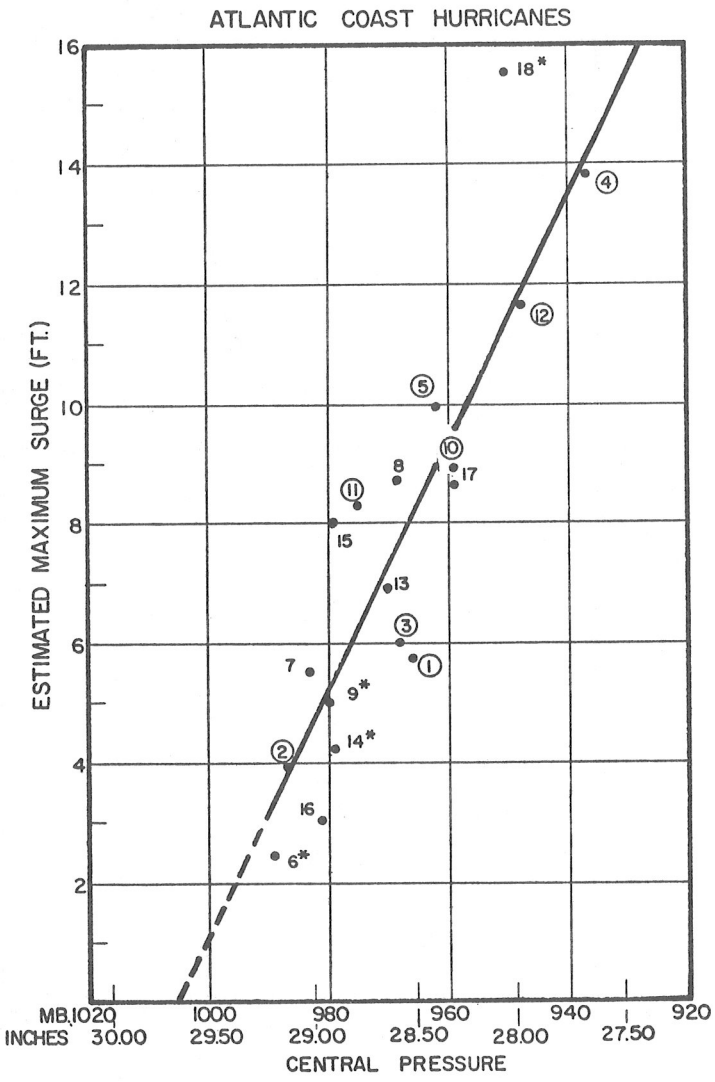

Figure 3.6. Regression of maximum surge height on central pressure for hurricanes entering the United States Atlantic Coastline north of Jacksonville, Florida. (Hoover, 1957)

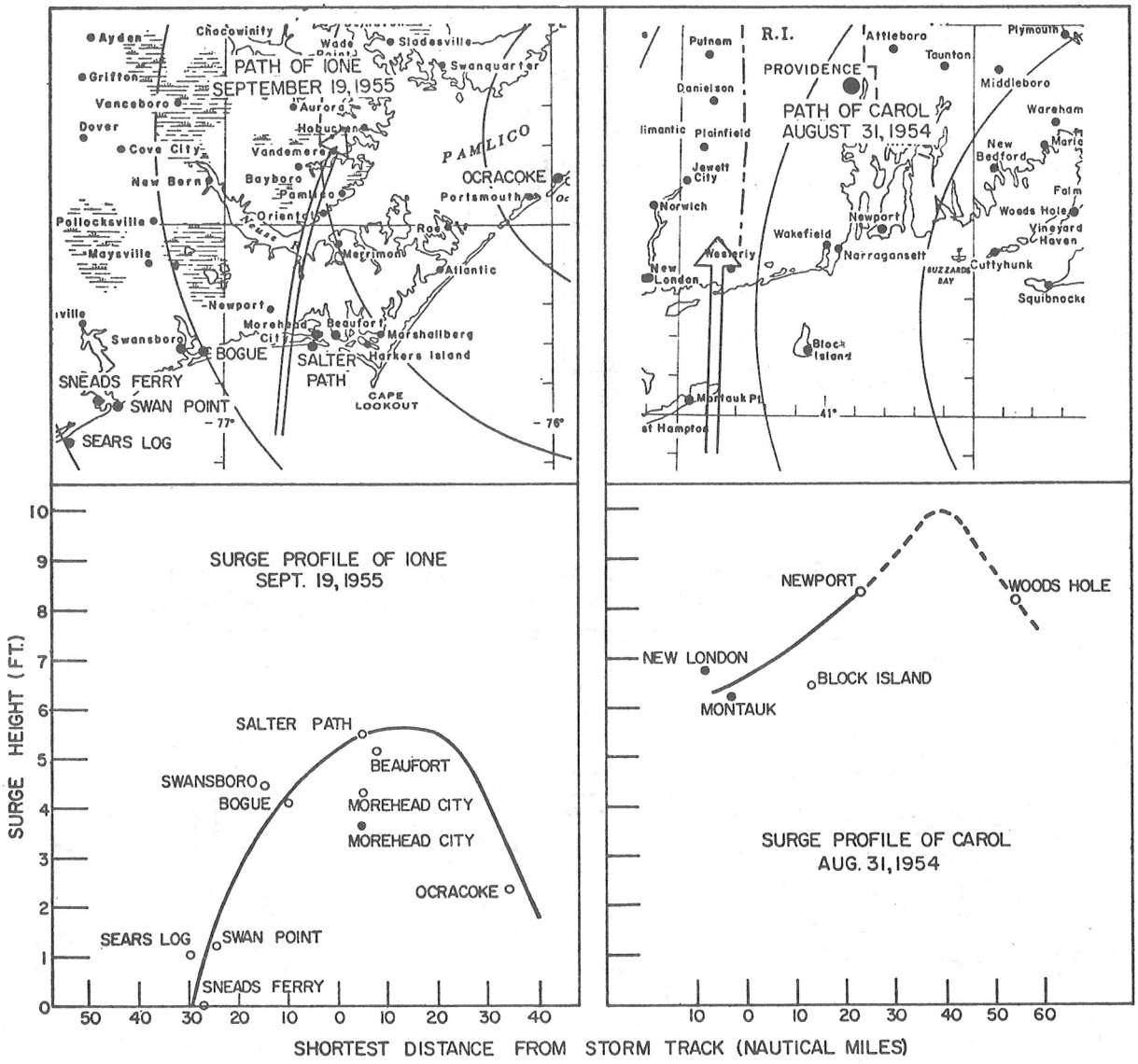

Figure 3.7. Storm surge profiles of hurricane Ione, September 19, 1955 and Carol, August 31, 1954. (Hoover, 1957)

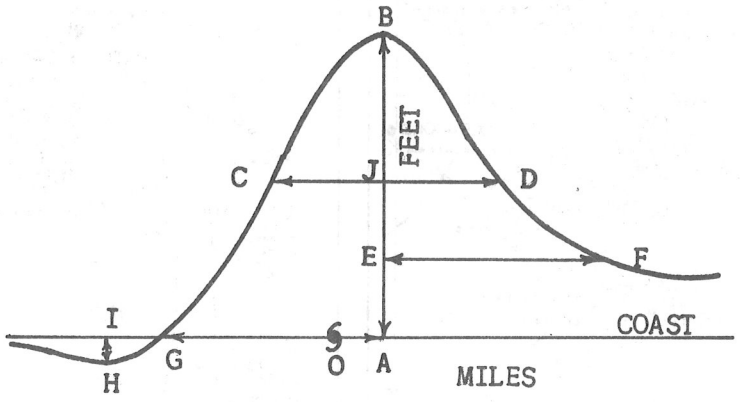

Figure 3.8. A typical computed coastal surge profile. The observer is on sea facing land. The various heights and distances are for later reference. (Jelesnianski, 1966)

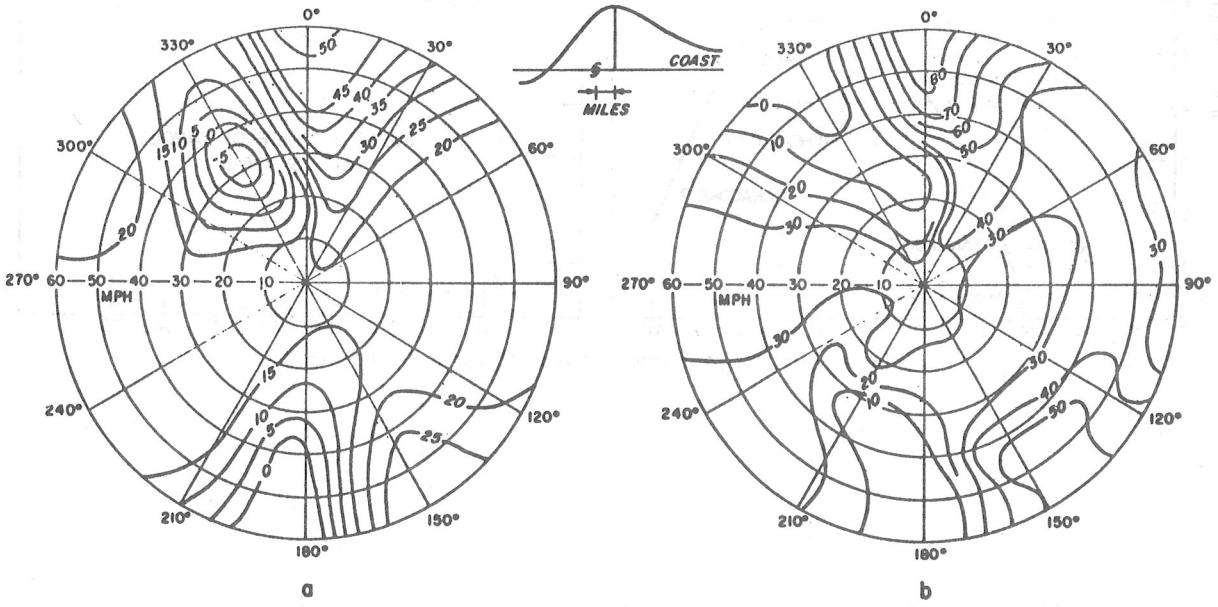

Figure 3.9. Contours of distance, in statute miles, from landfall position to point of peak surge on the coast. Radii are storm speeds, rays are crossing angles of storm track to the coast. (a) Radius of maximum wind, 15 statute miles. (b) Radius of maximum wind, 30 statute miles. (Jelesnianski, 1967)

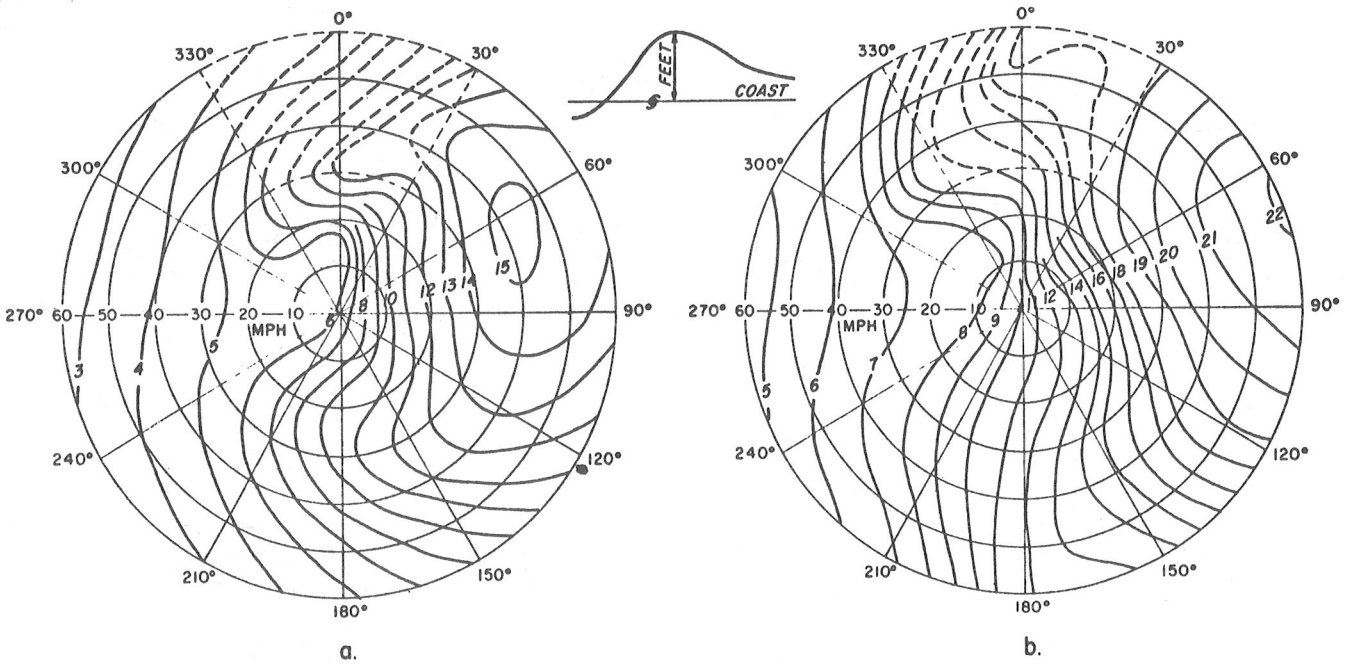

Figure 3.10. Contours of peak coastal surge values, in feet. Arguments are identical to Figure 3.9. (Jelesnianski, 1967)

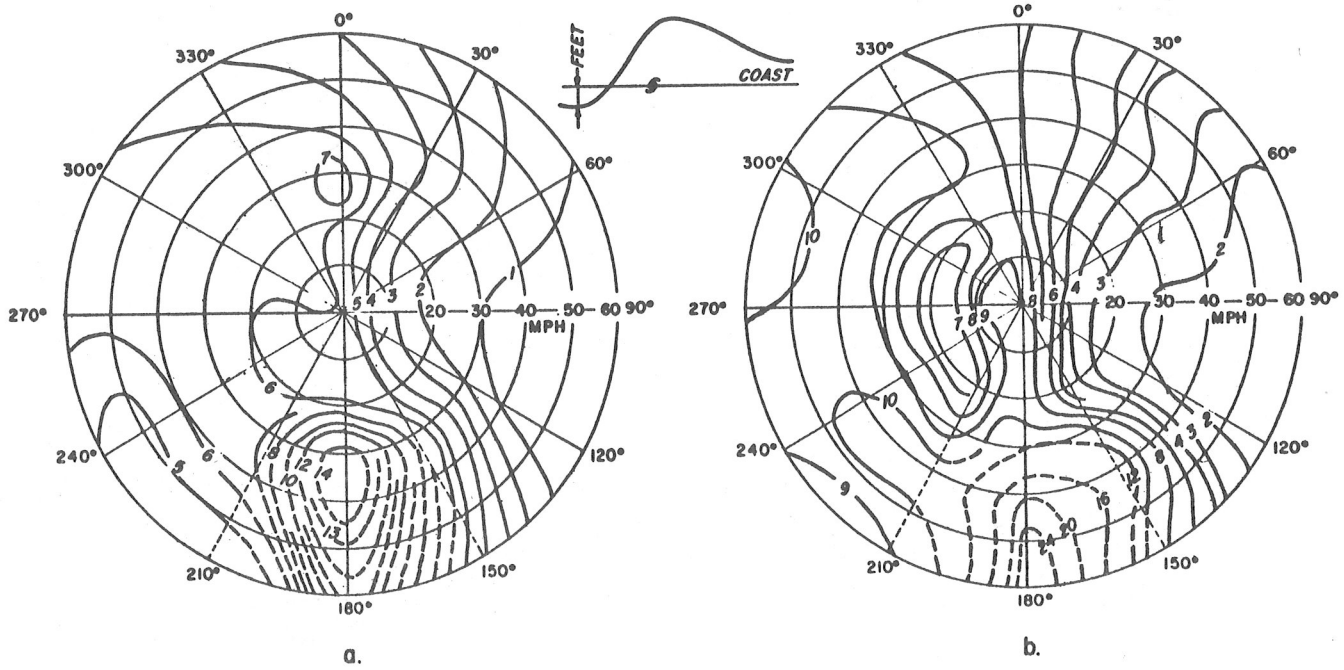

Figure 3.11. Same as Figure 3.10. for the minimum surge, portrayed at time of peak surge. The absolute minimum surge does not necessarily occur at time of peak surge. (Jelesnianski, 1967)

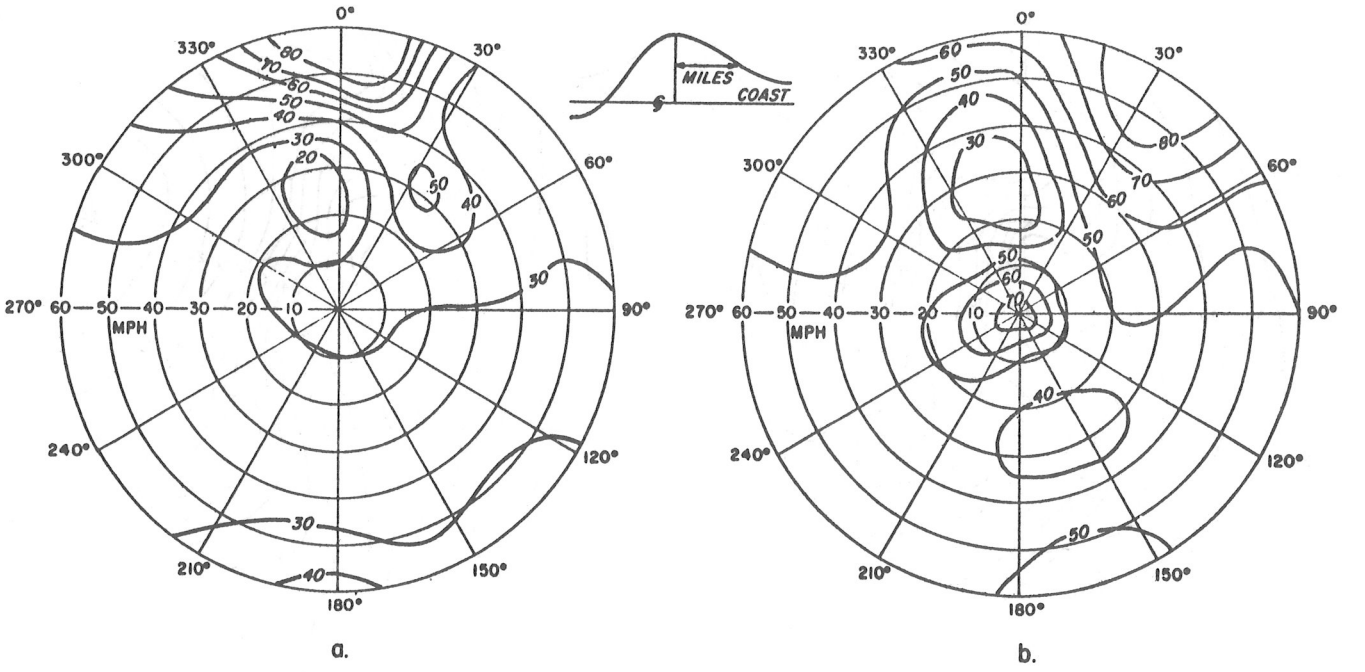

Figure 3.12. Contours of distance on coast, in statute miles, from point of peak surge to point on coast having ½ the peak surge, to the right of landfall. Arguments same as figure 3.9. (Jelesnianski, 1967)

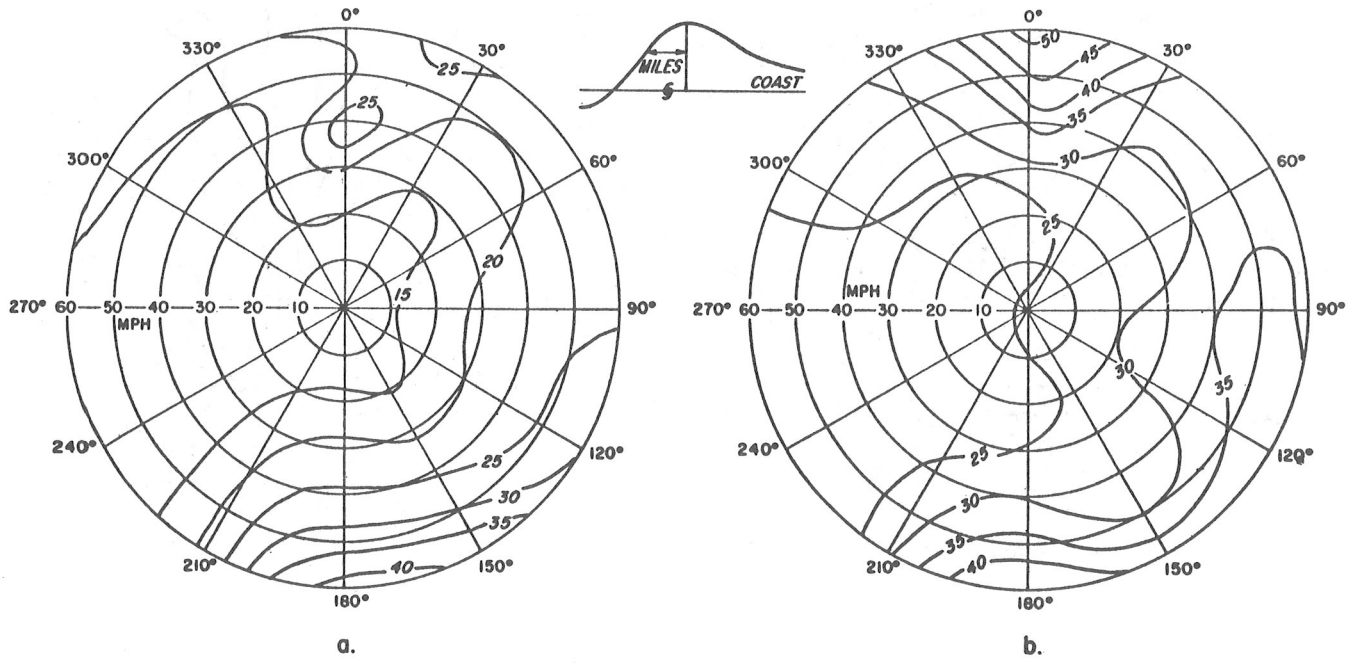

Figure 3.13. Same as Figure 3.12. but to left of landfall. (Jelesnianski, 1967)

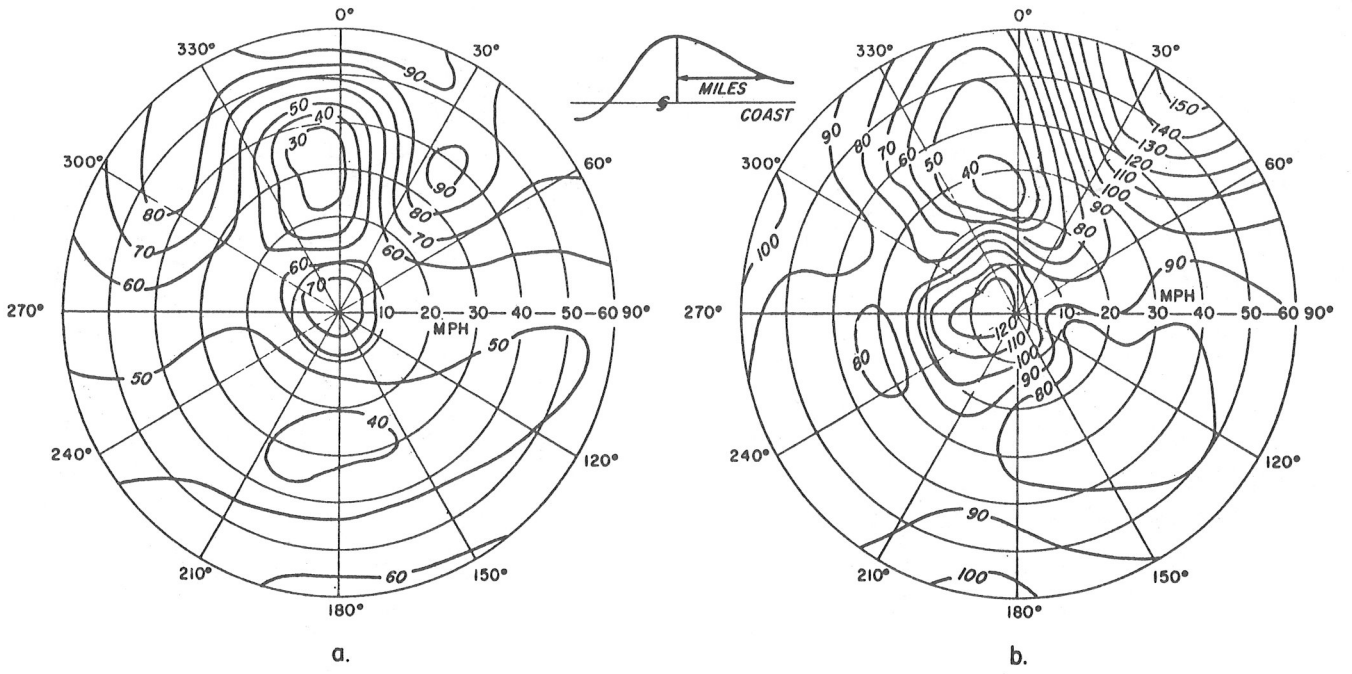

Figure 3.14. Same as Figure 3.12. but for $\frac{1}{4}$ peak surge value. (Jelesnianski, 1967)

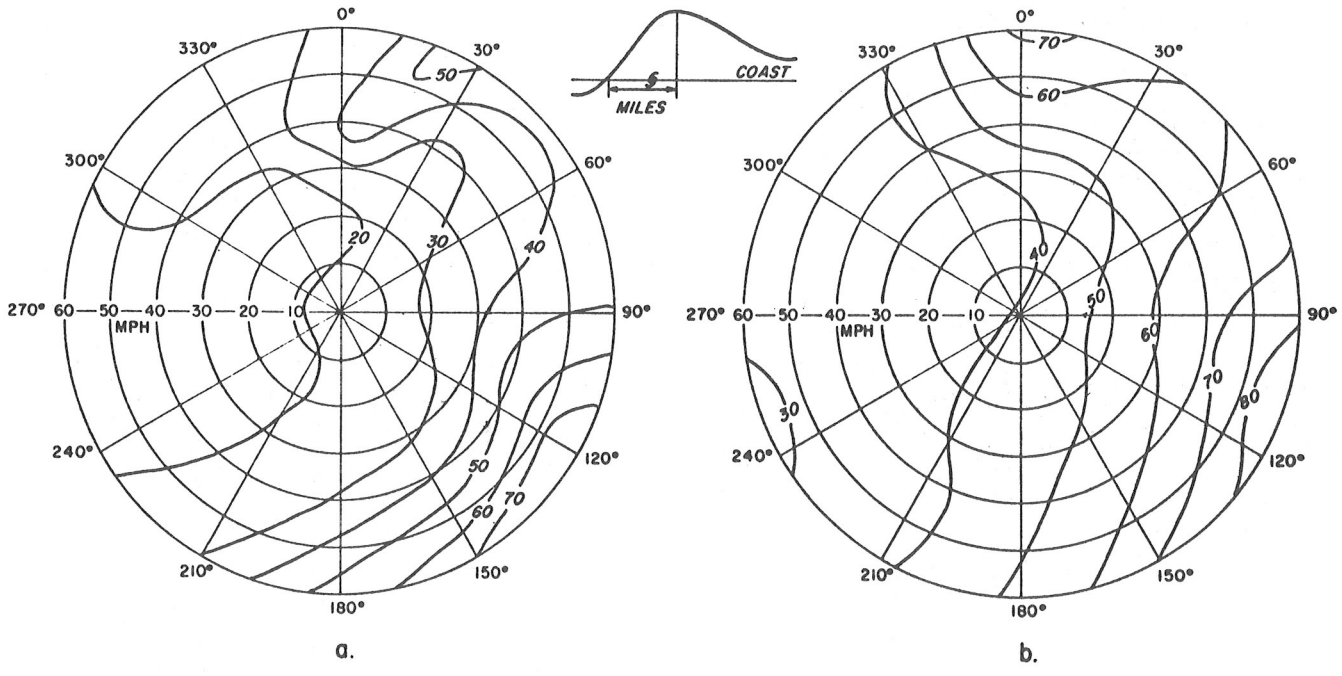

Figure 3.15. Distance, in statute miles, from peak surge to zero surge on the coast. Arguments same as Figure 3.9. (Jelesnianski, 1967)

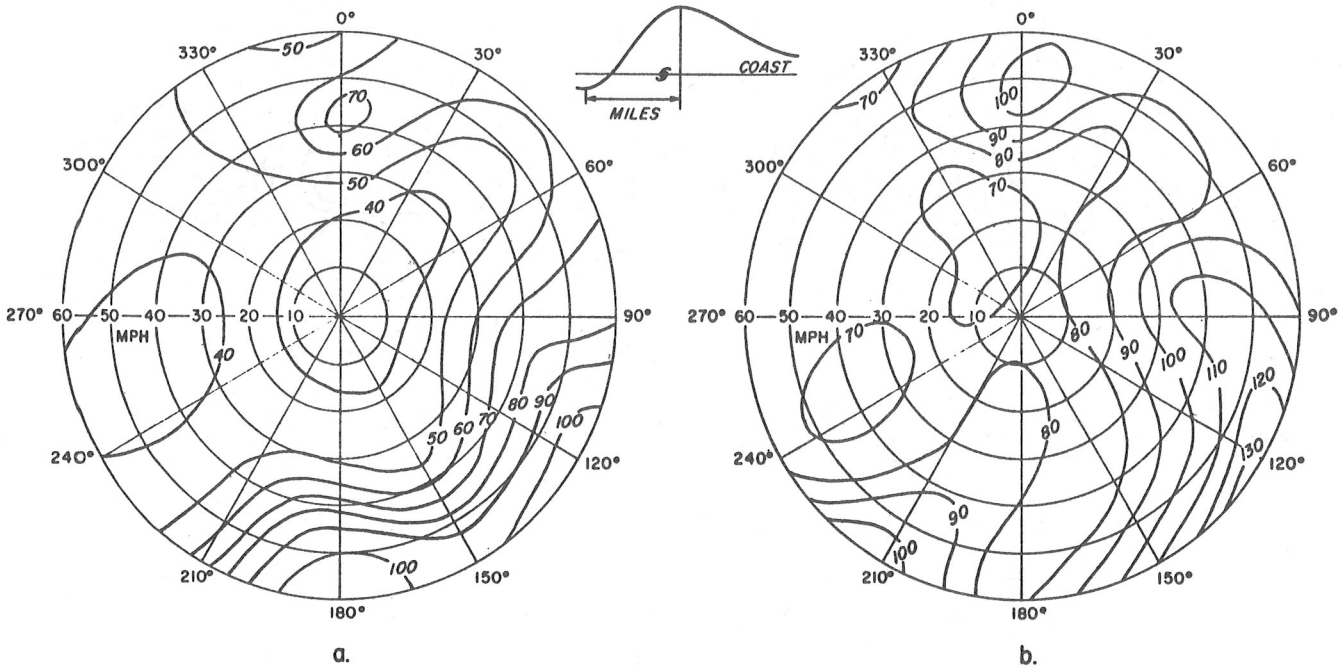

Figure 3.16. Distance, in statute miles, from peak surge to minimum surge on the coast. Arguments same as Figure 3.9. (Jelesnianski, 1967)

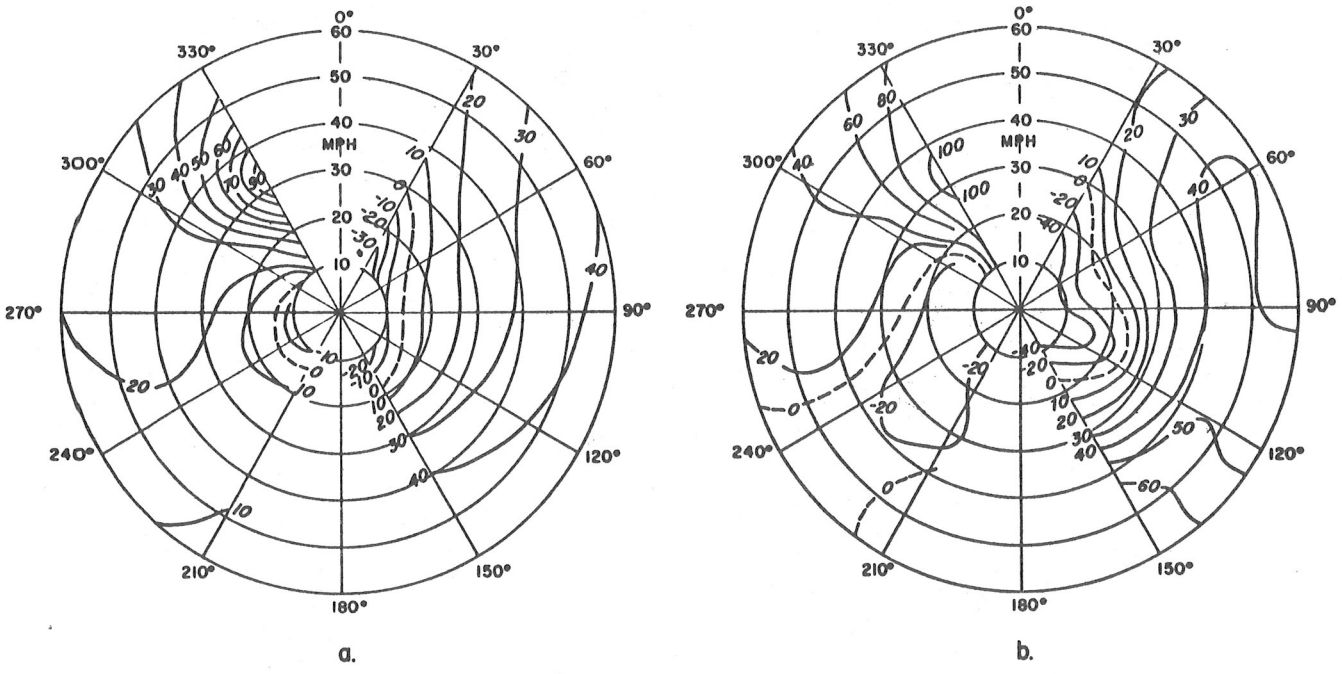

Figure 3.17. Arrival time, in minutes, of peak surge on the coast after storm landfall. Arguments same as Figure 3.9. (Jelesnianski, 1967)

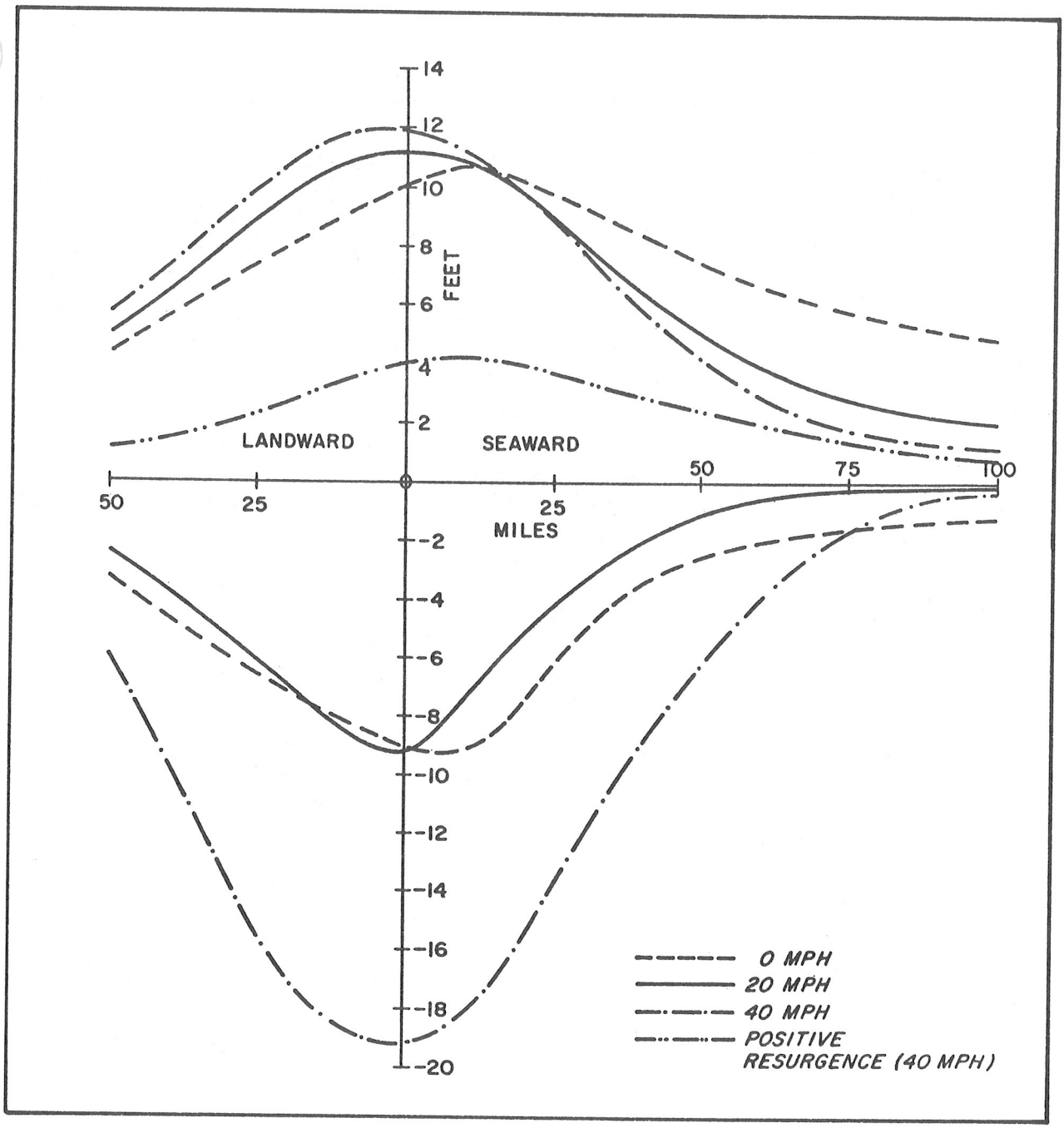

Figure 3.18. Height nomogram of the directly generated crest and trough, and the resurgence amplitude, for storms (standard storm and standard basin) moving at different speeds parallel to the coast. The abscissa is distance of the storm center from the coast in statute miles. (Jelesnianski, 1967)

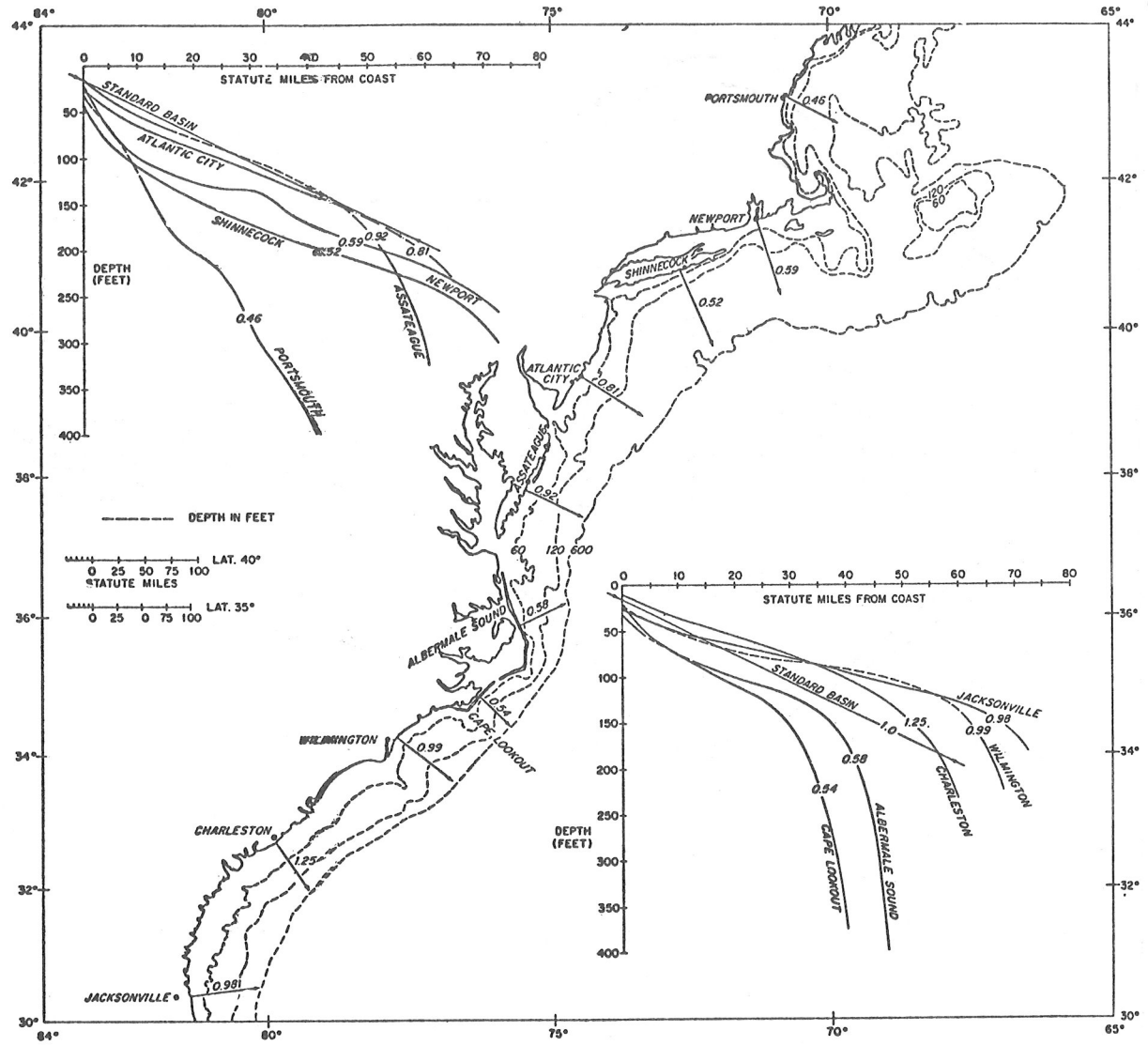

Figure 3.19. Correction factors at selected points along the Eastern Seaboard of the United States for depth profiles other than standard; the factors are used to correct precomputed surge heights in a standard basin. The inserts are the mean depth profiles of the selected points. (Jelesnianski, 1967)

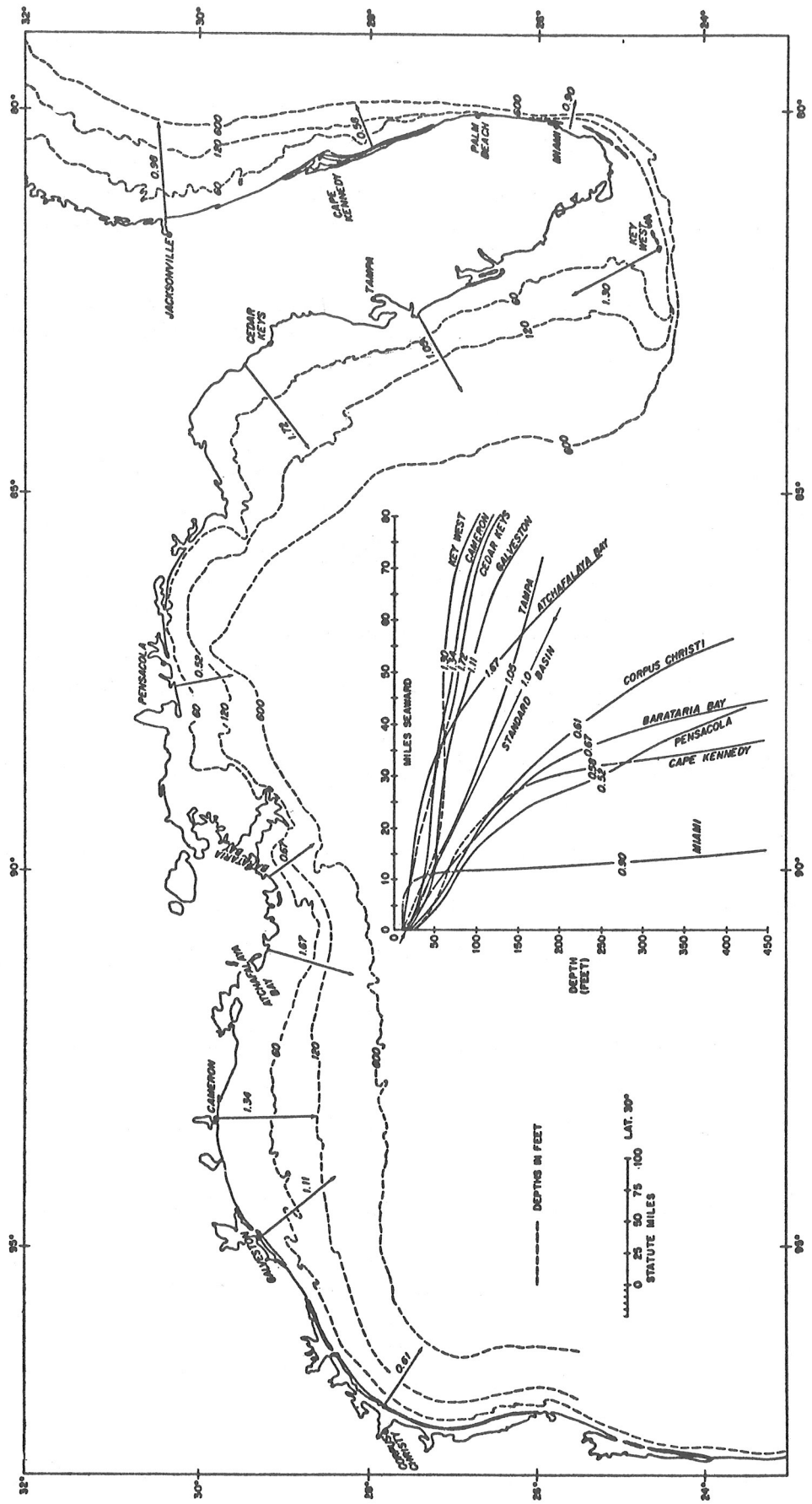

Figure 3.20. Same as Figure 3.19 for the Gulf States and Florida. (Jelesnianski, 1967)

IV. OCEAN SURFACE WAVES

Introduction

The most important geophysical phenomenon affecting the operation of ships is that of the waves on the surface of the ocean. These waves, of course, are caused by the action of the wind.

This section of this manuscript reviews certain basic wave characteristics, some historical background on empirical relationships, and selected wave forecasting methods that have been developed.

Basic wave characteristics

Discussion of basic wave characteristics can best begin with definitions of some of the relevant terms.

Figure 4.1 - from the Glossary of Oceanographic Terms (U.S. Naval Oceanographic Office, 1966) illustrates some basic wave characteristics.

Wave height is the vertical distance from trough to crest.

Significant wave height is the average height of the one-third highest waves.

Wave length is the horizontal distance between successive wave crests or troughs.

Wave period is time required for successive crests to pass a given point.

Wave speed is the forward speed of individual wave forms.

Group velocity is the forward speed of a wave group. In deep water group velocity is one-half wave velocity.

Wave frequency is the number of wave forms passing a stationary point per unit of time.

Fetch length is distance over water that the wind has essentially constant direction and speed.

Duration time refers to the length of time the wind blows over the fetch length.

Decay distance is the wave travel distance after leaving the wave generating area.

Wind-waves are wind generated waves still under the influence of the wind.

Fully developed sea is the maximum height to which wind-waves can be generated by a given wind speed blowing over sufficient fetch, regardless of duration.

Swell is the term applied to waves that have propagated from their area of generation.

The wave speed, for waves of relatively small height as compared to wave length, is given in H. O. Pub. 604 (U.S. Navy Hydrographic Office, 1951) as:

$$C = \sqrt{\frac{g L}{2\pi} \tanh \frac{2\pi d}{L}}$$

where C is wave speed, L is wave length, d is depth, and g is acceleration of gravity.

For very deep water d/L is large and $\tanh \frac{2\pi d}{L}$ approaches 1. The speed for deep water waves is therefore:

$$C = \sqrt{\frac{g L}{2\pi}}$$

In relatively shallow water d/L is small and $\tanh \frac{2\pi d}{L}$ approaches $\frac{2\pi d}{L}$ and therefore

$$C = \sqrt{gd}$$

Generally, waves in depths greater than one-half the wave length will have characteristics of deep water waves; waves in depths of less than 1/25 the wave length will have characteristics of shallow water waves (U.S. Navy Hydrographic Office, 1951). From this consideration, the speed of deep water waves depends on wave length, whereas the speed of shallow water waves is dependent on depth.

The group velocity, or speed at which wave trains travel out of the deep-water area of wave generation, is one-half the wave speed or phase velocity. The reason commonly given for this is that the leading wave is attenuated by expending some energy in setting the water particles in motion. Each wave in turn leaves some energy to be absorbed by the following wave. The result is that waves continually dissipate at the leading edge of the wave train and new waves form at the rear of the train. Deacon (1949) has reported that frequency analyses of wave spectra show that wave trains travel across oceans at a speed within five percent of the theoretical group velocity.

The interrelation of wave speed, length and period for deep water waves has been summarized according to theory in H. O. 604 (U.S. Navy Hydrographic Office, 1951) as:

$$C = \frac{L}{T} = \sqrt{\frac{gL}{2\pi}}$$

$$L = 2\pi \frac{c^2}{g} = \frac{gT^2}{2\pi}$$

$$T = \sqrt{2\pi \frac{L}{g}} = 2\pi \frac{c}{g}$$

Where C is wave speed, L is wave length, and T is wave period.

When C is in knots, L in feet and T in seconds, these become:

$$C = 1.34 \sqrt{L} = 3.03\ T$$

$$L = 0.555\ C^2 = 5.12\ T^2$$

$$T = 0.442 \sqrt{L} = 0.33\ C$$

The movement of the water particles and the variation in circular paths with depth are shown in figure 4.2 from H. O. 604 (U.S. Navy Hydrographic Office, 1951). The individual water particles of the wave move in circular paths. The radius of such paths (r) depends on the height (H), and length (L) of the waves and varies with depth (d) according to:

$$r = \frac{H\, e^{\frac{-2\pi d}{L}}}{2}$$

Historical background

There have been many empirical relationships derived which relate the wave height to wind conditions and fetch length. A review of some of these relationships as presented in The Oceans (Sverdrup, Johnson and Fleming, 1942) and in Physical Oceanography (Defant, 1961) is given below.

The first empirical formula for wave height was by T. Stevenson in 1851:

$$H = 1/3 \sqrt{F}$$

where H is greatest wave height in meters and F is fetch length in kilometers.

Boergen in 1890 developed a relationship between wave height and duration time of the wind:

$$H = Hm/(1 + \frac{a}{t})$$

where H is wave height, Hm is the maximum wave height for the wind speed, t is the duration time of the wind and a is a constant determined from observations.

In 1934, Cornish obtained the formula:

$$H = 0.48W$$

where H is height of the highest wave in meters, and W is wind speed in meters per second.

Zimmerman, Patton and Marmer, in 1932, for the height of highest wave (H) obtained:

$$H = 0.44W$$

where W is wind speed in meters per second.

In 1935, Rossby and Montgomery proposed:

$$H = \frac{0.3}{g}W^2$$

where

H is maximum wave height in meters

W is wind speed in meters per second

g is acceleration of gravity

and the constant 0.3 was selected to fit the available data.

The Sverdrup-Munk technique of forecasting wind-waves and swell

Before 1942, the science of ocean wave forecasting was limited to a few empirical relationships. These were not consistent with each other. World War II amphibious operations created an urgent need for sea and swell forecasts. The naval and military operation planners needed wind-wave and swell forecasts in order to anticipate wave conditions near the shores where amphibious operations were to be carried out.

The task of developing a forecast method for operational use was given to Dr. Sverdrup and Dr. Munk at Scripps Institution of Oceanography. By the summer of 1943 they had developed the method. Kinsman (1965) in his discussion of the method points out the great significance it had by stating, "...there are some thousands of World War II veterans alive today who would have been dead in the surf had Sverdrup and Munk not done their best with what they had."

Advances in wave theory and techniques for statistical analysis and description of waves have rendered the Sverdrup-Munk technique rather obsolete. However, the method (as modified by Bretschneider (1952a)) is still in rather wide use, because it continues to be one of the simplest and fastest methods for use by a forecaster to produce wave forecasts that agree reasonably well with observations. It is interesting that comparison of the growth of wave height by a recently developed method (Marks et al., 1968) shows good agreement with the results of the Sverdrup-Munk method.

The wave forecast relationships originally derived were modified slightly by Bretschneider in 1952 by adding more recent data to the original data of Sverdrup and Munk.

To use the method, one determines the wind speed, duration time and fetch length from analyzed and prognostic weather charts and then from graphs determines the significant wave length and period for the point of forecast. The determination of swell is made by entering another graph with the wave period and the wave decay distance (distance the waves travel as swell from their point of origin).

The wind-wave forecast graphs (U.S. Army Coastal Engineering Research Center, 1966) given as figures 4.3 and 4.4 are the forecasting technique of Sverdrup and Munk as revised by Bretschneider (commonly called the S-M-B method). The wave height for any particular wind speed can be limited by either the fetch length or duration time unless both of them are great enough for fully developed wave conditions to exist. The wave forecast graph of figures 4.3 and 4.4 is entered with wind speed, fetch length and duration time, and the lowest height indicated either by duration time or fetch length is the forecast. An example in the use of these charts is taken from Technical Report No. 4 of the U.S. Army Coastal Engineering Research Center (1966). The example is for a 35 knot wind of 10 hours duration and a fetch length of 200 nautical miles. Entering figure 4.3 at 35 knots from the left side, a duration of 10 hours is met before a fetch length of 200 nautical miles which indicates the duration time to be the limiting factor. The wave height is read from the graph as 14.7 feet, the wave period as 9.6 seconds. If the fetch had been 80 nautical miles with duration still 10 hours, the fetch would be the limiting factor. The wave height and period would then be 12.7 feet and 8.7 seconds.

Dotted lines of constant H^2T^2, which can be thought of as lines of constant wave energy, are included in figures 4.3 and 4.4. These are used for making wave forecasts when the value of the fetch or wind speed changes between synoptic map times. Adjustment to the fetch and duration times are made by following along these lines of constant wave energy. A detailed description of these adjustments is given in Technical Report No. 4 of the U.S. Army Coastal Engineering Research Center (1966).

As the waves propagate out of the area of generation the various wave components separate because of the different component speeds. The resulting significant heights and period, are determined as a function of wave period at the end of the fetch and the decay distance, which is the wave travel distance from the end of fetch to the forecast point.

Figure 4.5 shows the wave period at the end of decay distance (T_D), the ratio of the wave height at end of decay to the wave height at the end of fetch (H_D/H_F), and the travel time from end of fetch to forecast point (t_D), as functions of wave period at end of fetch (TF) and the decay distance (D). The following paragraph from H.O. 604 gives instructions for the use of figure 4.5.

"Figure 4.5 is the decay diagram. Enter on the left with the wave period at the end of the fetch. Proceed horizontally to the vertical representing decay distance. At this intersection read the reduction factor H_D/H_F, the travel time, and the period at the end of the decay. The inset on this plate gives the wave speed and wave length appropriate to the wave period."

An example for waves advancing through a region of calm wind is reproduced here from H.O. 604:

Given HF = 18 feet

TF = 9 seconds

D = 600 miles

From figure 4.5 T_D = 12.1 seconds

H_D/H_F = 0.46 H_D = 8.3 ft.

t_d = 33 hours

Whenever the waves travel through an area of wind which is other than calm the height and period are modified differently, depending on whether the wind is following or opposing the waves. An effective decay distance is substituted for the actual decay distance. For following winds the effective decay distance is less than the actual decay distance and for opposing winds the effective decay distance is greater than the actual decay distance. The magnitude of the ratio of effective decay distance to actual decay distance depends upon the difference between the wave speed and the wind speed.

Figure 4.6 from Bretschneider(1952a),includes the fetch length as a factor in determining the height and period of swell. This figure indicates that for waves leaving the fetch with a given period, the shorter the fetch the greater the increase of period and the greater the decrease of height. The reason for including fetch length as a factor in swell decay as given by Bretschneider (1952a),is that greater wind speeds are necessary to generate a given period in short fetches. Such waves are higher and steeper than those generated in longer fetches and will therefore decay more rapidly.

The increase in wave period is determined from the upper part of figure 4.6 by entering horizontally with the wave period, going vertically to the curve of decay distance, then horizontally to the fetch length and vertically to the ratio of swell period to wave period at end of fetch. The lower portion of the figure is used similarly to determine the decrease in height of the swell. Examples of each type of determination are shown in the figure.

The Pierson-Neumann-James method of forecasting ocean waves

The Pierson-Neumann-James method of forecasting ocean waves, commonly called the PNJ method, is described in detail in Hydrographic Office Publication No. 603 (U.S. Navy Hydrographic Office, 1955). This report gives only a brief outline of the method.

The PNJ method is based on statistics and treats the surface waves as a combination of small size waves of various heights, periods and directions. The wave heights summed over the frequency range are represented by the wave spectrum. The spectrum is estimated from the wind field and the wave characteristics are determined from the wave spectrum.

This method considers a variable called E, with the dimensions of feet squared to describe some of the properties of wave heights. A definition of E, from H. O. 603 is "twice the variance of a large number of values from points equally spaced in time as chosen from a wave record."

Some of the statistical characteristics of wave height as related to E are:

Most frequent wave height will be	1.41	$\sqrt{E}$ feet
Average height will be	1.77	$\sqrt{E}$ feet
Significant height will be	2.83	$\sqrt{E}$ feet
Average height of 1/10 highest	3.60	$\sqrt{E}$ feet.

The distribution of the squares of the wave height with frequency is described by the spectrum of the waves. The forecast of the spectrum, which is determined by meteorological conditions, is the first step in the wave forecasting procedure. Figure 4.7 shows wave spectra for fully developed seas at three wind speeds. In this figure it can be seen that the most significant frequency extends toward lower frequency values for higher wind speeds.

Co-cumulative spectra curves (C.C.S.) are used instead of spectrum curves for the integration of the spectra. The construction of the C.C.S. curves from the spectrum is illustrated in figure 4.8. Beginning at the high frequency end of the spectrum the area is summed and represented on the co-cumulative spectrum. These C.C.S. curves have been computed for various wind speeds.

The wave characteristics can be limited by either the length of the fetch or the duration time of the wind or both. For that reason the graphs containing the C.C.S. curves contain lines of wind duration for use when the generated sea is not fully developed because of a limitation of duration time. Other graphs containing the C.C.S. curves contain lines of equal fetch length for use when the generated sea is less than fully developed because of fetch length limitations.

There are certain disadvantages in using the C.C.S. curves because of the linear scales. Therefore the PNJ manual gives a set of distorted C.C.S. curves in which the E values are on a non-linear scale, the significant wave height scale is linear, and there is a change of scale after a certain point on the frequency scale.

So far, only wave generation as a function of wind speed, duration, and fetch length have been discussed. The PNJ manual points out that in considering wave propagation for the forecasting of swell two other processes are important.

One of these processes is the wave dispersion which is the separating out of the waves of different frequencies because of their different group velocities. The problem is to find the range of the periods which will have reached the forecast point at forecast time. Group velocity (C_g) can be expressed in knots as:

$$C_g = 1.515\ T$$

where T is the wave period in seconds. Distance traveled (D) in nautical miles is equal to speed times travel time:

$$D = 1.515\ T \times \text{time}$$

The shortest period of the waves (T_2) to be expected can be expressed as:

$$T_2 = \frac{D}{1.515\ t_{ob}}$$

where t_{ob} is the longest time the waves could have traveled from the generating area. The longest period of the waves to be expected (T_1) can be expressed as:

$$T_1 = \frac{D}{1.515\ (t_{ob} - t_w)}$$

where t_w is the number of hours after the waves in the storm began that these longest period waves began propagating toward the forecast point.

The other process in wave propagation is the angular spreading. This occurs because the waves in the generating area are traveling in many different directions. The angles from the edges of the fetch to the forecast point should be determined as illustrated in figure 4.9. Here only the waves moving in a direction from θ_3 to θ_4 can reach the forecast point.

The effects of dispersion and angular spreading are combined by determining T_2 and T_1, the shortest and longest periods which are expected and multiplying the difference of the values of E for each of these periods by the percent of relative wave energy as determined by the angular spreading.

PNJ refers to the formulae that determine the wave frequencies and wave directions at a forecast point as wave forecasting filters. They present various filters in H. O. 603 such as those for a storm moving to windward or the case of when the winds cease in a generating area.

In the case of waves arriving at a forecast point from two or more generating areas, the values of E associated with the various generating areas are added together and used to describe the wave conditions of the forecast point.

The U.S. Naval Oceanographic Office wave prediction system

The Naval Oceanographic Office wave prediction system is a two dimensional spectral method. The grid used at present for the specification of the wind and wave spectra is shown in figure 4.10. The resolution of spectra into 15 frequency bands for 12 directions requires 180 numbers for each of the 519 grid points.

References to this system of wave forecasting includes work of the following: Baer (1962), Pierson and Tick (1964) and Moskowitz (1966). Baer (1962) programmed the model for forecasting the wave spectra which used the Neumann spectrum and considered the angular dispersion of waves. Energy growth was determined from a tabulated form of the co-cumulative spectra curves of H. O. 603 (U.S. Navy Hydrographic Office, 1955).

The present system is based on a spectral form by Pierson and Moskowitz (1964) and derived from 460 wave records made on British weather ships with the Tucker shipborne wave recorders. An energy growth function is used along with the angular spreading factor.

At present the meteorological input is the computed wind at the 19.5 meter level as determined from the 1000 mb geostrophic wind at six hour intervals. Computations are made for three hour intervals, which requires that each set of geostrophic wind calculations be used twice.

In the wave spectra forecast three operations are considered: growth, dissipation, and propagation. In the growth step the contribution of the wind components with favorable directions (-90° to + 90°) is computed for each grid point. If the waves at the grid point are not fully developed the wave growth contributed by the favorable wind for the appropriate frequencies and directions is added to the waves present at the point.

The waves which are traveling within 90° against the wind are decreased in the dissipation step. This attenuation is greater for the shorter period waves.

By considering the growth and dissipation steps every three hours, the spectral fields are updated for each frequency and direction. The various wave components are then propagated, each in its own direction at the appropriate group velocity. Whenever the wave components reach nearby grid points the energy there is consequently increased. The propagation of swell is automatically accounted for in this process. Those wave components which propagate beyond the grid are eliminated from further consideration.

The output of this program is 180 numbers for each grid point representing the directional wave spectra. From these spectra, desired information such as significant wave height or direction can be extracted.

Weather Bureau automated wave forecast technique

The Weather Bureau wave forecast technique is patterned after that of the Fleet Numerical Weather Central (FNWC) (Hubert, 1964). The FNWC method is an adaptation of the Sverdrup-Munk-Bretschneider system. The adaptation and further development work at FNWC were accomplished by E. M. Carlstead, W. E. Hubert, N. M. Stevenson and others.

The Weather Bureau wave forecast program is run twice daily at the National Meteorological Center (NMC) and uses the wind forecast of the Primitive Equation (PE) Model as input. This description of the method is based upon two earlier reports by Pore and Richardson (1967, 1969).

The 1000-mb PE wind forecasts are the basis of the wind-wave forecasts. Comparison of these wind calculations with observed winds at the Ocean Station Vessels showed that the PE wind calculations should be adjusted by shifting them 20° toward low pressure and reducing their speeds to 86% of their calculated values. Data were examined in an effort to find the effect of low level atmospheric stability. Air-sea temperature difference data were compared to PE wind calculations and observed winds at the Ocean Station Vessels. Consideration of these data indicated that the PE wind forecasts should not be modified on the basis of air-sea temperature difference.

The wind-wave program is used for calculating the significant wave height and significant wave period. Significant wave height is defined as the average height of the one-third highest waves. Significant wave period is the average period of the one-third highest waves.

Calculations are made for points of the NMC octagonal grid as shown in figure 4.11. The program is given information which specifies which of the grid points are land or polar ice, so that wave forecasts will be made only for ocean areas. The distribution of land and ice is also considered in determining fetch length restrictions.

The wave forecasts are based upon the NMC Primitive Equation (PE) Model 1000-mb-level wind calculations. The winds for the 18-hour period prior to the time of the wave forecast are considered. To make a wind-wave forecast for time T, the winds at times T, T-6, T-12 and T-18 hours are used.

For any particular forecast time wind data are obtained from:

1. The current PE output tape, and

2. A wind and wave history tape updated by the previous program run made 12 hours earlier.

The duration of the wind is determined by comparing the wind direction at time T with that at time T-6, etc., until a wind shift of more than 22° is found. The duration is therefore determined to be 0, 6, 12, or 18 hours.

Once the duration at a grid point is determined, an effective wind speed is calculated for that duration time. The effective wind speed is a weighted mean such that the more recent winds are given heavier weight. Each wind contributes as much as all of the earlier winds in the calculation.

The expressions for wave height and period are:

$$H_w = K_1 V^2 D + K_2$$

$$T_w = V (K_3 + K_4 D) + K_5$$

where H_w is significant wave height,

T_w is significant wave period,

V is effective wind speed,

D is duration of wind, and

K's are constants.

At computation points near land or ice, consideration is given to the possibility of fetch limitations. A determination is made in the upstream direction from each computation point for the existence of land or ice within approximately 1 or 2 grid lengths. If land or ice is found within 1 grid length, the wave height is reduced to 70 percent of its value. Land or ice between 1 and 2 grid lengths causes the wave height to be reduced to 90 percent of the computed value.

Wind-wave calculations are made for +00, +12, +24, +36, and +48 hours from the time of the latest PE output. Variables which can be printed out include effective wind speed, significant wave height, period, and direction.

Calculations of swell are made for ocean points of the NMC octagonal grid. The program is given a map factor at each grid point. These map factors are used to determine the map projection distance the swell travels, since this distance is a function of latitude.

The swell forecasts are based upon the +00, +12, and +24 hour forecasts of the wind-waves. A minimum travel time of 15 hours is required before a wind-wave is considered to have moved from its generation area to become a swell. Therefore, to make a swell forecast for time T, wind-waves at times T-24, T-36, T-48, T-60, and T-72 hours are used.

For any particular forecast time wind-wave data and swell data are obtained from a wind and wave history tape updated by the previous program run made 12 hours earlier.

Starting from the oldest field on the wave history tape (T-72 hours), each wind-wave having a height greater than 5 feet is considered as a potential swell. A preliminary swell travel distance is computed. Travel distance (d) of waves depends on group velocity of the waves (C_g) and the travel time (t) in the following form:

$$d = C_g \times t$$

The group velocity (C_g) depends upon the period of waves as shown here:

$$C_g = A \times T$$

where T is the period of the waves,

and A is a constant.

As swell propagate from the area of generation, the longer period components (with the larger group velocities) outrun the shorter period components. This results in increasing periods of significant swell with increasing distance from the generation area.

The expression for approximate swell travel distance therefore is:

$$d = C_1 \overline{T} \; t \; m$$

where d is distance traveled,

$\overline{T}$ is the mean of the period of the waves (T_W) when they leave the generation area and their period (T_S) when they arrive as swell at the forecast point,

t is travel time,

m is the map factor at point of generation,

and C_1 is a constant.

Once the preliminary travel distance has been computed, a search is made along the entire path of the wave. If land or ice has been specified within 0.72 grid lengths of the path of the wave, the wind-wave is discarded.

Each wave train is allowed to spread 75 degrees either side of the center line of travel. A more accurate travel distance is computed for each grid point over water (affected point) within a 150 degree spread about the center line of swell propagation. The expression for computing this distance is the same as the expression for approximate swell travel distance, except m is replaced by $\bar{m}$, which is an average map factor over the area traveled. The affected point is then tested against a distance requirement. This requirement is that the affected point lies within the range of travel distance of the swell for the particular forecast period. If this requirement is satisfied, swell period and height are computed for the affected point by the following expressions:

$$T_s = (T_w^2 + C_2 t)^{\frac{1}{2}}$$

$$H_s = H_w (T_s / T_w)^{C_3} \cos \alpha$$

where T_s is the period of the swell,

T_w is the period of the wind-wave leaving the generation area,

t is travel time from generating point to affected point,

H_s is the swell height,

H_w is the initial wind-wave height,

α is the angle between direction of center line of swell propagation and direction to affected grid point,

and C_2 and C_3 are constants.

Since any grid point can be hit by many swells, only the greatest swell height is retained at the affected point.

Swell calculations are made for +24, +36, and +48 hours. Variables which can be printed out include swell height, period, and direction.

An overall wave condition, a combined-height field, is constructed as the square root of the sum of the squares of the wind-wave and swell heights.

Output charts prepared for facsimile transmission consist of 24- and 36-hour contoured charts of wind-wave height, swell height, and combined-wave height. These are drawn by the NMC curve follower (Electronic Associates, Inc.) on a 1:30,000,000 polar stereographic base map for the area of the NMC octagonal grid. A sample chart is shown in figure 4.12.

Sections of these hemispheric charts are extracted for facsimile transmission. Figure 4.13 is a sample Atlantic area chart for the East Coast FOFAX circuit. Figure 4.14 shows the area included for the West Coast FOFAX circuit and the Suitland-Honolulu-SW Pacific circuit. The combined-wave prognoses for a portion of the North Pacific as shown in figure 4.15 are included in the Alaskan prog package on the National Weather Facsimile Circuit.

This wave and swell forecasting system is for deep-water wave conditions on the high seas. At this point we feel that the wave conditions in off-shore waters of moderate depth may be adequately forecast. Certainly, breaker and surf forecasts are not to be implied from these high seas forecasts. Wave and swell heights are depicted by contours drawn at 3-foot intervals with maximum values printed at the centers. The discontinuous nature of waves at coastlines raises a problem in contouring of wave heights close to shore. This problem has been partially overcome by having some wave height contours drawn as intersecting the coast lines. These should be considered as terminating at that intersection. Exceptions are made in the cases where the surface wind is forecast to be offshore. Gradients of wind-wave heights in these cases are packed offshore in a realistic manner.

Although the significant wave height (defined as the average height of the one-third highest waves) is the variable which is forecast, other properties of wave height distribution are of value. Statistical analyses and theoretical investigations (U.S. Army Coastal Engineering Research Center, 1966) show the following relationships:

a. Mean wave height = 0.6 x significant wave height.

b. Mean height of highest 10% of waves = 1.3 x significant wave height.

c. Maximum wave height = 1.9 x significant wave height.

These relationships indicate possible wave heights, for any given forecast, to be almost double the significant wave height. Further discussion of the uses of wave forecasts from an operational viewpoint is contained in Technical Report No. 4 of U.S. Army Coastal Engineering Research Center (1966).

Little confidence can be placed in the wave forecasts in the vicinity of tropical storms. The spacing of NMC grid points precludes adequate depiction of wave conditions in these areas unless the storm is large enough to affect values of parameters at grid points at initial and forecast times.

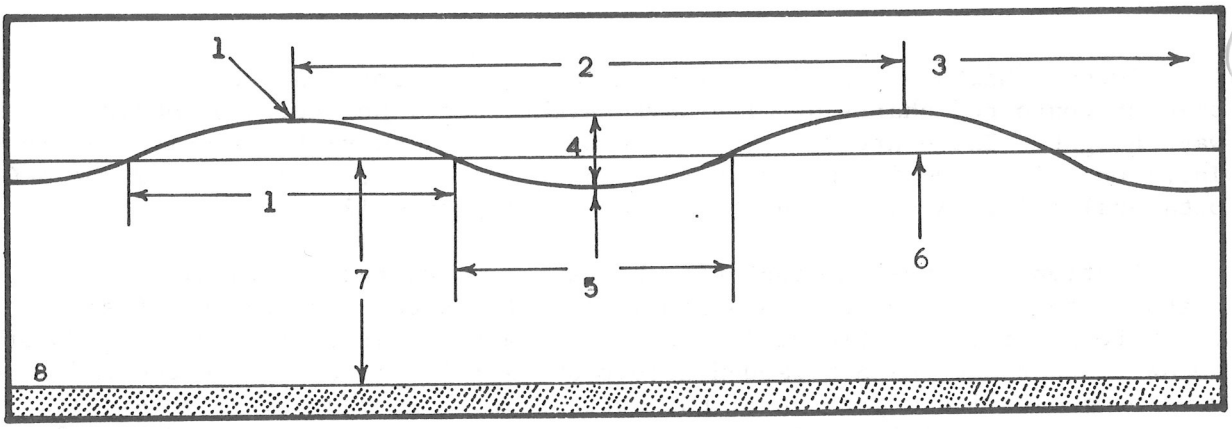

WAVE CHARACTERISTICS

1. Wave crest; 2. Wave length; 3. Direction of wave travel; 4. Height; 5. Wave trough; 6. Still water level; 7. Depth; 8. Ocean bottom

Figure 4.1. Illustration of several wave characteristics. (U.S. Naval Oceanographic Office, 1966)

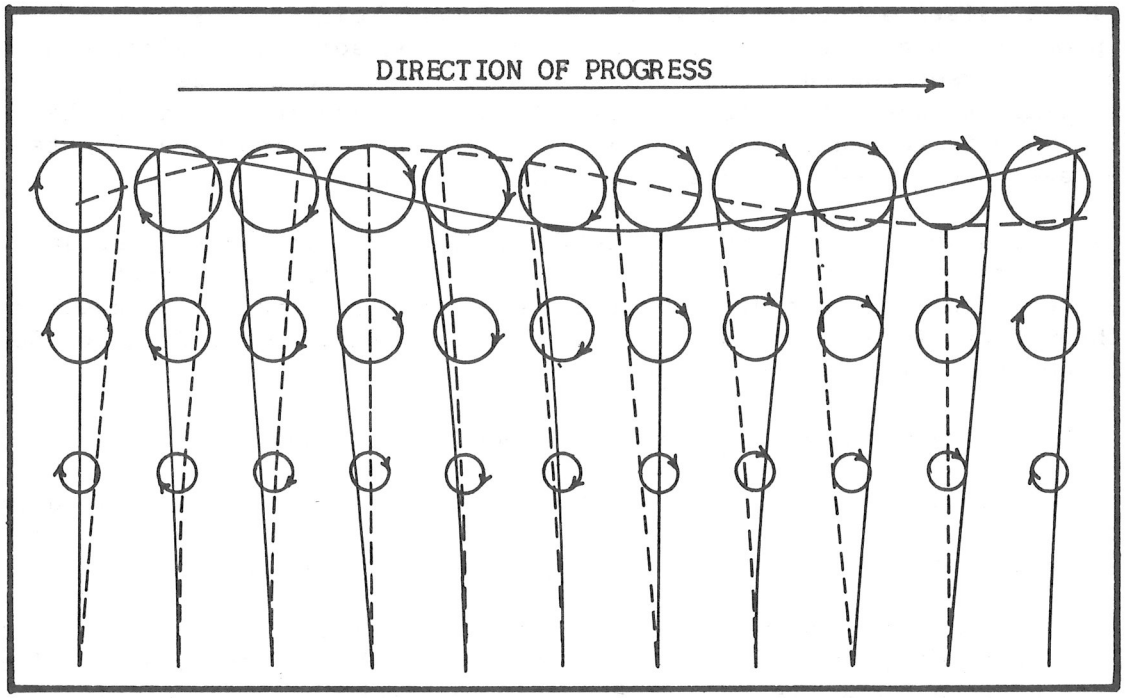

Figure 4.2. Movement of water particles in a deepwater wave. The circles show the paths in which the water particles move. The wave profiles and the positions of a series of water particles are shown at two instants which are one-fourth of a period apart. The solid, nearly vertical lines indicate the relative positions of water particles which lie exactly on vertical lines when the crest or trough of the wave passes and the dashed lines show the relative positions of the same particles one-fourth of a period later. (U.S. Navy Hydrographic Office, 1951)

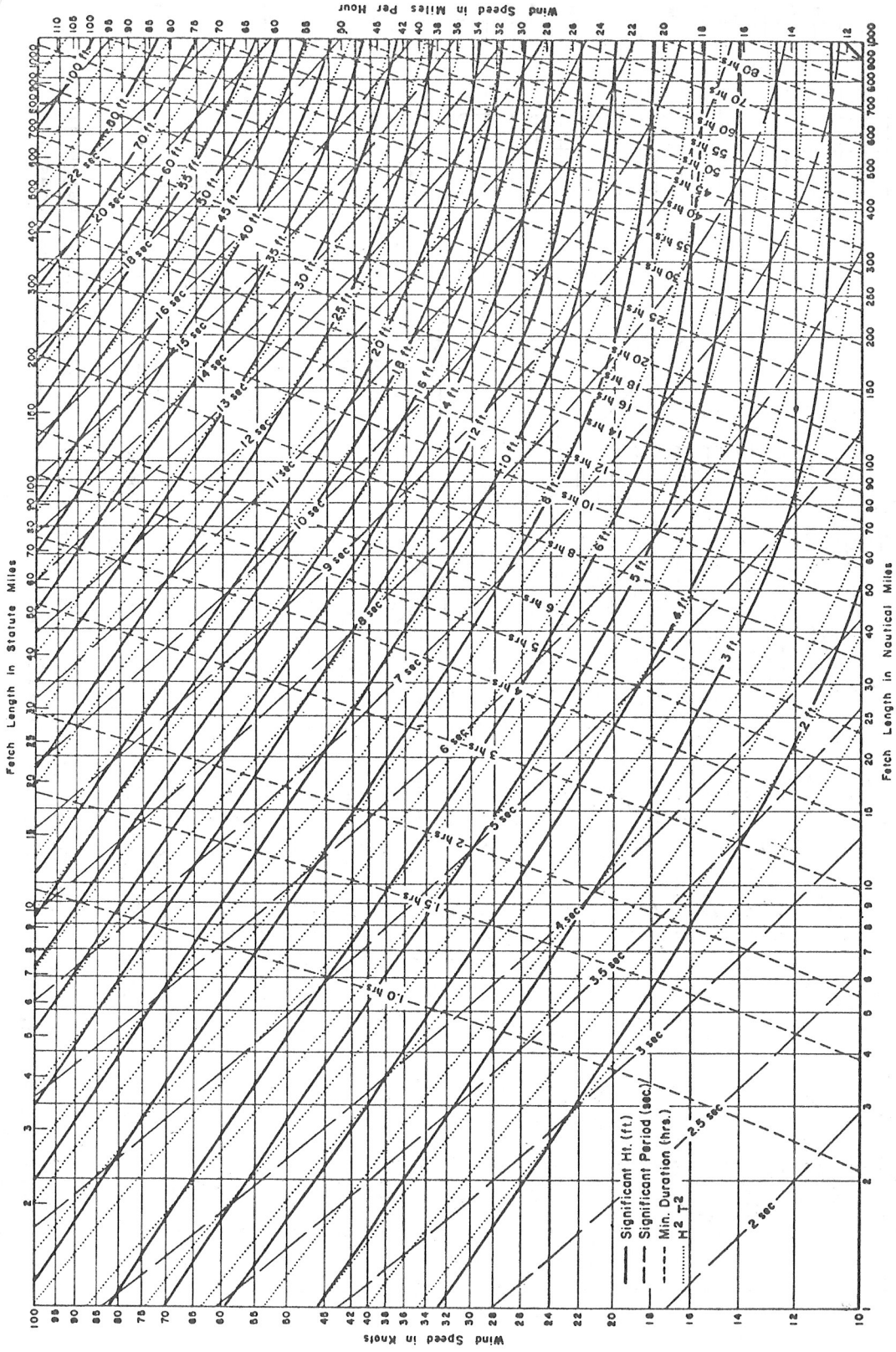

Figure 4.3. Deep water wave forecasting curves as a function of wind speed, fetch length and wind duration, for fetches of 1 to 1000 miles. (U.S. Army Coastal Engineering Research Center, 1966)

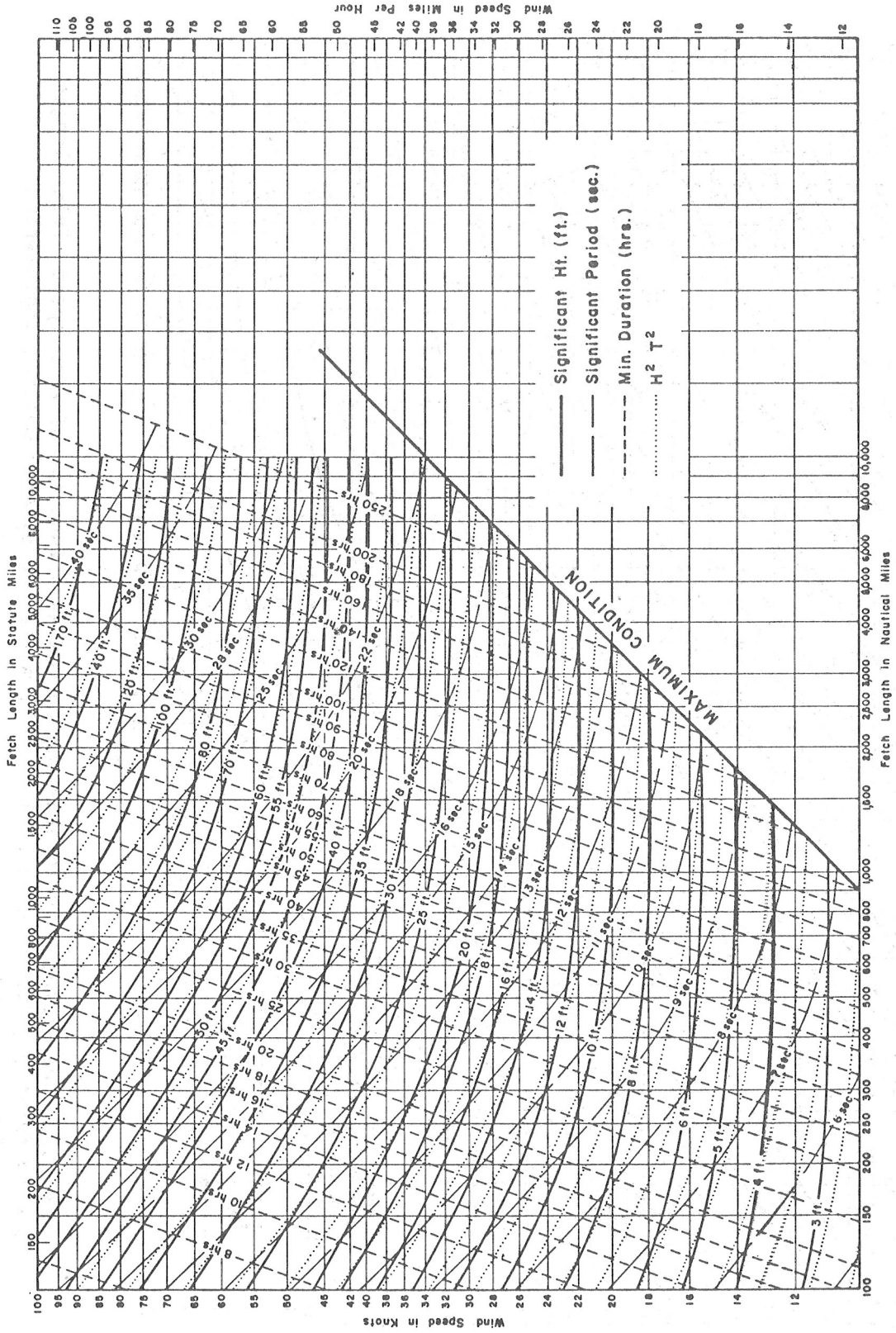

Figure 4.4. Deep water wave forecasting curves as a function of wind speed, fetch length and wind duration, for fetches of 100 to >1000 miles. (U.S. Army Coastal Engineering Research Center, 1966)

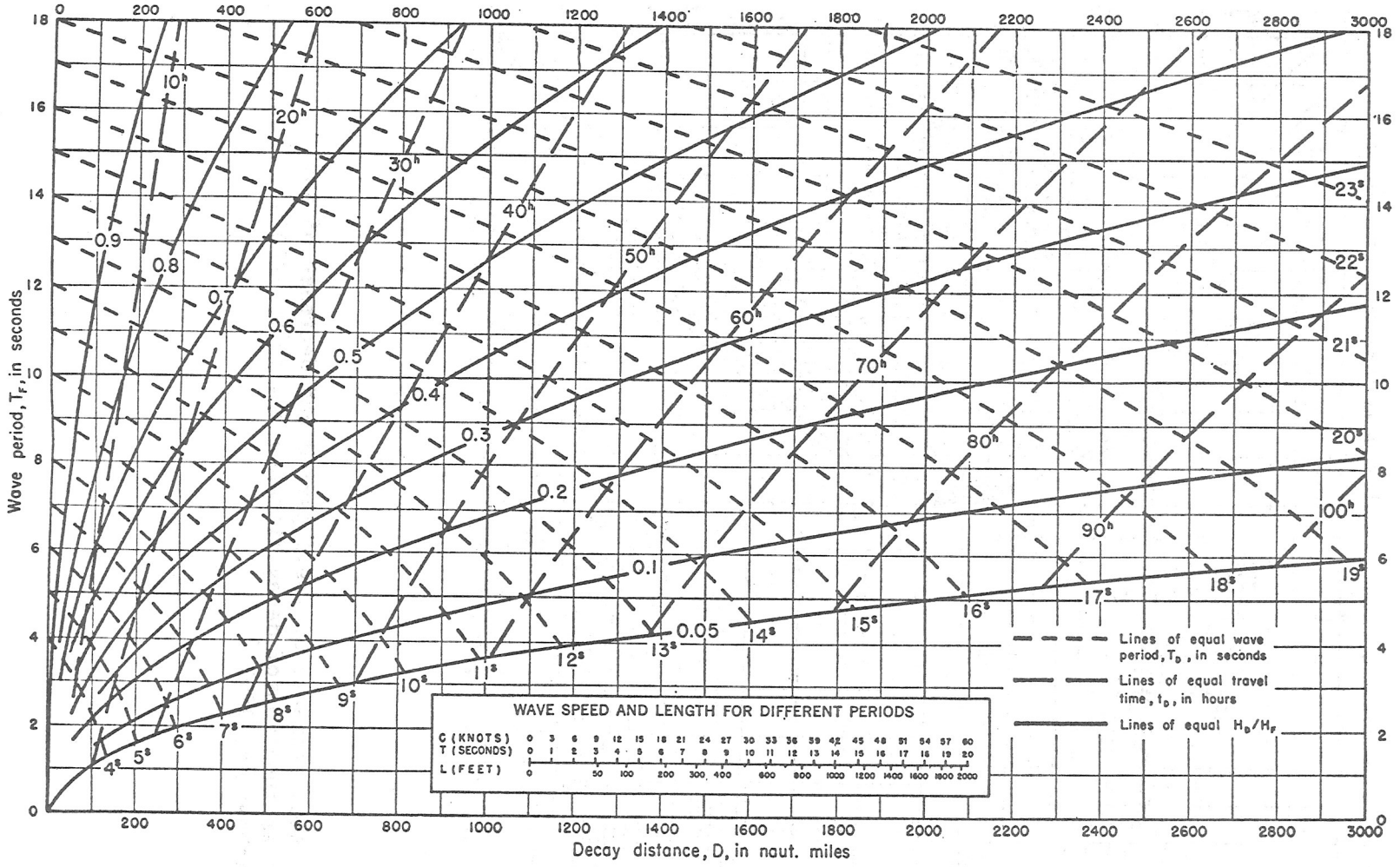

Figure 4.5. Wave period at end of decay distance, travel time, and ratio between wave height at end of decay distance and at end of fetch as functions of decay distance and wave period at end of fetch. (U.S. Navy Hydrographic Office, 1951)

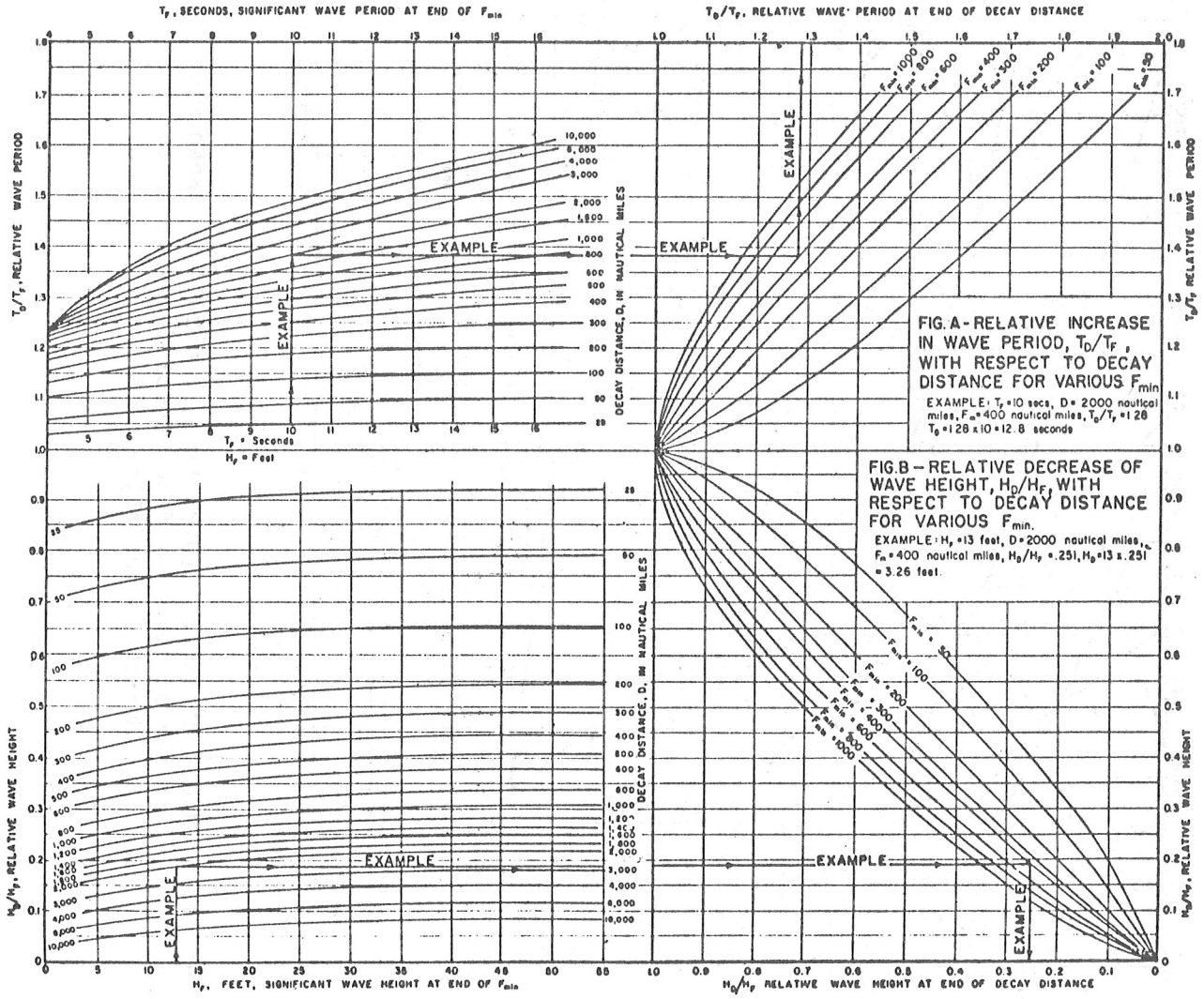

Figure 4.6. Increase of swell period and decrease of swell height as functions of decay distance and fetch length. (Bretschneider, 1952 a)

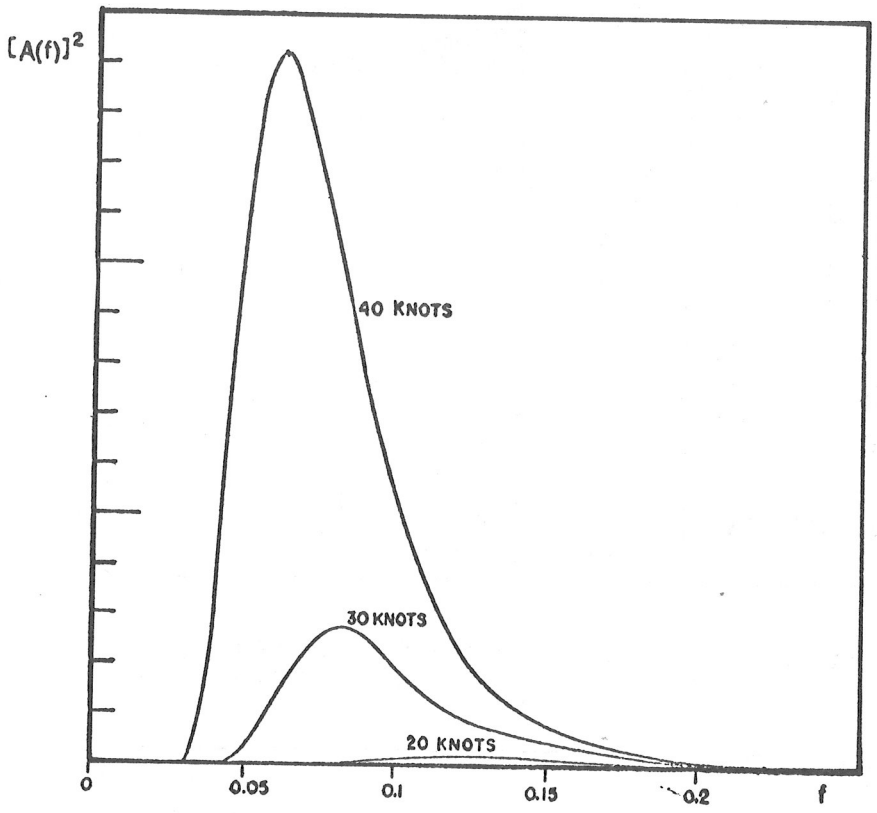

Figure 4.7. Continuous wave spectra for fully arisen sea at wind speeds of 20, 30 and 40 knots. The abscissa shows the scale of wave frequency, f. The area under the curves has the dimension of feet-square. The displacement of the maximum energy band is from high to low frequencies with increasing wind speeds. (U.S. Navy Hydrographic Office, 1955)

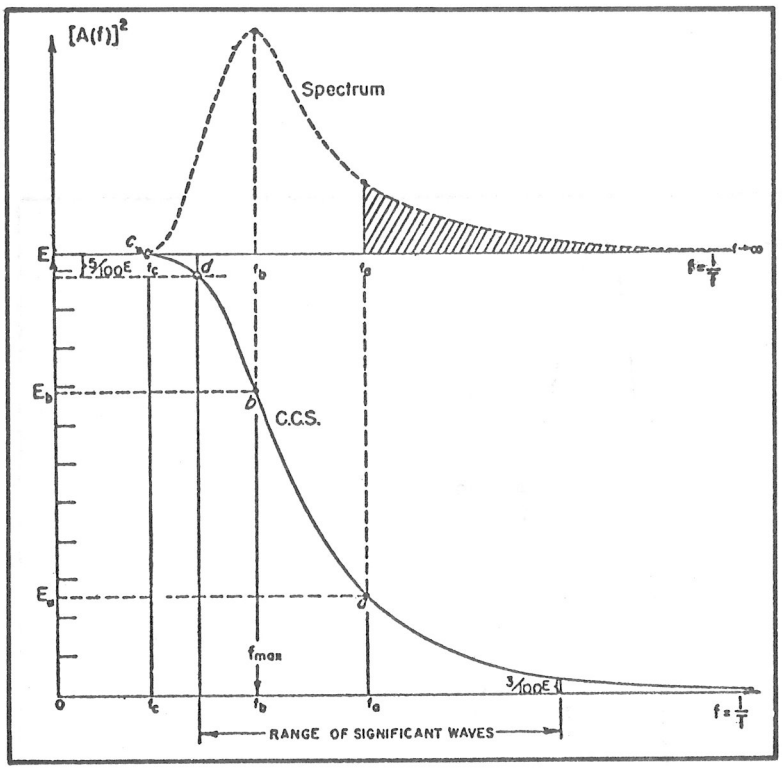

Figure 4.8. Wave spectrum and co-cumulative spectrum. (U.S. Navy Hydrographic Office, 1955)

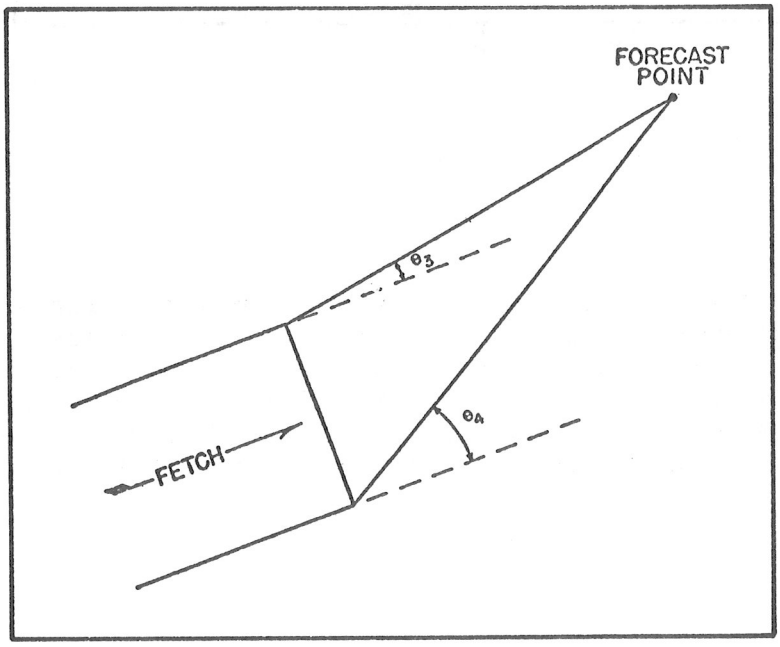

Figure 4.9. Limits of angular spreading of wave components leaving a fetch area which will affect the indicated forecast point. (U.S. Navy Hydrographic Office, 1955)

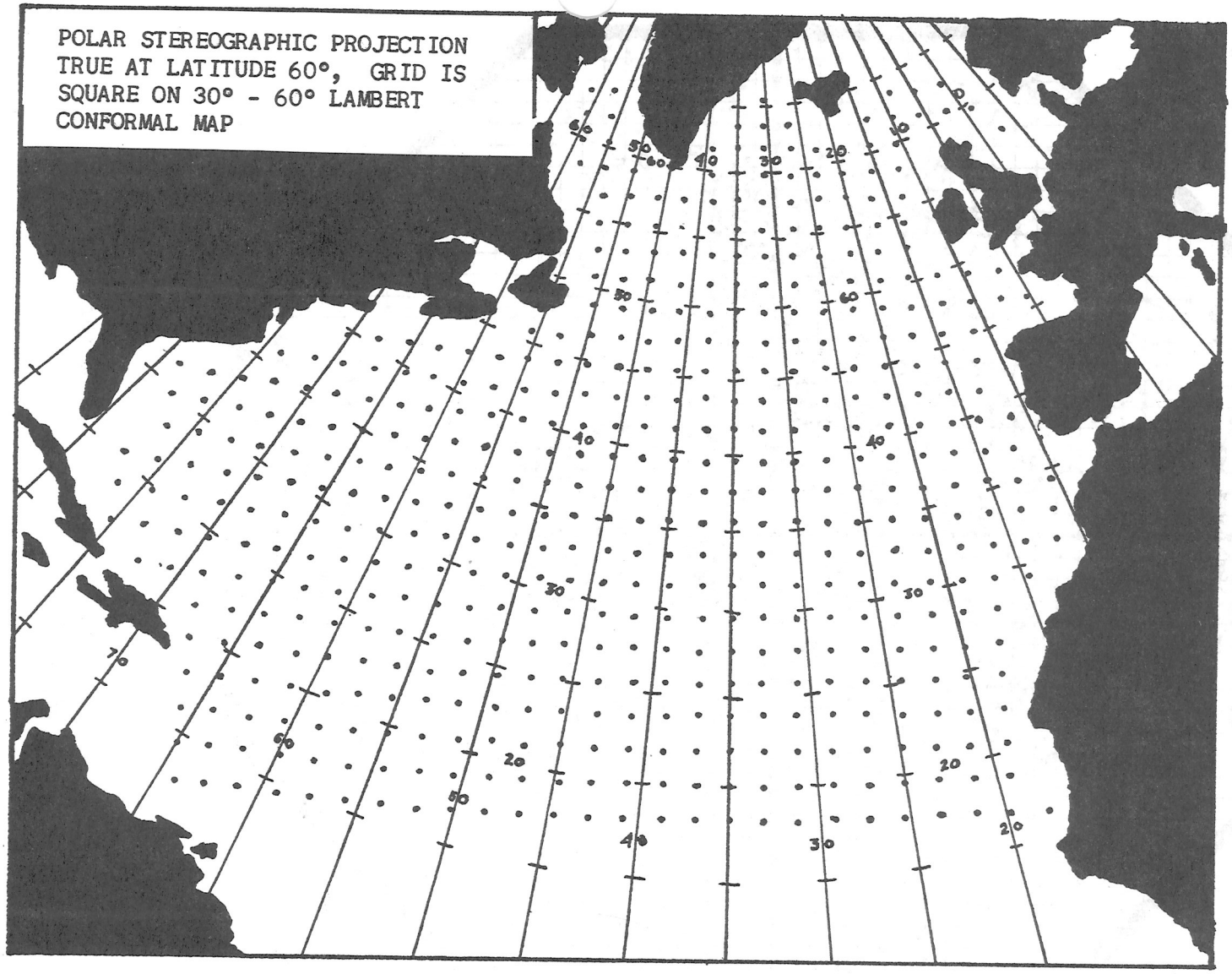

Figure 4.10. Grid used to specify wind and wave fields of the Naval Oceanographic Office Wave Prediction System. (Moskowitz, 1966)

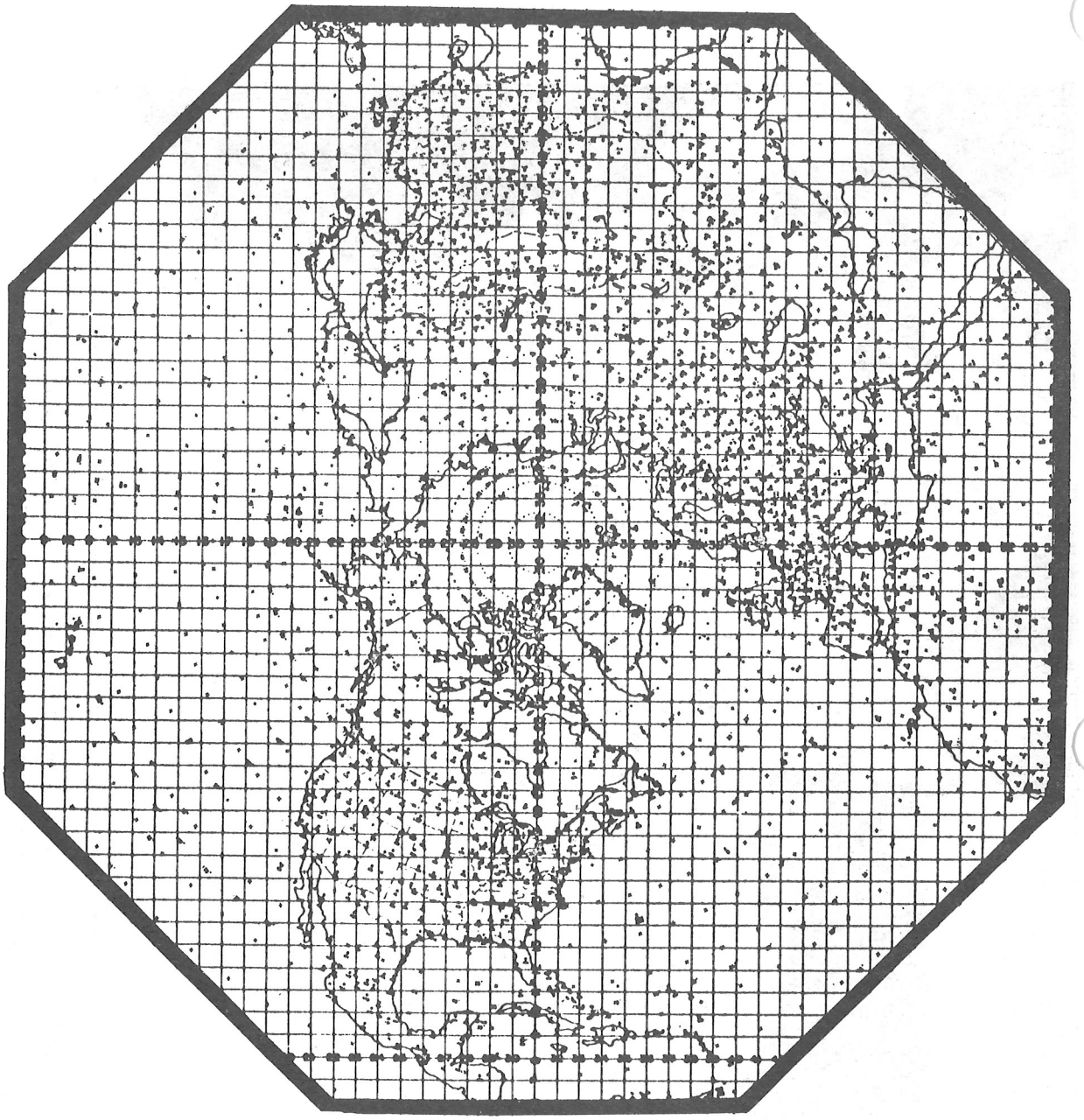

Figure 4.11. National Meteorological Center grid used for computation.

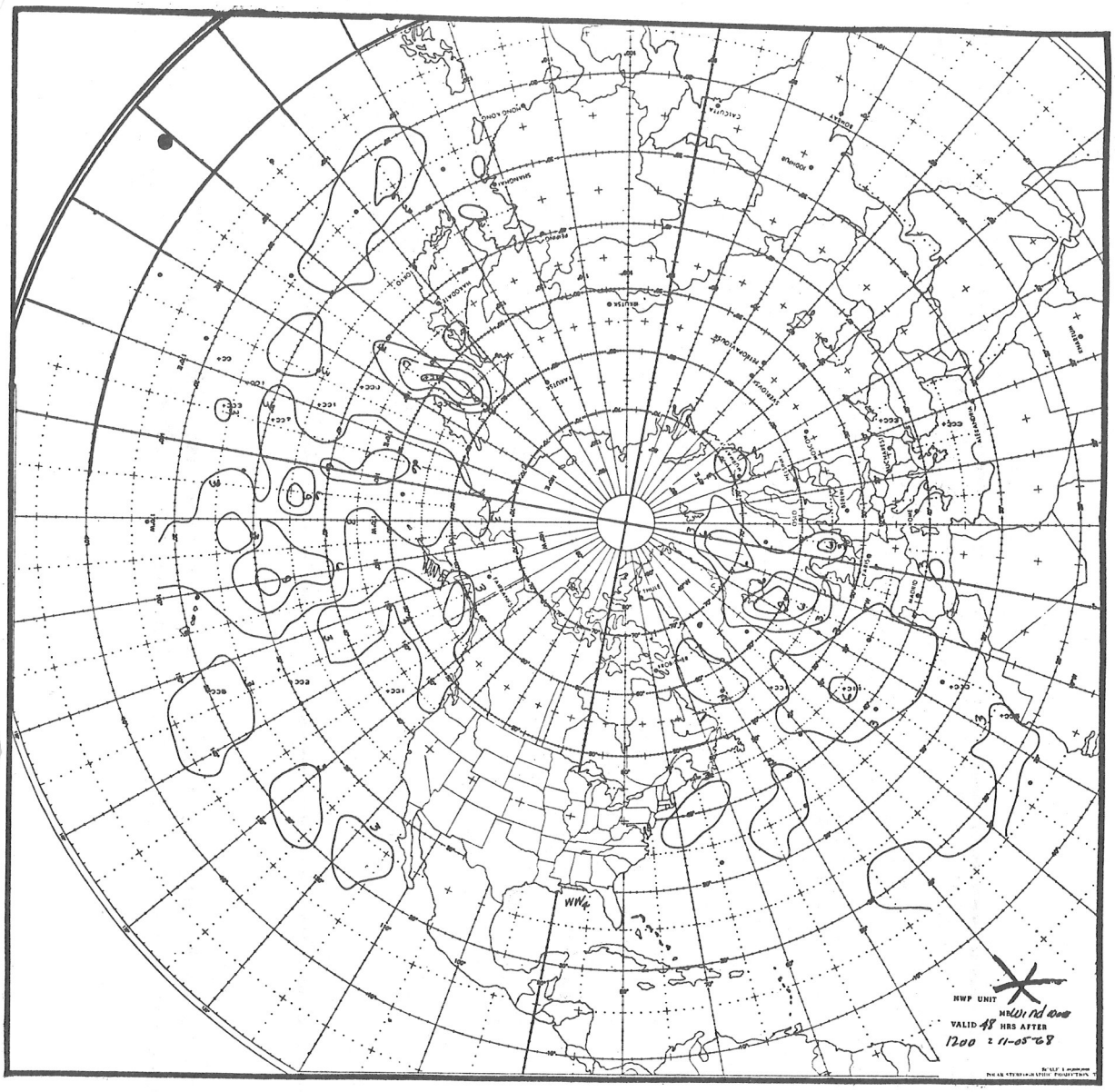

Figure 4.12. Sample wind-wave height forecast chart as prepared by the NMC curve follower. Contours are drawn at intervals of three feet. (Pore and Richardson, 1969)

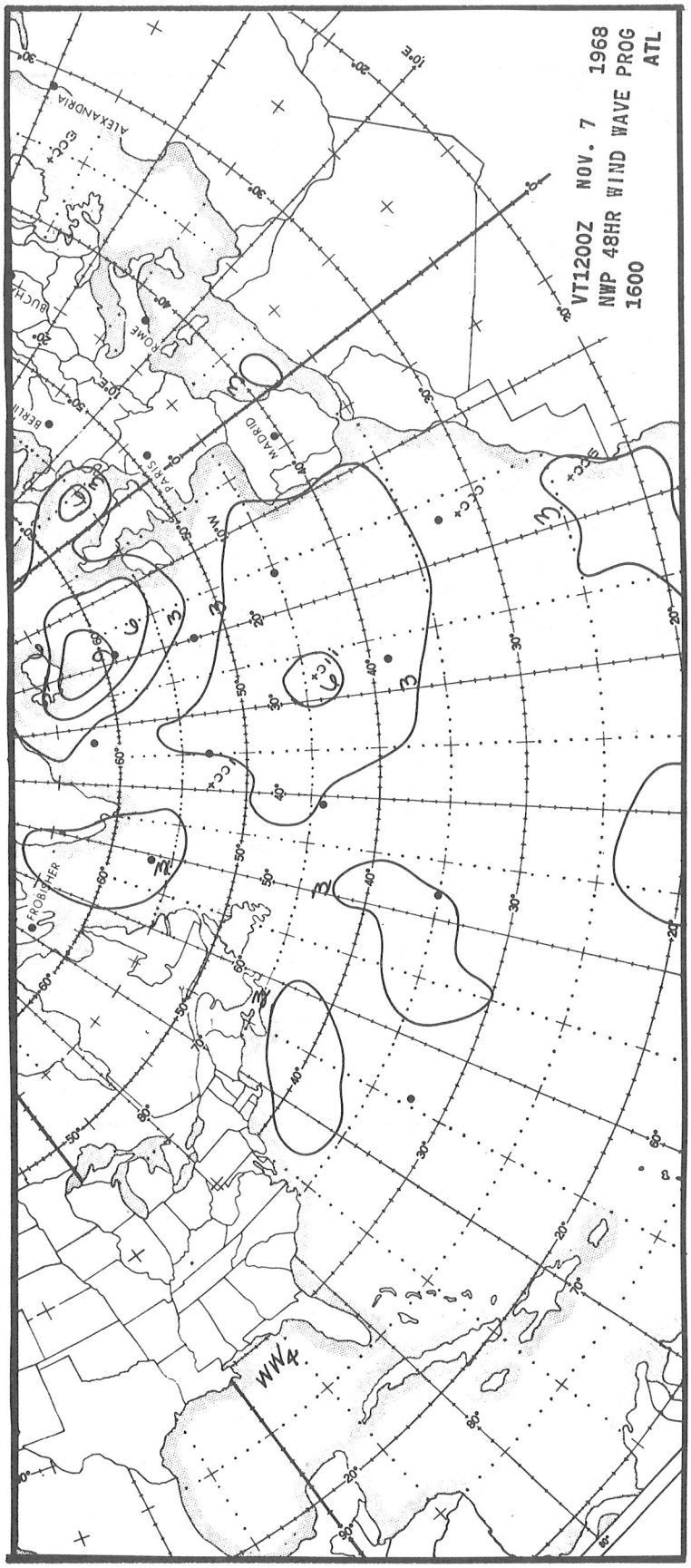

Figure 4.13. Sample wind-wave height forecast chart for East Coast FOFAX Facsimile circuit. Contour interval is three feet. (Pore and Richardson, 1969)

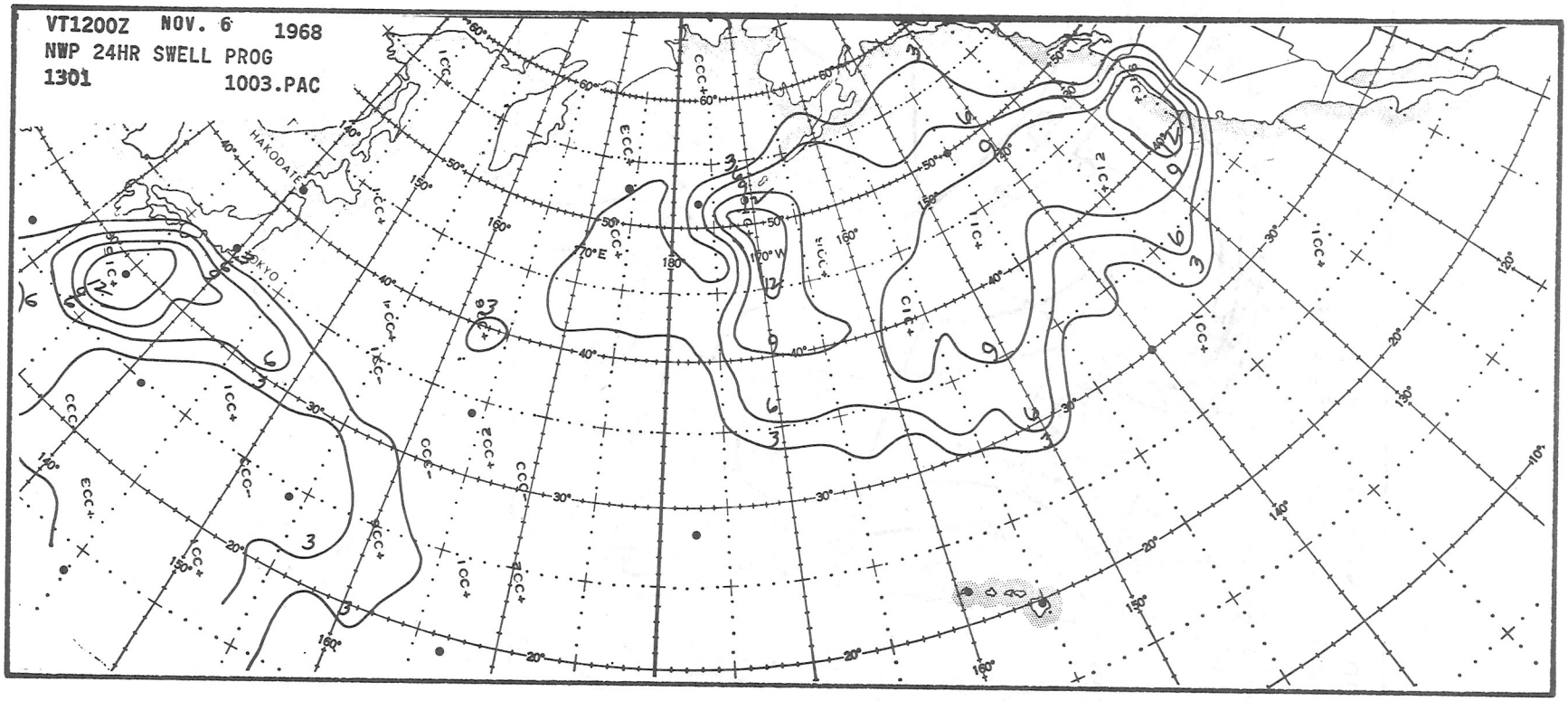

Figure 4.14. Sample swell height forecast chart for West Coast FOFAX and the Suitland-Hono-Southwest Pacific Facsimile Circuits. Contour interval is three feet. (Pore and Richardson, 1969)

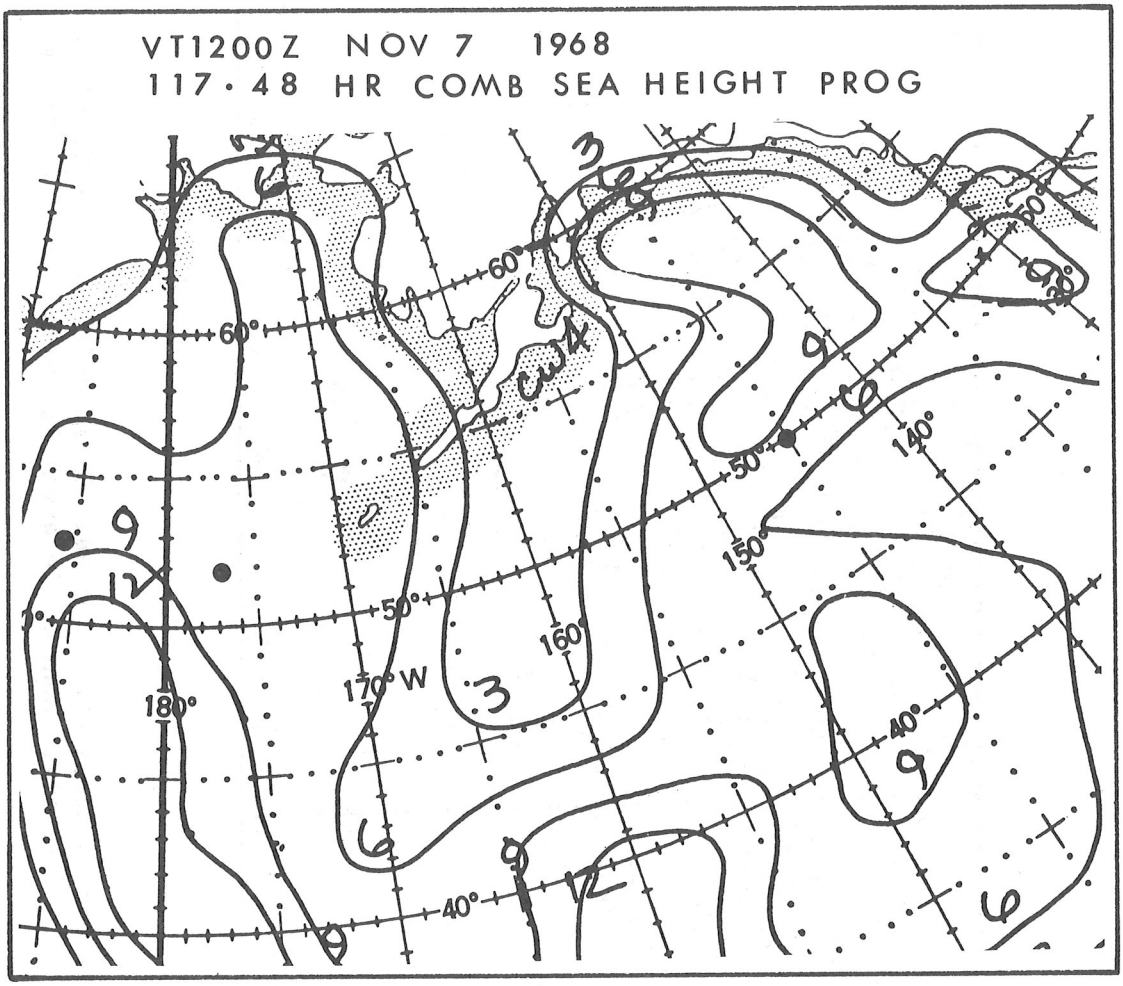

Figure 4.15. Sample of combined-wave height forecast chart which is included in the Alasken Prog package on the National Weather Facsimile Circuit. Contour interval is three feet. (Pore and Richardson, 1969)

V. BREAKERS

Introduction

As a wave approaches the shore, the wave speed decreases, the wave height increases, and the wave steepness increases. At some critical depth, when the forward speed of the top of the crest exceeds the wave speed, the wave becomes unstable and breaks. The breaking process dissipates the final energy of the wave and often results in physical changes of the beach. The transformation of waves into breakers is illustrated in figure 5.1.

Definitions

Several definitions applicable taken from Technical Report No. 4 of U.S. Army Coastal Engineering Research Center (1966) are:

Breaker - A wave breaking on the shore, over a reef, etc.

Breaker Depth - The still water depth at the point where the wave breaks

Surf - The wave activity in the area between the shore line and the outermost limit of breakers

Surf Zone - The area between the outermost breaker and the limit of wave uprush.

Shoaling and Refraction

As the waves approach shore and their speed is decreased there are two effects to alter the wave characteristics. These are shoaling and refraction.

The shoaling effect is expressed in H. O. Pub. No. 234 (U.S. Navy Dept., 1944) as:

$$\frac{H}{H_o} = \sqrt{\frac{1}{2}\,\frac{1}{n}\,\frac{1}{C/C_o}}$$

where

H_o is deep water wave height,

H is wave height at point in question,

C_o is deep water wave speed,

C is wave speed at point in question, and

n is fraction of energy carried forward with advancing waves at at point in question.

The fraction n is expressed as:

$$n = \tfrac{1}{2}\left[1 + \frac{4\pi\,(d/L)}{\sinh\,(4\,\pi\,d/L)}\right]$$

where

d is the depth at point in question, and

L is wavelength at point in question.

As the waves first reach the shoal area the height initially decreases because the effect of n is more important than the effect of the C/C_o term. At a depth of about 0.06 of the initial wave length the wave has regained its initial height. Progressing on into shallower water the wave then becomes higher. This shoaling effect is shown graphically in figure 5.2 from H. O. Pub. No. 602 (U.S. Navy Hydrographic Office, 1953). Here the ratio of height to deep water wave height is shown as a function of the ratio of depth to deep water wave length. Also included in this graph is a curve showing the change of wave length and wave speed. Laboratory experiments with wave tanks and field observations are in rough agreement on the initial decrease and then the increase of wave heights because of shoaling.

Wave refraction as defined in the Glossary of Oceanographic Terms (U.S. Naval Oceanographic Office, 1966) as "the process by which the direction of a train of waves moving in shallow water at an angle to the contours is changed." As a wave progresses shoreward from deep water at an angle to the bottom contours, the inshore portion of the wave crest will be in shallower water and consequently will have a lower speed than the portion of the wave in deeper water. The resulting bending of the wave crest is such that the crest tends to conform to the bottom contour pattern. This refraction results in changes of the wave direction and changes of the wave height.

The wave bending and wave height changes can be determined by the construction of a wave refraction diagram which is defined (U.S. Naval Oceanographic Office, 1966) as "A drawing showing position of wave crests and/or orthogonals in a given area for a specific deep water wave period and direction." An example of a refraction diagram is shown in figure 5.3. Here the orthogonals or wave rays are constructed everywhere perpendicular to the wave fronts. The change in spacing of adjacent wave rays indicates whether the wave energy is being spread out or converged as the wave progresses shoreward. The refraction coefficient is a measure of this divergence or convergence and is the square root of the distance between adjacent wave rays in deep water to the spacing between the same rays at the location for which the wave information is desired.

The manual construction of wave refraction diagrams is described in H. O. Pub. No. 605 (U.S. Navy Hydrographic Office, 1954b) and will be only briefly reviewed here. Starting at a depth of half the deep water wave length, contours are selected which adequately represent the details of the bottom topography. At these contours the wave speed is determined by considering the depth and the wave length. The change of the angle of bending from one contour to the next is related to the wave speed at the two depths by Snell's Law which is illustrated in figure 5.4. For a point between two wave rays the refraction coefficient, K, is expressed as:

$$K = \sqrt{\frac{b}{b_o}}$$

where

b is the spacing between the wave rays in deep water, and

b_o is the spacing at the point in question.

The wave refraction process has been treated numerically with the use of electronic computers (Griswold and Nagle, 1962; Harrison and Wilson, 1964). Such methods determine the wave rays based upon a grid of depth values of the area.

The combined effects of shoaling and refraction are then described as:

$$\frac{H}{H_o} = \sqrt{\frac{1}{2}\ \frac{1}{n}\ \frac{1}{C/C_o}}\quad \sqrt{\frac{b}{b_o}}$$

where all symbols are as described earlier.

Waves break before they reach the shoreline of course and wave theory and observations indicate the depth of breaking to be a function of the breaker height. As given in Supplement to H. O. 234 (U.S. Navy Hydrographic Office, 1954a) this relationship is:

$$d_b = 1.3\ H_b$$

where

d_b is the depth of breaking in feet, and

H_b is the breaker height in feet.

Figure 5.5 shows the change in wave direction and height caused by refraction in coastal areas with straight and parallel bottom contours. Here the refraction coefficient is given as a function of depth, deep water wave length and the angle of wave approach in deep water. This figure can be used instead of an actual refraction diagram for areas in which the bottom contours are approximately straight and parallel. Figure 5.6 gives the breaker height (H_b) as a function of the wave period and the deep water wave height for waves that approach the coast directly with no refraction. The inset shows the

the relationship of the period (T) to the depth (d) and the wavelength (L) in the surf zone for waves either before or after breaking.

As an example of the use of figures 5.5 and 5.6, consider the following situation: the deep water waves have a height of 10 feet and a period of 10 seconds. The angle of wave crests to the bottom contours is 40°. To determine the breaker height and the depth of breaking, we first determine the deep water wave length (L_o) to be 5.12 times period squared or 512 feet. At this step we don't know the exact breaking depth so we cannot enter figure 5.5 with the precise value of d/L_o, but since the deep water wave height is 10 feet and the shoaling factor will increase the height while the refraction effect will reduce the height, the breaking depth won't be too far from 10 feet. Estimating the depth of breaking to be in the range between 5 and 15 feet, we can enter figure 5.5 with d/L_o of .010 for d_b of 5 feet and .029 for d_b of 15 feet. For α_o of 40° refraction coefficient is 0.88 for breaking depth of 5 feet and 0.89 for breaking depth of 15 feet. Multiplying the deep water wave height by K of 0.88, the height is reduced to 8.8 feet by refraction. Entering figure 5.6 with H_o equal to 8.8 feet and period equal to 10 seconds, we determine the breaker height to be 11.2 feet. The depth of breaking is 1.3 times breaker height or 1.3 times 11.2 which is 14.5 feet.

Types of breakers

Breakers are roughly classified into three types, spilling, plunging, or surging. These types are described in Glossary of Oceanographic Terms (U.S. Naval Oceanographic Office, 1966) as:

Spilling breakers break gradually over a considerable distance;

Plunging breakers tend to curl over and break with a crash; and

Surging breakers peak up, but then instead of spilling or plunging they surge up on the beach face.

The three types of breakers are illustrated in figure 5.7. The type of breaker depends upon the slope of the beach with spilling, plunging, and surging breakers occurring respectively on flat, steep, and very steep beaches.

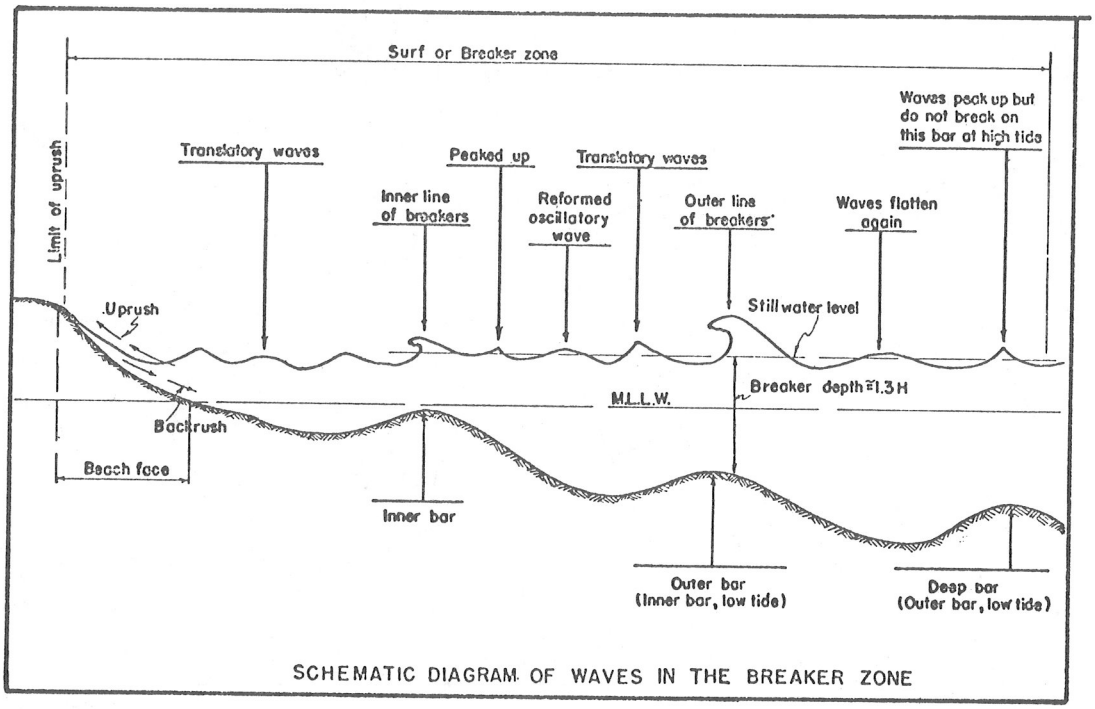

Figure 5.1. Schematic diagram of waves in the breaker zone. (U.S. Army Coastal Engineering Research Center, 1966)

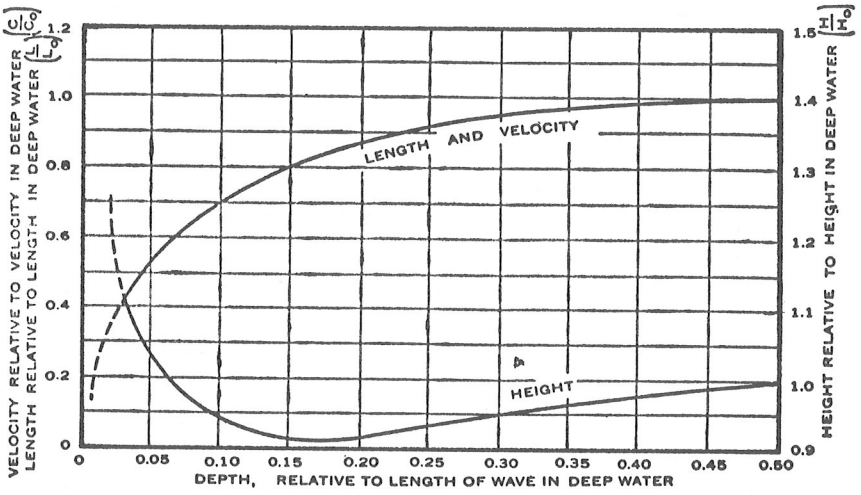

Figure 5.2. Theoretical changes in dimensions of waves as they shoal. (U.S. Navy Hydrographic Office, 1953)

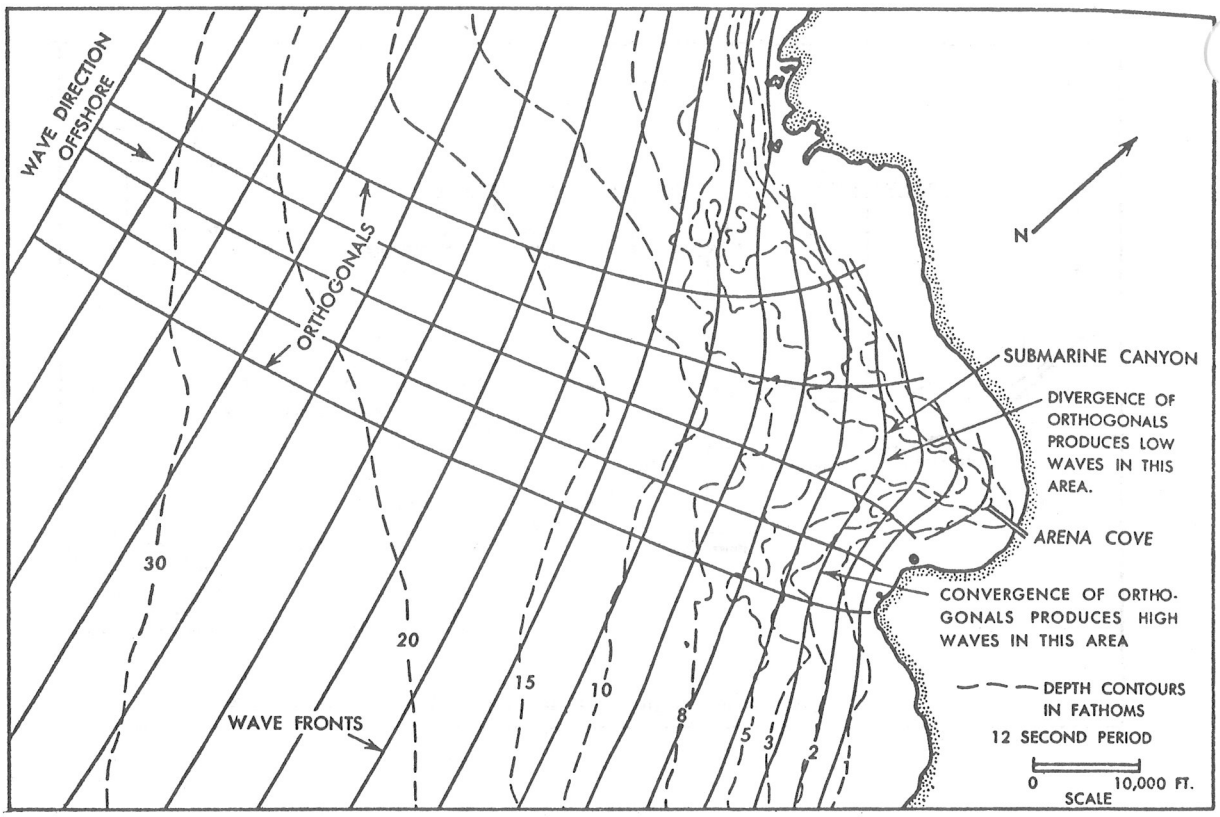

Figure 5.3. Example of wave refraction diagram. (U.S. Naval Oceanographic Office, 1966)

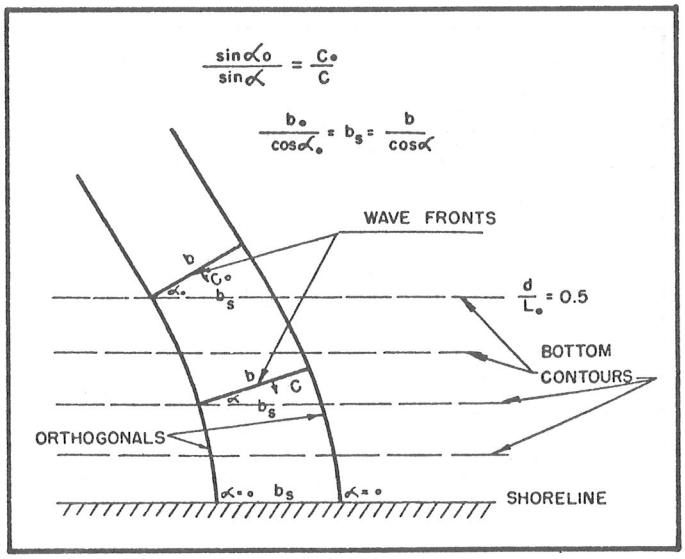

Figure 5.4. Wave refraction assuming a gradual change in wave velocity. (U.S. Navy Hydrographic Office, 1954b)

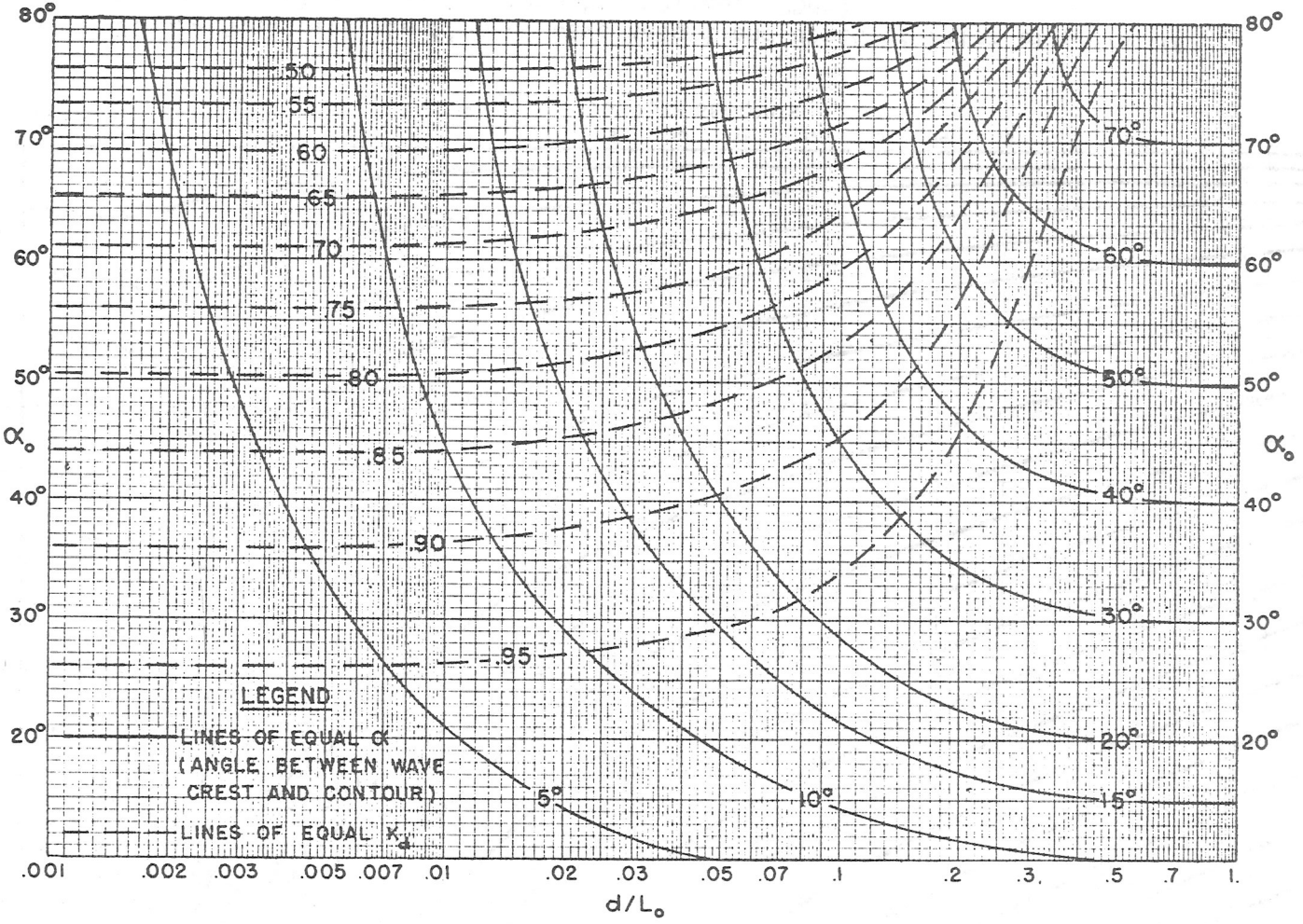

Figure 5.5. Change in wave direction and height due to refraction on beaches with straight, parallel depth contours. (U.S. Navy Hydrographic Office, 1954b)

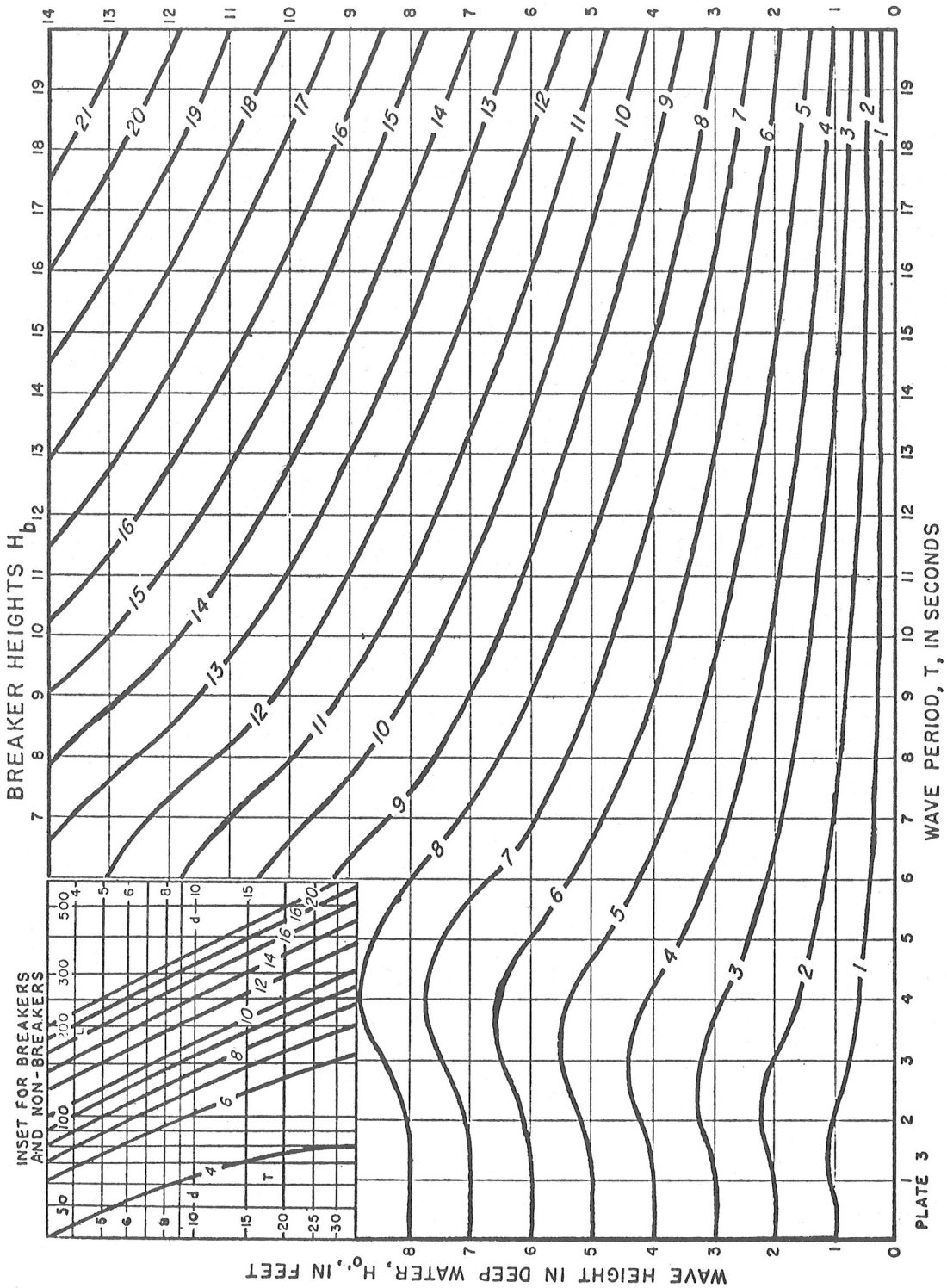

Figure 5.6. Determination of wave height and depth of water at point of breaking. (U.S. Navy Hydrographic Office, 1954a)

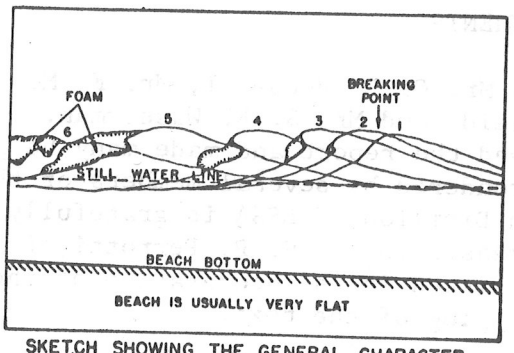

SKETCH SHOWING THE GENERAL CHARACTER OF SPILLING BREAKERS

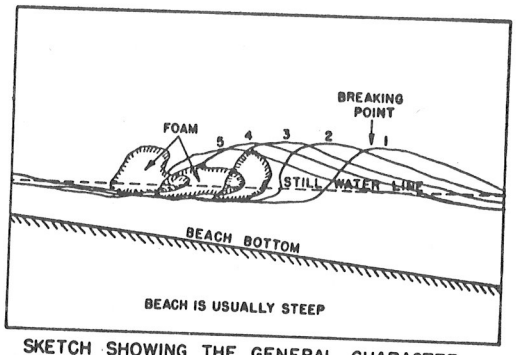

SKETCH SHOWING THE GENERAL CHARACTER OF PLUNGING BREAKERS

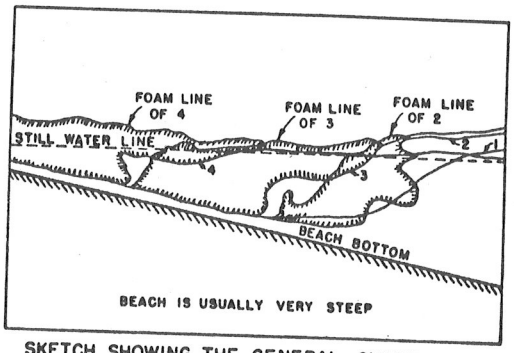

SKETCH SHOWING THE GENERAL CHARACTER OF SURGING BREAKERS

Figure 5.7. Diagrams of the three types of breakers. Each sketch consist of a series of profiles of the wave form as it appears before breaking, during breaking and after breaking. (U.S. Army Coastal Engineering Research Center, 1966)

ACKNOWLEDGMENTS

The author expresses appreciation to Mr. G. B. Burdwell, Mr. E. M. Carlstead, Mr. M. W. Mull, Mr. G. C. Shields and Mr. S. E. Wasserman, Weather Bureau marine experts who reviewed the report and made many helpful suggestions. The editorial assistance rendered by several members of the Scientific Information and Documentation Division of ESSA is gratefully acknowledged. Appreciation is also expressed to Mr. H. P. Perrotti of Techniques Development Laboratory who assisted in the preparation of the figures and to Rosina Lopresti for the typing of the text.

REFERENCES AND BIBLIOGRAPHY

L. Baer, "An Experiment in Numerical Forecasting of Deep Water Ocean Waves," Technical Report LMSC-801296, Missiles and Space Division, Lockheed Aircraft Corporation, Sunnyvale, Calif., 1962.

W. Bascom, Waves and Beaches, Science Study Series, Doubleday and Company, Inc., Garden City, New York, 1964, 267 pp.

C. L. Bretschneider,"Revised Wave Forecasting Relationships", Proc. 2nd Conference on Coastal Engineering, Houston, Council on Wave Research, Univ. of California, 1952a.

C. L. Bretschneider, "The Generation and Decay of Wind Waves in Deep Water," Trans. American Geophysical Union, Vol. 33, No. 3, June 1952b, pp. 381-389.

I. M. Cline, "Relation of Changes in Storm Tides on Coast of the Gulf of Mexico to the Center and Movement of Hurricanes", Monthly Weather Review, Vol. 48, No. 3, March 1920, pp. 127-146.

I. M. Cline, Tropical Cyclones, The MacMillan Company, New York, 1926, 301 pp.

Coast and Geodetic Survey, Tide Tables, High and Low Water Predictions, East Coast North and South America, 1970a, 290 pp.

Coast and Geodetic Survey, Tide Tables, High and Low Water Predictions, West Coast North and South America, 1970b, 226 pp.

W. C. Conner, R. H. Kraft, and D. L. Harris, "Empirical Methods for Forecasting the Maximum Storm Tide Due to Hurricanes and Other Tropical Storms," Monthly Weather Review, Vol. 85, No. 4, April 1957, pp. 113-116.

G. E. R. Deacon, "Recent Studies of Waves and Swell," Annals of the New York Academy of Sciences, Vol. 51, Art. 3, 1949, pp. 475-482.

A. Defant, Physical Oceanography, Pergamon Press, New York, Oxford, London, Paris, Vol. II, 1961, 598 pp.

W. L. Donn, "An Empirical Basis For Forecasting Storm Tides," Bulletin of the American Meteorological Society, Vol. 39, No. 12, 1958, pp. 640-647.

R. W. Fairbridge, Encyclopedia of Oceanography, Reinhold Publishing Corp., New York, N. Y., 1966, 1021 pp.

G. M. Griswold and F. W. Nagle, "Wave Refraction by Numerical Methods," Mimeo. Rept., U.S. Navy Weather Research Facility, 1962, 19 pp.

D. L. Harris, "Hurricane Audrey Storm Tide," National Hurricane Research Project Report No. 23, 1958, 19 pp.

D. L. Harris, "The Equivalence Between Certain Statistical Prediction Methods and Linearized Dynamical Methods," Monthly Weather Review, Vol. 90, August 1962, pp. 331-340.

D. L. Harris, "Coastal Flooding by the Storm of March 5-7, 1962," Manuscript of the U.S. Weather Bureau, Washington, D.C., January 1963a, 22 pp.

D. L. Harris, "Characteristics of the Hurricane Storm Surge," U.S. Weather Bureau, Technical Paper No. 48, Washington, D.C., 1963b, 139 pp.

D. L. Harris, N. A. Pore, and R. A. Cummings, "Tide and Tidal Current Prediction by High Speed Digital Computer," International Hydrographic Review, Vol. XLII, No. 1, January 1965, pp. 95-103.

W. Harrison and W. S. Wilson, "Development of a Method for Numerical Calculation of Wave Refraction," U.S. Army Corps of Engineers, Technical Memorandum No. 6, October 1964, 64 pp.

S. D. Hicks,"The Tide Prediction Centenary of the United States Coast and Geodetic Survey," International Hydrographic Review, Vol. XLIV, No. 2, July 1967, pp. 121-131.

M. N. Hill, The Sea, Vol. 1, Physical Oceanography, John Wiley and Sons, Inc., 1966, 864 pp.

R. A. Hoover, "Empirical Relationships of the Central Pressures in Hurricanes to the Maximum Surge and Storm Tide," Monthly Weather Review, Vol. 85, No. 5, May 1957, pp. 167-174.

W. E. Hubert, "Operational Forecasts of Sea and Swell," First U.S. Navy Symposium on Military Oceanography, 17-19 June 1964, U.S. Navy Oceanographic Office, Washington, D.C., pp. 113-124.

A. D. Hustead, "An Empirical Method of Forecasting Meteorologically Produced Tidal Departures From the Normal Astronomical Tide in the Norfolk, Va., Tidal Basin for a Specific Wind Direction," Manuscript of the U.S. Weather Bureau, Washington, D.C., August 1955, 5 pp.

C. P. Jelesnianski, "Numerical Computations of Storm Surges Without Bottom Stress," Monthly Weather Review, Vol. 94, No. 6, June 1966, pp. 379-394.

C. P. Jelesnianski, "Numerical Computations of Storm Surges with Bottom Stress," Monthly Weather Review, Vol. 95, No. 11, November 1967, pp. 740-756.

B. Kinsman, Wind Waves--their generation and propagation on the ocean surface, Prentice-Hall, Inc., Englewood Cliffs, N. J., 1965, 676 pp.

W. Marks, T. R. Goodman, W. J. Pierson, Jr., L. J. Tick and L. A. Vassilopoulos, "An Automated System for Optimum Ship Routing," Paper presented at meeting of The Society of Naval Architects and Marine Engineers, Nov. 13-16, 1968.

H. A. Marmer, Tidal Datum Planes, Special Publication No. 135, U.S. Coast and Geodetic Survey, Revised 1951 Edition, 142 pp.

A. R. Miller, "The Effect of Steady Winds on Sea Level at Atlantic City," Meteorological Monographs, American Meteorological Society, Vol. 2, 1957, pp. 24-31.

R. G. Miller, "The Screening Procedure. Studies in Statistical Weather Prediction," Final Report, Contract No. AF19(604)-1590, Hartford, Conn., Travelers Weather Research Center, 1958, pp. 86-95.

L. I. Moskowitz, "The Automated Wave Prediction Program of the U.S. Naval Oceanographic Office," Informal Manuscript Report No. 0-9-66, U.S. Naval Oceanographic Office, June 1966, 9 pp., Unpublished Manuscript.

V. A. Myers, "Characteristics of United States Hurricanes Pertinent to Levee Design for Lake Okeechobee, Florida," Hydrometeorological Report No. 32, U.S. Weather Bureau and U.S. Army Corps of Engineers, Washington, D. C., 1954, 106 pp.

National Academy of Sciences, Ocean Wave Spectra, Proceedings of a Conference, Prentice-Hall, Inc., Englewood Cliffs, N. J., 1963, 357 pp.

G. Neumann and W. J. Pierson, Principles of Physical Oceanography, Prentice-Hall, INC., Englewood Cliffs, N. J., 1966, 545 pp.

W. J. Pierson, Jr. and L. J. Tick, "Wave Spectra Hindcasts and Forecasts and their Potential Uses in Military Oceanography," U. S. Navy Symposium on Military Oceanography, 17-18-19 June 1964, U.S. Naval Oceanographic Office, pp. 125-141.

W. J. Pierson, Jr., and L. Moskowitz, "A Proposed Spectral Form for Fully Developed Wind Seas Based on the Similarity Theory of S. A. Kitaigorodskii," Journal of Geophysical Research, Vol. 69, No. 24, Dec. 1964, pp. 5181-5190.

N. A. Pore, "The Storm Surge," Mariners Weather Log, Vol. 5, No. 5, September 1961, pp. 151-156.

N. A. Pore, "The Relation of Wind and Pressure to Extratropical Storm Surges at Atlantic City," Journal of Applied Meteorology, Vol. 3, No. 2, April 1964a, pp. 155-163.

N. A. Pore, "Extratropical Storm Surges at Breakwater Harbor, Delaware," Manuscript of the U.S. Weather Bureau, Washington, D.C., June 1964b, 9 pp.

N. A. Pore, "The Weather Bureau Tide Observing Network," Mariners Weather Log, Vol. 8, No. 4, July 1964c, pp. 108-110.

N. A. Pore, "Chesapeake Bay Extratropical Storm Surges," Chesapeake Science, Vol. 6, No. 3, September 1965, pp. 172-182.

N. A. Pore and R. A. Cummings, "A FORTRAN Program for the Calculation of Hourly Values of Astronomical Tide and Time and Height of High and Low Water," Weather Bureau Technical Memorandum TDL-6, January 1967, 17 pp.

N. A. Pore and W. S. Richardson, "Interim Report on Sea and Swell Forecasting," Weather Bureau Technical Memorandum TDL-13, December 1967, 21 pp.

N. A. Pore and W. S. Richardson, "Second Interim Report on Sea and Swell Forecasting," ESSA Technical Memorandum WBTM TDL 17, January 1969, 17 pp.

J. Proudman, Dynamical Oceanography, Dover Publications, Inc., New York, N.Y., 1952, 409 pp.

H. U. Roll, Physics of the Marine Atmosphere, Academic Press, New York and London, 1965, 426 pp.

P. Schureman, Manual of Harmonic Analysis and Prediction of Tides, Special Publication No. 98, Coast and Geodetic Survey, Revised 1940 Edition, Reprinted 1958, 317 pp.

P. Schureman, Tide and Current Glossary, Special Publication No. 228, Coast and Geodetic Survey, Revised 1949 Edition, Reprinted 1963, 40 pp.

H. U. Sverdrup, M. W. Johnson, and R. H. Fleming, The Oceans, Prentice-Hall, Inc., New York, 1942, 1087 pp.

A. E. Tancreto, "A Method for Forecasting the Maximum Surge at Boston due to Extratropical Storms," Monthly Weather Review, Vol. 86, No. 6, June 1958, pp. 197-200.

U.S. Army Coastal Engineering Research Center, "Shore Protection Planning and Design," Technical Report No. 4, Third Edition, 1966, 580 pp.

U.S. Naval Oceanographic Office, Glossary of Oceanographic Terms, SP-35, Second Edition, Washington, D.C., 1966, 204 pp.

U.S. Navy Department, "Breakers and Surf, Principles in Forecasting," Hydrographic Office Publication No. 234, November 1944, 52 pp.

U.S. Navy Department, "Wind, Sea, and Swell: Theory of Relations for Forecasting," H.O. Pub. No. 601, U.S. Hydrographic Office, March 1947, 44 pp.

U.S. Navy Hydrographic Office, "Techniques for Forecasting Wind Waves and Swell," H.O. Pub. No. 604, Washington, D.C., 1951, 37 pp.

U.S. Navy Hydrographic Office, Wind Waves at Sea, Breakers and Surf, Hydrographic Office Publication No. 602, Washington, D.C., 1947, Reprinted 1953, 177 pp.

U.S. Navy Hydrographic Office, "Supplement to Breakers and Surf, Principles in Forecasting", Hydrographic Office Publication No. 234, U.S. Navy Hydrographic Office, Washington, D.C., November 1950, Reprinted 1954a, 16 pp.

U.S. Navy Hydrographic Office, "Graphical Construction of Wave Refraction Diagrams," Hydrographic Office Publication No. 605, Washington, D.C., Jan. 1948, Reprinted 1954b, 45 pp.

U.S. Navy Hydrographic Office, Practical Methods for Observing and Forecasting Ocean Waves by means of Wave Spectra and Statistics, H.O. Pub. No. 603, 1955, 284 pp.

W. S. von Arx, An Introduction to Physical Oceanography, Addison-Wesley Publishing Company, Inc., Reading, Mass., 1962, 422 pp.

R. L. Wiegel, Oceanographical Engineering, Prentice-Hall, Inc., Englewood Cliffs, N.J., 1964, 532 pp.

B. D. Zetler, "Tidal Characteristics From Harmonic Constants," Journal of the Hydraulics Division, Proceedings of the American Society of Civil Engineers, Vol. 85, No. HY 12, December 1959, pp. 77-87.

GPO 911-782

(Continued from inside front cover)

WBTM TDL 16 Objective Visibility Forecasting Techniques Based on Surface and Tower Observations. Donald M. Gales, October 1968. (PB-180 479)

WBTM TDL 17 Second Interim Report on Sea and Swell Forecasting. N. A. Pore and Lt. W. S. Richardson, USESSA, January 1969. (PB-182 273)

WBTM TDL 18 Conditional Probabilities of Precipitation Amounts in the Conterminous United States. Donald L. Jorgensen, William H. Klein, and Charles F. Roberts, March 1969. (PB-183 144)

WBTM TDL 19 An Operationally Oriented Small-Scale 500-Millibar Height Analysis. Harry R. Glahn and George W. Hollenbaugh, March 1969. (PB-184 111)

WBTM TDL 20 A Comparison of Two Methods of Reducing Truncation Error. Robert J. Bermowitz, May 1969. (PB-184 741)

WBTM TDL 21 Automatic Decoding of Hourly Weather Reports. George W. Hollenbaugh, Harry R. Glahn, and Dale A. Lowry, July 1969. (PB-185 806)

WBTM TDL 22 An Operationally Oriented Objective Analysis Program. Harry R. Glahn, George W. Hollenbaugh, and Dale A. Lowry, July 1969. (PB-186 129)

WBTM TDL 23 An Operational Subsynoptic Advection Model. Harry R. Glahn, Dale A. Lowry, and George W. Hollenbaugh, July 1969. (PB-186 389)

WBTM TDL 24 A Lake Erie Storm Surge Forecasting Technique. William S. Richardson and N. Arthur Pore, August 1969. (PB-185 778)

WBTM TDL 25 Charts Giving Station Precipitation in the Plateau States From 850- and 500-Millibar Lows During Winter. August F. Korte, Donald L. Jorgensen, and William H. Klein, September 1969. (PB-187 476)

WBTM TDL 26 Computer Forecasts of Maximum and Minimum Surface Temperatures. William H. Klein, Frank Lewis, and George P. Casely, October 1969. (PB-189 105)

WBTM TDL 27 An Operational Method for Objectively Forecasting Probability of Precipitation. Harry R. Glahn and Dale A. Lowry, October 1969. (PB-188 660)

WBTM TDL 28 Techniques for Forecasting Low Water Occurrences at Baltimore and Norfolk. Lt. (jg) James M. McClelland, USESSA, March 1970. (PB-191 744)

WBTM TDL 29 A Method for Predicting Surface Winds. Harry R. Glahn, March 1970. (PB-191 745)